ANALYSIS OF LANE CHANGES FOR VEHICLE STRINGS ON HIGHWAYS: STRING STABILITY, DRIVING SAFETY AND COMFORT

HARUN BUĞRA SAĞLAM

SEPTEMBER 2017

ANALYSIS OF LANE CHANGES FOR VEHICLE STRINGS ON HIGHWAYS:
STRING STABILITY, DRIVING SAFETY AND COMFORT

A THESIS SUBMITTED TO
THE GRADUATE SCHOOL OF NATURAL AND APPLIED
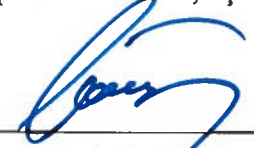SCIENCES OF
ÇANKAYA UNIVERSITY

BY
HARUN BUĞRA SAĞLAM

IN PARTIAL FULFILLMENT OF THE REQUIREMENTS FOR THE
DEGREE OF
DOCTOR OF PHILOSOPHY
IN
THE DEPARTMENT OF
ELECTRONIC AND COMMUNICATION ENGINEERING

SEPTEMBER 2017

Title of the Thesis: Analysis of Lane Changes for Vehicle Strings on Highways:
String Stability, Driving Safety and Comfort
Submitted by **Harun Buğra SAĞLAM**

Approval of the Graduate School of Natural and Applied Sciences, Çankaya
University.

Prof. Dr. Can ÇOĞUN
Director

I certify that this thesis satisfies all the requirements as a thesis for the degree of
Doctor of Philosophy.

Prof. Dr. Sıtkı Kemal İDER
Head of Department
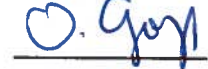
This is to certify that we have read this thesis and that in our opinion it is fully
adequate, in scope and quality, as a thesis for the degree of Doctor of Philosophy.

Assoc. Prof. Dr. Klaus Werner SCHMIDT
Supervisor

Examination Date: 14.09.2017

Examining Committee Members

Assoc. Prof. Dr. Klaus Werner SCHMIDT	(Çankaya Univ.)	
Prof. Dr. Mehmet Kemal LEBLEBİCİOĞLU	(METU)	
Assoc. Prof. Dr. Orhan GAZİ	(Çankaya Univ.)	
Assoc. Prof. Dr. Umut ORGUNER	(METU)	
Asst. Prof. Dr. Serap Altay ARPALİ	(Çankaya Univ.)	

STATEMENT OF NON-PLAGIARISM PAGE

I hereby declare that all information in this document has been obtained and presented in accordance with academic rules and ethical conduct. I also declare that, as required by these rules and conduct, I have fully cited and referenced all material and results that are not original to this work.

Name, Last Name   : Harun Buğra, SAĞLAM

Signature   :

Date   : 14.09.2017

ABSTRACT

SAĞLAM, Harun Buğra

Ph.D., Department of Electronic and Communication Engineering

Supervisor: Assoc. Prof. Dr. Klaus Werner SCHMIDT

September 2017, 140 pages

An important aim of intelligent transportation systems (ITS) is the full or partial replacement of human driver functionality. Cooperative adaptive cruise control (CACC) is a recent technology for automating the longitudinal vehicle motion. Fulfilling the condition of string stability, CACC enables safe vehicle following at small inter-vehicle spacings and hence supports the formation of tight vehicle strings for improving the road capacity. In its classical realization, CACC is limited to the case where vehicle strings are already formed and all vehicles in a string follow each other on the same lane of a road. However, practical driving situations include the case of vehicles entering or leaving a string and performing maneuvers different from only vehicle following.

This thesis is concerned with the effect of additional maneuvers due to lane changes (vehicles entering or leaving) on the safety of vehicle strings. Lane changes include gap opening and closing maneuvers and are subject to measurement inaccuracies and sensor errors due to changes of the vehicle locations. Accordingly, the effect of these maneuvers on the longitudinal vehicle motion has to be analyzed.

As the first contribution, the thesis argues that the described measurement inaccuracies during lane changes can be modeled by input signal impulses of the respective vehicle. Moreover, opening/closing gap maneuvers can be realized by the generation of suitable feedforward input signals that are nonzero for a limited time. Respecting that multiple lane changes can occur in a vehicle string, the thesis proposes to study the effect of repeated input signals (impulses or time-limited input signals) on the output signal norm of LTI systems. The second contribution of the thesis is extending the definition of string stability to additional disturbances that can be applied to any vehicle in the string. Respecting the same idea, the third contribution of the thesis shows that a bound on the output signal norm of stable LTI systems exists if the repeated input signals (impulses or time-limited signals) are separated by a non-zero dwell-time. Additionally, an original computational procedure for finding a tight bound on the output signal norm is provided. The fourth contribution is the adaptation of these computational methods to the case of stable LTI systems with multiple inputs and outputs. The fifth contribution is the application of the obtained results to vehicle strings. It is shown that suitable analytical bounds for the relevant output signals such as distance error or acceleration can be determined and the results are validated by simulations. The last major contribution is the development of new numerical methods for bounding the matrix exponential function for large LTI systems based on the Jordan canonical form and the Schur decomposition. The evaluation of such norms is needed when computing the output signal norm of large LTI systems such as long vehicle strings.

Keywords: Intelligent Transportation System, platooning, cooperative adaptive cruise control, linear systems, impulse inputs, time-limited inputs, vehicle following, string stability, driving safety, feedforward signal, matrix exponential bound.

ÖZ

SAĞLAM, Harun Buğra

Doktora, Elektronik ve Haberleşme Mühendisliği Anabilim Dalı

Tez Yöneticisi: Doç. Dr. Klaus Werner SCHMIDT

Eylül 2017, 140 sayfa

Akıllı ulaştırma sistemlerinin önemli amaçlarından biri insan sürücü fonksiyonalitesini kısmi veya tümüyle devralabilmektir. Kooperatif otomatik seyir kontrolü (CACC) boylamsal araç hareketinin otomasyonu için yeni sayılabilecek bir teknolojidir. Dizi kararlılığı koşulunu sağlamak kaydıyla, CACC küçük araç arası boşluklarda güvenli araç takibini mümkün kılmakta ve yol kapasitesini iyileştirmek hedefiyle sıkı araç dizilerinin oluşumunu desteklemektedir. Klasik gerçeklenişiyle düşündüğümüzde, CACC araç dizilerinin oluşmuş olduğu ve tüm araçların yolun aynı şeridinde birbirini takip ettiği durumlarla sınırlandırılmıştır. Bununla birlikte pratik öngörülen sürüş durumları diziye giren ve çıkan araçları içermekte olup dizide sadece öndeki aracı takip etmenin yanı sıra farklı manevralar icra etmeyi gerektirir.

Bu tez araç dizilerindeki (araçlar girerken ve çıkarken) şerit değişikliklerinden dolayı yapılan ek manevraların araç dizileri üzerindeki emniyet etkileri ile ilgilenmektedir. boşluk açma ve kapama manevralarını içerecek şekilde şerit değişikliklerini düzenleyen kontrolcüler araç lokasyonunun değişiminden dolayı ölçüm hataları ve sensör bozulmalarına maruz kalabilmektedir. Uygun şekilde, bu manevraların aracın boylamsal hareketi üzerine etkileri analiz edilmelidir.

İlk önemli katkısı olarak bu tez, şerit değişikliği sırasında tanımlanan bu ölçüm hatalarının ilgili aracın girdi sinyal impulse'ları olarak modellenebildiğini tartışmaktadır. Bunun yanında, takip boşluğu açma/kapama manevraları uygun tanımlanmış, sınırlı bir süre sıfır-dışı olan ileribesleme girdi sinyallerinin üretimi ile gerçekleştirilebilmektedir. Bir araç dizisinde birden fazla şerit değişikliği olabileceği fikrine sadık kalarak, bu tez tekrar eden girdi sinyallerinin (impulse'lar veya zaman-sınırlı girdi sinyalleri) LTI sistemlerin sinyal çıktı normları üzerindeki etkilerinin çalışılmasını önermektedir. Bu tezin ikinci katkısı dizi kararlığı tanımına herhangi bir araç üzerindeki ek bozulmaları uygulayarak genişletmesidir. Aynı fikre sadık kalarak bu tezin yaptığı üçüncü katkıysa, eğer tekrar eden girdi sinyalleri (impulse veya zaman-sınırlı sinyaller) sıfır-harici bir ikamet-zamanı ile ayrılmışsa kararlı LTI sistemlerin çıktı sinyal normu üzerinde bir sınır göstermesidir. Ek olarak, çıktı sinyal normu üzerinde orijinal şekilde, sıkı bir sınır hesaplama prosedürü sunmaktadır. Dördüncü katkısı ise, bu hesaplama yöntemlerini kararlı çok-girdili çok-çıktılı LTI sistemler üzerine adapte edebilmesidir. Beşinci katkısıysa, elde edilen sonuçların araç dizilerine uygulanabilmesidir. Mesafe hatası, ivme hatası gibi çıktı sinyallerin uygun analitik sınırlarını belirlenebildiği gösterilmekte ve sonuçlar simülasyonlarla geçerli kılınmaktadır. Son büyük katkısıysa, büyük LTI sistemler için matris eksponansiyel fonksiyonların Jordan kanonik form ve Schur kırılımı temelinde yeni numerik metodlar geliştirmesidir. Bu normların değerlendirme ihtiyacı, uzun araç dizileri gibi büyük LTI sistemlerin çıktı sinyal normunun hesaplanması sırasında ortaya çıkmıştır.

Anahtar Kelimeler: Akıllı Ulaştırma Sistemleri, araç dizileri, kooperatif otomatik seyir kontrolü, lineer sistemler, impulse girdileri, zaman-sınırlı girdiler, araç takibi, dizi kararlılığı, sürüş emniyeti, ileri beslemeli sinyal, matris exponansiyel sınır.

ACKNOWLEDGEMENTS

TABLE OF CONTENTS

CHAPTERS:

List of Figures

List of Tables

LIST OF ABBREVIATIONS

ACC	Adaptive Cruise Control
CACC	Cooperative Adaptive Cruise Control
ITS	Intelligent Transportation Systems
LTI	Linear Time-Invariant
PD	Proportional Derivative
V2I	Vehicle to Infrastructure
V2V	Vehicle to Vehicle
v_i	Velocity of Vehicle i
d_i	Actual Inter-Vehicle Distance of Vehicle i
$d_{i,r}$	Desired Inter-Vehicle Distance of Vehicle i
r_i	Standstill Distance of Vehicle i
H	Time Headway Constant
e_i	Spacing Error of Vehicle i
q_i	Rear Bumper Position of Vehicle i
L_i	Length of Vehicle i
G_i	Plant Model of Vehicle i
θ	Communication Delay
ϕ	Actuator (Plant) Time Delay
Γ_i	Complementary Sensitivity of Vehicle i
τ_i	Time Constant of Driveline Dynamics
H(s)	Spacing Policy
K_{fb}	Feedback Controller
K_{ff}	Feedforward Controller
a_i	Acceleration of Vehicle i
u_i	Control Input of Vehicle i
$u_i{}^{ff}$	Feedforward Input

CHAPTER 1

INTRODUCTION

Transportation systems form the backbone of national economic prosperity, which provides reliable transportation of passenger traffic and freight movement for domestic and international trade. The ever-growing demands of traffic during the last few decades exceeds existing road transportation infrastructure and resources. This leads to an increased frequency and severity of traffic problems, such as traffic congestion, traffic accidents and environmental pollution [1]. Additionally, a considerable number of people die from roadway crashes on highways, and growing traffic demand causes significant congestion on major urban areas and corridors in each country. While driver error has been considered as the leading cause of most crashes, limited transportation infrastructure capacity is one of the primary reasons of congestion.

For these reasons, a robust solution in the future lies in efficient application of presently available means of road transportation and infrastructure [2]. Intelligent Transportation Systems (ITS) are a possible solution to reduce these issues, maximize the efficiency of existing transportation system capacity, and to improve traffic safety [3, 4, 5]. ITS can be classified as traffic infrastructure based, vehicle categories based, diverse roads based, vehicle to road based or vehicle to vehicle based technologies [6, 7, 8, 9]. In particular, the introduction of automation into vehicles [10, 11, 12] and wireless communication in a connected vehicular environment can improve safety and mobility efficiency. They can also reduce environmental impact of transportation systems.

It is observed that the most important factor for traffic breakdown is the human driving behavior [7]. That is, the design of control strategies for automatic

driving is essential to avoid traffic breakdown. Starting from automation of vehicles and highways, protocols for coordination of vehicle strings are established. Such protocols can either be entirely distributed based on vehicle to vehicle (V2V) communication or they can include a central roadside unit for vehicle to infrastructure (V2I) communication. This thesis focuses on cooperative adaptive cruise control (CACC) as a vehicle to vehicle based technology. The functionality of CACC is based on signal communication and distance measurement among vehicles in a platoon. Its main aim is to improve the highway traffic flow and driving safety [13, 14, 15] by increasing the road capacity by small inter-vehicle distances (traffic throughput).

In the recent literature, CACC is commonly realized using predecessor following [14, 16]. That is, each vehicle obtains data from its direct predecessor vehicle [8, 13, 17, 18, 19, 20, 21, 22, 21, 23]. When realizing vehicle following, it is important to ensure driving comfort and safety. Hence, it is important that fluctuations in the motion of any vehicle are attenuated along a vehicle string. This intuitive requirement is formally described by the condition of string stability [8, 24, 25, 26, 27]. Hence, CACC has to be designed so as to fulfill string stability and the literature provides various methods. Designs based on PD-controllers are proposed in [8, 13, 20, 23] and H_∞-control is employed in [22]. Model-predictive control is applied in [9], [28] uses consensus control and [29] uses receding-horizon control to achieve string-stability for speed-change maneuvers. It is important to note that all the cited research works are based on the assumption that vehicle strings are already formed. That is, all vehicles in a string already travel back to back on the same lane of a road and disturbances to the string are only introduced by the leader vehicle. However, the case of vehicles entering or leaving a string and the case of vehicles performing maneuvers different from only following in a string are not considered.

Accordingly, this thesis identifies that it is important to analyze the effect of additional disturbances within vehicle strings. Hereby, the main focus is the effect of lane changes (vehicles entering or leaving) in vehicle strings. Consider the case of a new vehicle entering in front of some vehicle V. When completing such

maneuver, it is the case that the leader vehicle of vehicle V changes. Due to measurement inaccuracies, this has the effect of a jump in the state of vehicle V (for example distance error) and can be modeled by an impulse input signal. In addition, the preparation of lane changes requires opening gaps, which are achieved by applying certain feedforward signals to vehicle V. Since such maneuvers can be performed in a bounded time, time-limited input signals are suitable for this task. Following the previous discussion and respecting the fact that the described maneuvers can occur many times in a vehicle string, the thesis extends the classical setting of CACC to scenarios including repeated state jumps (impulse inputs) and repeated exogenous time-limited input signals within vehicle strings. In addition, the thesis provides a detailed analysis of the effect of such additional maneuvers on the successor vehicles in order to establish driving safety.

The main contributions of the thesis are listed as follows:

1. In the existing literature, the notion of string stability is defined for the case of vehicle strings, where the only disturbance signal is introduced by the leader vehicle. The thesis extends the definition of string stability to additional disturbances that can be applied to any vehicle in the string. In particular, the case of impulsive and time-limited exogenous disturbance inputs is considered and conditions for the verification of the extended version of string stability are derived.

2. It is necessary to quantify the effect of additional disturbances for the practical application of CACC in vehicle strings. Modeling a vehicle string with CACC by a stable LTI system, the thesis develops general methods for computing norm bounds on output signals when applying repeated input impulses and time-limited input signals to stable LTI systems. In this context, it is desired that output signals such as the distance error between vehicles remain bounded in order to ensure driving safety even if maneuvers are repeatedly executed. Accordingly, the thesis first shows that a bound on the output signal norm exists if the repeated input signals (impulses or time-limited signals) are separated by a non-zero dwell-time. Moreover, an

3

original computational procedure for finding a close (fitting tightly) bound on the output signal norm is developed.

3. Vehicle strings have a special interconnection structure and each vehicle is associated with an input and output signal. To this end, the computational methods in item 2. are adapted to the case of stable LTI systems with multiple inputs and outputs.

4. The bound computations in item 2. and 3. are formulated for general LTI systems. In accordance with the aim of studying lane changes in vehicle strings, the developed methods are applied to vehicle strings as the second main contribution of the thesis. Suitable analytical bounds for the relevant output signals such as distance error or acceleration are determined and validated by simulations. Together, it is shown that a safe and comfortable driving distance is guaranteed even if an arbitrary number of longitudinal maneuvers is performed in vehicle strings with many vehicles.

5. The developed computational methods require the numerical computation of a certain bounding function for the norm bound of the impulse response matrix. It turns out during the thesis study, that this bound computation becomes infeasible for large LTI systems. To this end, the thesis proposes new numerical methods based on the Jordan canonical form and the Schur decomposition for bounding the matrix exponential function for large LTI systems.

This thesis is organized as follows. Chapter 2 provides background information regarding vehicle strings, CACC and string stability. In Chapter 3, lane change maneuvers in vehicle strings are described, suitable models are presented and string stability under additional disturbance signals is investigated. Chapter 4 determines analytical bounds for the effect of repeated input signals on the output signal norm of LTI systems. Chapter 5 applies the general bound computations to vehicle strings and evaluates driving safety under repeated lane changes. Chapter 6 develops computational methods for bounding the impulse response matrix norm. Chapter 7 gives conclusion and discusses directions for future work.

CHAPTER 2

BACKGROUND

The main subject of this thesis is the use of cooperative adaptive cruise control (CACC) during lane changes. This chapter provides the necessary background information about vehicle following and CACC. Section 2.1 introduces the concept of vehicle following together with CACC. A state space model for the CACC control loop is derived in Section 2.2 and string stability is introduced as an important condition for safe vehicle following in Section 2.3. Section 2.4 provides simulations of vehicle strings for illustration.

2.1 CACC and Vehicle Following

CACC is an extension of standard Adaptive Cruise Control (ACC) [30, 31], feeding additional data by wireless communication to allow short-distance automatic vehicle following. CACC takes an important role in the future traffic control, where vehicles follow each other in so-called *vehicle strings* at small inter-vehicle spacing [13, 26, 32] as shown in Fig. 2.1. As a special feature, data is communicated from one or more predecessor vehicles. Different versions such as the leader-following, the predecessor following or the leader-predecessor following strategy are investigated in the literature. In this thesis, we employ the predecessor following strategy, where vehicle $i-1$ provides state information to vehicle i via V2V communication. The practical advantage of this strategy is that communication is only required with the closest vehicle, which increases the reliability and allows for small response times. Hence, this is the most basic strategy [14, 16, 33] that is most frequently used in the recent literature.

Fig. 2.1 shows the common vehicle following scenario. L_i, q_i and v_i denote
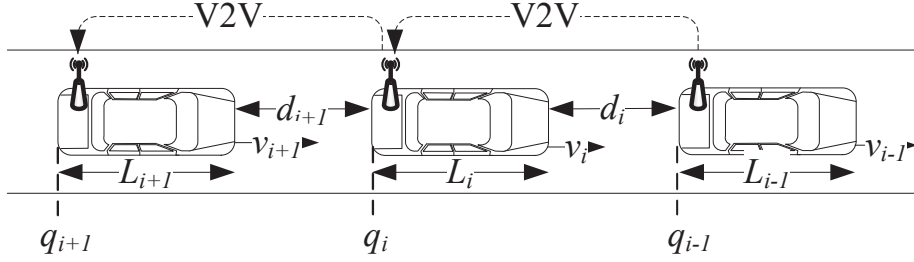
Figure 2.1: Vehicle following scenario in a vehicle string.

the length, rear bumper position and velocity of vehicle i, respectively. Here d_i is the gap between vehicle $i-1$ and vehicle i that is defined as

$$d_i(t) = q_{i-1}(t) - q_i(t) - L_i. \tag{2.1}$$

It is assumed that d_i can be measured by vehicle i via sensors (RADAR or LIDAR) [6, 13, 33]. In addition, data such as the acceleration or velocity of the predecessor vehicle can be obtained via wireless (V2V) communication. Introducing the desired distance $d_{i,r}$ of vehicle i, the distance error e_i is evaluated as

$$e_i = d_{i,r} - (q_{i-1} - q_i). \tag{2.2}$$

In this scenario, the vehicle spacing $q_{i-1} - q_i$ should be small in order to increase the traffic capacity. On the other hand, a sufficient vehicle spacing must be guaranteed in order to ensure driving safety. This task can be accomplished by using *cooperative adaptive cruise control* (CACC) with the property of *string stability* that ensures the attenuation of fluctuations in the motion of a leader vehicle along the vehicle string [8, 26, 27]. In particular, bounds for the L_2-norm or the L_∞-norm of the distance error e_i can be established [8].

A frequently used spacing policy for CACC is given by the constant headway time policy [33] as shown in (2.3).

$$d_{i,r} = r_i + h v_i. \tag{2.3}$$

6

Here, $d_{i,r}$ in (2.2) represents the desired spacing between vehicle $i-1$ and vehicle i. It depends on the *distance at standstill* r_i and the *headway time* h_i. That is, at zero velocity, the desired distance is r_i and $d_{i,r}$ increases proportional to v_i. The spacing error $e_i(t)$ is then equal to:

$$e_i(t) = d_i(t) - d_{i,r}(t) = (q_{i-1}(t) - q_i(t) - L_i) - (r_i + hv_i(t)). \qquad (2.4)$$

Regarding the vehicle plant, we employ the linear model

$$G_i(s) = \frac{Q_i(s)}{U_i(s)} = \frac{e^{-\phi_i s}}{(1 + s\,\tau_i)\,s^2}, \qquad (2.5)$$

that is frequently used in the recent literature [21, 23, 33]. τ_i is the time constant of the *driveline dynamics* and ϕ_i is the *actuator time delay* that can be different for each vehicle i. This model is obtained from a nonlinear model of the driveline dynamics based on feedback linearization and low-level control [34, 35, 36]. The low-level control loop ensures that τ_i is constant over a wide range of normal driving situations [13, 37] which are predominant for CACC. The control objective in this chapter is, as in the literature, only for the case of homogeneous strings, where all vehicles have the same dynamic properties and use the spacing policy in (2.3) [20, 33]. That is, we assume that $G_i = G$ with $\tau_i = \tau$ and $\phi_i = \phi$ for all vehicles i.

CACC controller is designed for the feedback loop in Fig. 2.2. Here, the input signal u_{i-1} of vehicle i is transmitted to vehicle i via V2V communication and $D = e^{-\theta s}$ represents a potential communication delay. $H = 1 + hs$ is used to implement the spacing policy in (2.3) with the constant headway h and K is the controller transfer matrix which can be written as

$$K = \begin{bmatrix} K_{ff} & K_{fb} \end{bmatrix}. \qquad (2.6)$$

K_{ff} is a feedforward controller transfer function for controlling acceleration data by wireless communication and K_{fb} is a feedback controller transfer function for controlling the spacing error $e_i(s)$ between the desired distance and the actual distance. Then, the transfer function Γ is found from Fig. 2.2 for all i:
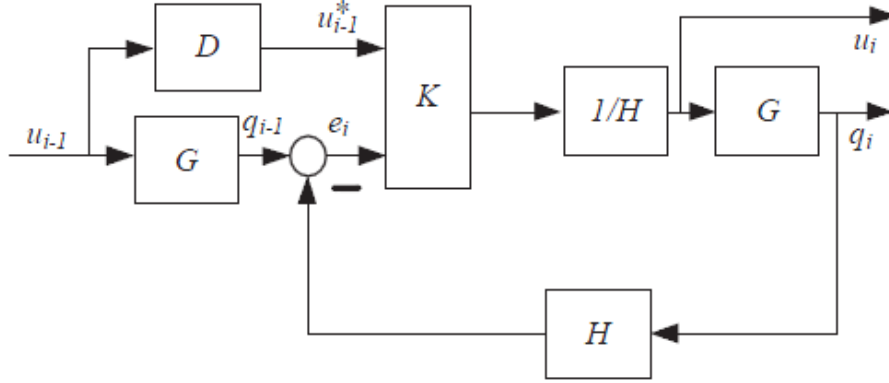
Figure 2.2: Feedback loop for CACC.

$$\Gamma(s) := \frac{U_i(s)}{U_{i-1}(s)} = \frac{DK_{ff} + GK_{fb}}{H(1 + GK_{fb})}.$$ (2.7)

2.2 State Space Model of the CACC Loop

Consider the feedback loop in 2.2. No communication delay is assumed, where $D(s) = 1$. As a basis for state-space design, the following vehicle model is adopted:

$$\begin{bmatrix} \dot{e}_i \\ \dot{v}_i \\ \dot{a}_i \end{bmatrix} = \begin{bmatrix} v_{i-1} - v_i - ha_i \\ a_i \\ -\frac{1}{\tau}a_i + \frac{1}{\tau}u_i \end{bmatrix}$$ (2.8)

The controller state-space model can now be formulated in accordance with Fig. 2.2.

$$\begin{bmatrix} \dot{\eta}_i \\ Y_{K,i} \end{bmatrix} = \begin{bmatrix} A_K \eta_i + \begin{bmatrix} b_1 & b_2 \end{bmatrix} \begin{bmatrix} u_{i-1} \\ e_i \end{bmatrix} \\ C_K \eta_i + \begin{bmatrix} d_1 & d_2 \end{bmatrix} \begin{bmatrix} u_{i-1} \\ e_i \end{bmatrix} \end{bmatrix}$$ (2.9)

where $A_K, C_K, Y_{K,i}$ and b_1, b_2, d_1, d_2 depend on H_∞ controller designed. Moreover,

$Y_{K,i}$ is the unfiltered controller output and its effect for the system can be generated as

$$\dot{u}_i = -\frac{1}{h}u_i + \frac{d_1}{h}u_{i-1} + \frac{d_2}{h}e_i + \frac{C_K}{h}\eta_i \tag{2.10}$$

Using (2.8) to (2.10) and defining the overall system state as $x_i = \begin{bmatrix} e_i & v_i & a_i & u_i & \eta_i \end{bmatrix}^T$ with error e_i, velocity v_i, acceleration a_i, control input u_i and controller state η_i of vehicle i, the following vehicle model in the string, is thus obtained:

$$\underbrace{\begin{bmatrix} \dot{e}_i \\ \dot{v}_i \\ \dot{a}_i \\ \dot{u}_i \\ \dot{\eta}_i \end{bmatrix}}_{} = \underbrace{\begin{bmatrix} 0 & -1 & -h & 0 & 0 \\ 0 & 0 & 1 & 0 & 0 \\ 0 & 0 & -\frac{1}{\tau} & \frac{1}{\tau} & 0 \\ \frac{1}{h}d_2 & 0 & 0 & -\frac{1}{h} & \frac{1}{h}C_k \\ b_2 & 0 & 0 & 0 & A_k \end{bmatrix}}_{A_0}\begin{bmatrix} e_i \\ v_i \\ a_i \\ u_i \\ \eta_i \end{bmatrix} + \underbrace{\begin{bmatrix} 0 & 1 & 0 & 0 & 0 \\ 0 & 0 & 0 & 0 & 0 \\ 0 & 0 & 0 & 0 & 0 \\ 0 & 0 & 0 & \frac{1}{h}d_1 & 0 \\ 0 & 0 & 0 & b_1 & 0 \end{bmatrix}}_{A_1}\begin{bmatrix} e_{i-1} \\ v_{i-1} \\ a_{i-1} \\ u_{i-1} \\ \eta_{i-1} \end{bmatrix} \tag{2.11}$$

where A_0 is the part of the dynamic matrix that depends on the own state for each vehicle, while A_1 is the part of the dynamic matrix that depends on the predecessor state for each vehicle (interconnection).

The first vehicle in the platoon, not having a preceding vehicle, namely the leader vehicle $(i = r)$ employs the open-loop controller to direct the platoon. Using the above state definition, the leader reference vehicle model may be formulated as

$$\begin{bmatrix} \dot{q}_r \\ \dot{v}_r \\ \dot{a}_r \end{bmatrix} = \underbrace{\begin{bmatrix} 0 & 1 & 0 \\ 0 & 0 & 1 \\ 0 & 0 & -\frac{1}{\tau} \end{bmatrix}}_{A_r}\begin{bmatrix} q_r \\ v_r \\ a_r \end{bmatrix} + \underbrace{\begin{bmatrix} 0 \\ 0 \\ \frac{1}{\tau} \end{bmatrix}}_{B_r}u_r \tag{2.12}$$

with A_r and B_r, reflecting the dynamic matrix of the leader vehicle and the input

vector for the exogenous input u_r of the leader vehicle. The signal connections of a vehicle string are shown in Fig. 2.3.
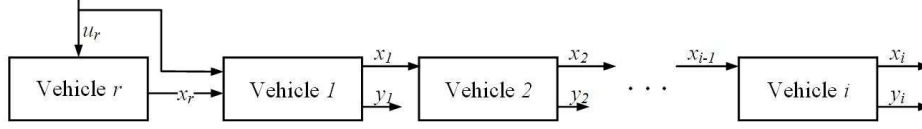
Figure 2.3: Normal string with input.

Individual models are derived in (2.11) and (2.12), considering the single state space model for a vehicle. Regarding a vehicle string with the connections in Fig. 2.3, a string with n vehicles and the output matrix C is modeled as

$$\dot{x}_r = A_r x_r + B_r u_r$$
$$\dot{x}_1 = A_{1,r} x_r + A_0 x_1 + B_1 u_r$$
$$\dot{x}_i = A_1 x_{i-1} + A_0 x_i, \quad i = 2, \ldots.$$

$$\dot{x} = Ax + Bu_r \tag{2.13}$$
$$y_i = C_i x. \tag{2.14}$$

with

$$x = \begin{bmatrix} x_r \\ x_1 \\ x_2 \\ \vdots \\ x_n \end{bmatrix} ; \quad A = \begin{bmatrix} A_r & 0 & 0 & \cdots & 0 & 0 \\ A_{1,r} & A_0 & 0 & \cdots & 0 & 0 \\ 0 & A_1 & A_0 & \cdots & 0 & 0 \\ \vdots & \ddots & \ddots & \ddots & \vdots & \vdots \\ 0 & 0 & 0 & \cdots & A_1 & A_0 \end{bmatrix} ; \quad B = \begin{bmatrix} B_r \\ B_1 \\ 0 \\ \vdots \\ 0 \end{bmatrix} \tag{2.15}$$
$$C_i = \begin{bmatrix} 0 & \cdots & 0 & C & 0 & \cdots 0 \end{bmatrix}$$

The control objective is to ensure that the (closed-loop) vehicle string dynam-

ics exhibits an asymptotically stable equilibrium for which it holds that [38]

$$\lim_{t\to\infty} e_i(t) = 0 \qquad (2.16)$$

for $u_r(t) = 0$. This control objective implies that all intervehicle distance errors $e_i(t)$ converge to zero when the velocity of the leader reference vehicle $v_r(t)$ goes to a constant velocity $\overline{v_r}$ (which is the case for $u_r = 0$). As a result, it holds that

$$\lim_{t\to\infty} v_i(t) = \overline{v_r} \qquad (2.17)$$

Now, (2.16) and (2.17) together imply that all vehicles follow at the desired inter-vehicle distance with equal velocity $\overline{v_r}$.

2.3 String Stability

2.3.1 Definition

The major goal of vehicle-following in dense traffic, (which is essential using CACC), is subject to requirements related to safety, comfort and scalability with respect to string length [26]. In order to fulfill these requirements, the vehicle string is desired to exhibit string-stable behavior. The CACC must be designed such that disturbances are attenuated along a vehicle string. That is, a small variation in the speed or acceleration of any vehicle i should not lead to increasing variations in the motion of its follower vehicles. This is equivalent to distance errors that are not amplified upstream from vehicle to vehicle in a vehicle string [33].

The stated condition is captured by the notion of strict string stability in the literature [20, 31, 33, 39]. Here, the most general definition of string stability is given in [33] and is hence employed in this work. The definition considers a state-space model of the vehicle string with N vehicles.[1] The homogenous vehicle string model (2.13) is a special, linear case of the following interconnected state-

---

[1]Note that $N \in \mathbb{N}$ can be any integer and the dynamics of different vehicles can be different in the general definition.

space system:

$$\dot{x}_r = f_r(x_r, u_r), \tag{2.18}$$

$$\dot{x}_1 = f_1(x_1, x_r, u_r), \tag{2.19}$$

$$\dot{x}_i = f_i(x_i, x_{i-1}), i = 2, 3, \dots, N, \tag{2.20}$$

$$y_i = h(x_i). \tag{2.21}$$

representing a general, possibly nonlinear, heterogeneous interconnected system with the same state relation structure as the model (2.13). Here, u_r is the external input signal of the reference leader vehicle, x_i is the state vector of each vehicle and y_i is the respective output signal for $i = 1, 2, \dots, N$. Note that, u_r in (2.19) might be dropped if u_r is embedded into A_r as part of the system state such that the reference input is moved in front of the spacing policy transfer function $1/H$ of Fig. 2.2. The overall state vector is written as $\begin{bmatrix} x_r & x_1 & x_2 & \cdots & x_N \end{bmatrix}^T$, where $\bullet^T$ denotes the transpose. Then, the general string stability definition starts from an equilibrium solution $\bar{x}$ for $u_r = 0$ of the system in (2.18) to (2.21). Two notions of string stability are defined as follows.

Definition 1 ($\mathscr{L}_p$ string stability)**.** *The system in* (2.18) *to* (2.21) *with the equilibrium solution $\bar{x}$ is*

1. *string stable if there exist class $\mathscr{K}$ functions α, β such that for any initial state x(0), any exogenous input signal $u_r \in \mathscr{L}_p$ and $i \in \{1, \dots, N\}$, it holds that*

$$||y_i - C_i \bar{x}||_{\mathscr{L}_p} \leq \alpha(||u_r||_{\mathscr{L}_p}) + \beta(||x(0) - \bar{x}||).$$

2. *strictly string stable if 1. holds and additionally for all $i \in \{2, \dots, N\}$ it holds that*

$$||y_i - C_i \bar{x}||_{\mathscr{L}_p} \leq ||y_{i-1} - C_{i-1} \bar{x}||_{\mathscr{L}_p}.$$

The string stability conditions can be explained as follows. 1. of Definition 1 considers the $\mathscr{L}_p$ norm of the output deviation from the equilibrium output for each vehicle. This deviation should be bounded by the $\mathscr{L}_p$ norm of the applied

input signal u_r (exogenous input) and the $\mathscr{L}_p$ norm of the deviation of the initial condition from the equilibrium point. In addition, strict string stability in 2. of Definition 1 requires that disturbances along a vehicle string are attenuated along the vehicle string. That is, the $\mathscr{L}_p$ norm of the follower deviation must be smaller than that of the predecessor.

The most relevant norms for the practical application of Definition 1 are the $\mathscr{L}_2$-norm and the $\mathscr{L}_\infty$-norm. Sufficient conditions for string stability are derived for both norms in the following sections.

2.3.2 Conditions for $\mathscr{L}_2$ String Stability using CACC

Now, we look at the case of the $\mathscr{L}_2$ norm where the energy content of a signal is measured. $\mathscr{L}_2$ string stability is defined such that the energy (represented by the $\mathscr{L}_2$ norm) of the output signal is not larger than the energy of the input signal [40]. Limiting the discussion to the case of linear systems and considering $\Gamma(s)$ is the frequency-domain equivalent of the $\mathscr{L}_2$-induced norm, then the conditions in Definition 1 can be simplified to operator norms. To this end, we use the transfer functions with the external input u to the vehicle, the acceleration a or the velocity v as relevant output signal for string stability. Next, we define the so-called string-stability transfer functions $\Gamma_{\eta,i}$ where $\eta \in u, a, v$. Assuming a linear system representation with input u or a or v of the preceding vehicle, we note that

$$\Gamma_i(s) = \frac{U_i(s)}{U_{i-1}(s)} = \frac{A_i(s)}{A_{i-1}(s)} = \frac{V_i(s)}{V_{i-1}(s)}. \tag{2.22}$$

for the transfer function between the control inputs of each preceding and follower vehicles. Hereby, $U_i(s)$ denotes the Laplace transform of the signal $u_i(t)$, $A_i(s)$ denotes the Laplace transform of the signal $a_i(t)$, $V_i(s)$ denotes the Laplace transform of the signal $v_i(t)$.

To this end, the model (2.15) is first formulated in the Laplace domain as follows:

$$Y_i(s) = P_i(s) U_i(s) + O_i(s) x(0), \tag{2.23}$$

13

with $x(0)$ denoting the initial (time-domain) condition, and $P_i(s) = C_i(sI - A)^{-1}B$ and $O_i(s) = C_i(sI - A)^{-1}$. $P_i(s)$ is the transfer function formulated in the Laplace domain, according to interconnected system reference input u_r and selected output depending on C_i.

Combining (2.22) and (2.23), by factorization, the string stability complementary sensitivity is

$$\Gamma_i(s) = P_i(s)P_{i-1}(s)^{-1}. \tag{2.24}$$

Here, it is assumed that, $P_{i-1}(s)^{-1}$ exists. The following theorem can now be stated.

Theorem 1 ($\mathscr{L}_2$ Stability)**.** *The system is $\mathscr{L}_2$ string stable if:*

1. *$||P_1(j\omega)||_{H_\infty}$ exists;*

2. *$||\Gamma_i(j\omega)||_{H_\infty} \leq 1, i = 2, 3, \ldots, N;$*

with $\Gamma_i(s)$ as in (2.24). $||\bullet||_\infty$ denotes the H_∞-norm.

A proof of Theorem 1 is given in [8]. When considering homogeneous strings and assuming that 1. in Theorem 1 is fulfilled by the plant, it must hold that

$$||\Gamma(j\omega)||_{H_\infty} \leq 1. \tag{2.25}$$

2.3.3 Conditions for $\mathscr{L}_\infty$ String Stability using CACC

Until now, only $\mathscr{L}_2$ string stability has been considered. As [33] suggested, physically, this can be motivated by the requirement of energy dissipation along the string. Obviously, the induced $\mathscr{L}_\infty$ norm can be used instead. In the scope of vehicle following, the motivation for using this norm would be traffic safety, since the $\mathscr{L}_\infty$ norm is directly related to maximum overshoot. The conditions for $\mathscr{L}_\infty$ string stability can be analogous with Definition 1. The difference is taking the $\mathscr{L}_1$ norm of string impulse response.

Theorem 2 ($\mathscr{L}_\infty$ Stability)**.** *The system is $\mathscr{L}_\infty$ string stable if*

1. $||p_1(t)||_{\mathscr{L}_1}$ *exists*

2. $||\gamma_i(t)||_{\mathscr{L}_1} \leq 1$.

$p_1(t)$ *and* $\gamma_i(t)$ *denote the impulse responses corresponding to* $P_1(s)$ *and* $\Gamma_i(s)$.

As [40] suggested, using $||\gamma(t)||_{\mathscr{L}_1}$ in the time-domain to obtain analytical results even in cases with relatively simple transfer functions can be quite difficult to analyze. Fortunately, it is possible to replace $||\gamma(t)||_{\mathscr{L}_1} \leq 1$ by sufficient conditions:

Corollary 1. *The system is* $\mathscr{L}_\infty$ *string stable if*

1. $||p_1(t)||_{\mathscr{L}_1}$ *exists*

2. $||\Gamma_i||_{H_\infty} \leq 1$

3. $\gamma_i(t) \geq 0$

That is, it is only required to check the H_∞ norm of $\Gamma_i(s)$ and to verify if the impulse response $\gamma_i(t)$ is non-negative.

In summary, $\mathscr{L}_2$ string stability is satisfied with proper controller synthesis in accordance with $||\Gamma_i(s)||_\infty \leq 1$. $\mathscr{L}_\infty$ string stability needs the additional condition of a non-negative impulse response. Although it is difficult to fulfill this condition by design, it turns out in this thesis that the used controllers automatically fulfill this condition. Regarding the practical meaning of both conditions, with $\mathscr{L}_2$ string stability, we only know that $||u_i||_2 \leq ||u_{i-1}||_2$. Concerning $\mathscr{L}_\infty$ string stability, we additionally know that $||u_i||_\infty \leq ||u_{i-1}||_\infty$.

There are various controller design methods for string stability using CACC. Considering the feedback loop in Fig. 2.2, a recent method suggests to use H_∞ controller synthesis [33]. The method is based on the requirement that

$$||\Gamma(s)||_\infty \leq 1. \tag{2.26}$$

In addition, [33] considers the closed-loop sensitivity as

$$S(s) = \frac{E_i(s)}{U_{i-1}(s)} = \frac{G(1 - DK_{ff})}{1 + GK_{fb}}. \tag{2.27}$$

In order to fulfill string-stability, (2.26) has to be fulfilled. At the same time, it is desired to minimize the position error $e_i(t)$. Hence, the H_∞ control problem

$$\min_K \left\| \begin{matrix} \Gamma(s) \\ S(s) \end{matrix} \right\|_\infty \leq 1 \tag{2.28}$$

is solved. Hereby, both the vehicle and the communication delay are described by Pade approximations, yielding a sufficiently accurate phase in the frequency interval of interest. The lower fractional transformation (LFT) and the corresponding matrix P are shown in Fig. 2.4.

$$P = \begin{bmatrix} 0 & \dfrac{1}{H} \\ G & -G \\ D & 0 \\ G & -G \end{bmatrix}$$
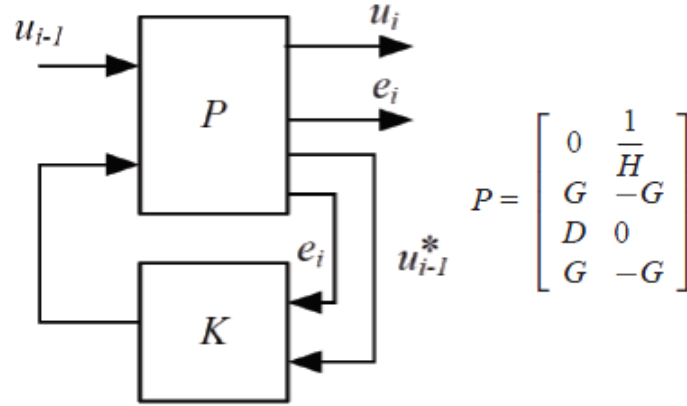
Figure 2.4: H_∞ control design for CACC.

In this thesis, we generally use H_∞ computations for LTI plants. The input u_{i-1} is an exogenous input representing the disturbance acting on the system. The output u_i and e_i are outputs of the system, whose dependence on the exogenous input u_i which we want to minimize. The outputs are the measurements we make on the system which we shall use to choose our input e_i, which in turn is the tool we have to minimize the effect of u_{i-1} to u_i and e_i. At the same time, we do not want the states to become too large while we try to regulate our performance. The effect of u_{i-1} on u_i after closing the loop is measured in terms of the energy attenuation and the worst disturbance u_{i-1} in accordance with our $\mathcal{L}_2$ string stability criteria. Moreover, in line with the $\mathcal{L}_2$ string stability condition, the H_∞ norm of

the transfer function Γ should be less or equal to a bound value, 1. In particular, the function of Matlab/Simulink **hinfsyn** is applied to minimize the infinity norm in (2.28) while obtaining a stable feedback loop in Fig. 2.2. The partitioned plant P in analogy to [33] is used for this purpose.

2.4 Simulations for CACC with String Stability Conditions

Our simulation platform is based on MATLAB/SIMULINK to evaluate the performance of CACC for homogenous vehicle strings. Heterogeneous strings under CACC are explicitly studied in [41]. An example experiment is accomplished for 7 vehicles as shown in Fig. 2.5. In order to quantify values of τ_i, we refer to prac-
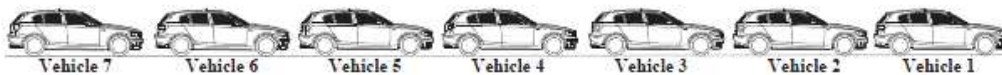
Figure 2.5: Vehicle string with 7 vehicles.

tical experiments in [26], where a value of $\tau \approx 0.4$ is obtained. That is, we choose $\tau_i = 0.4$ for each vehicle, assume wireless communication time delay $\theta = 0.02$s. and design K according to (2.28). The string stability complementary sensitivity $\Gamma_i(s) = \Gamma(s)$ (independent of i) is illustrated in Fig. 2.6 where (2.26) is satisfied.
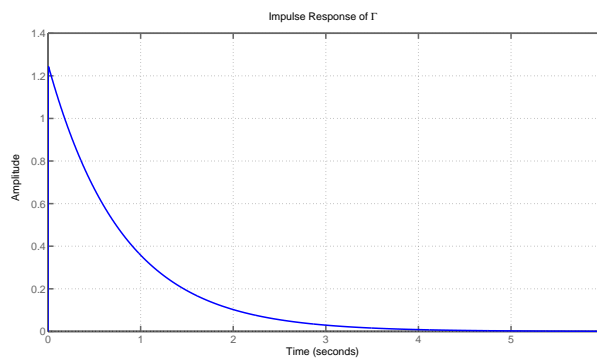
Figure 2.6: Impulse response of Γ.
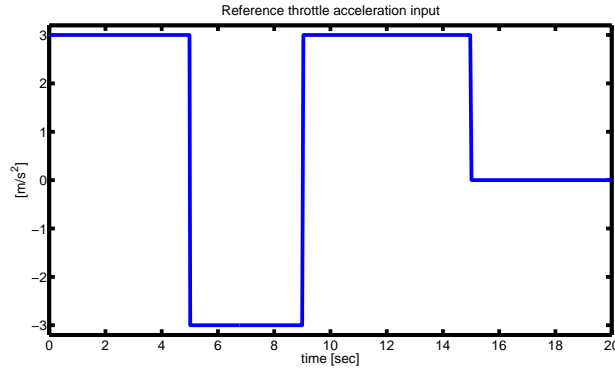
Figure 2.7: Input signal u_r of the leader reference vehicle.

In our simulation, the leader vehicle is provided with the input signal in Fig. 2.7. That is, sharp accelerations of $3\,\text{m/s}^2$ and $-3\,\text{m/s}^2$ are given in order to study a difficult vehicle following scenario. The simulation result is shown in Fig. 2.8. It can be seen from the vehicle positions that each vehicle follows its predecessor at a safe distance. In addition, the velocity and acceleration plot suggest that the disturbance provided by the input signal is attenuated along the string (the respective signal amplitudes decrease along the string). That is, strict string stability is confirmed.

In contrast, string stability is violated in the scenario of Fig. 2.9. After changing the communication delay to $\theta = 0.5$s., performing the same maneuver of the leader vehicle 1, it now holds that the acceleration and velocity of the follower vehicles are amplified which is clearly undesirable. This is very similar scenario of ACC where this method is always criticized as creating traffic jams. It is evident that the signals of vehicle 2 (which is represented by the green line) are amplified compared to its predecessor vehicle 1 (which is represented by the blue line) and each vehicle follows its predecessor vehicle with amplification. In addition the position plot (left-upper side) shows that the vehicles follow each other at an extremely unsafe distance.
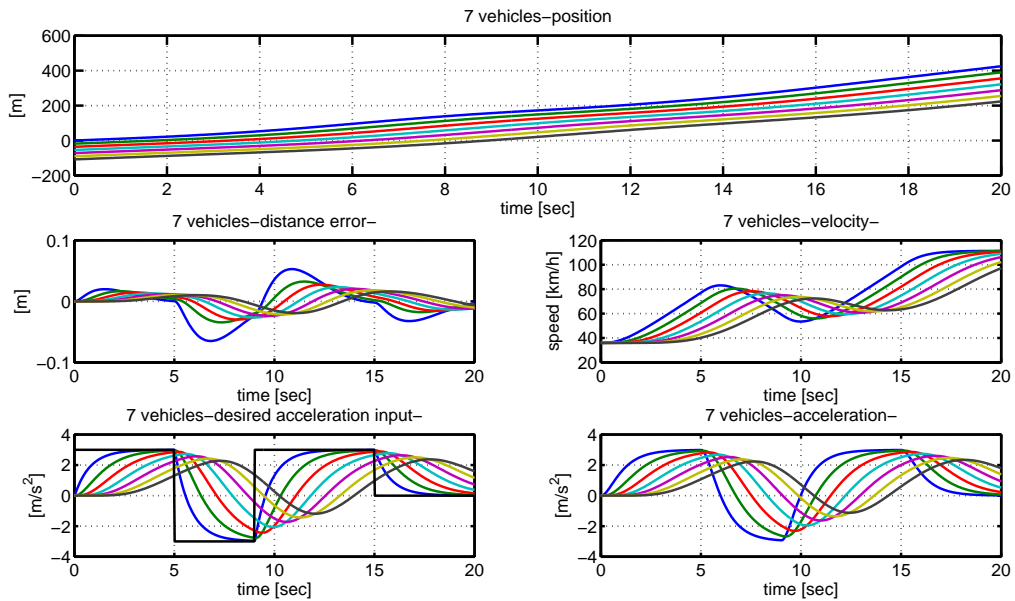
Figure 2.8: Vehicle string with 7 homogenous vehicles performing an acceleration/deceleration maneuver and CACC design that fulfills $\mathscr{L}_\infty$ strict string stability. Each line represents the motion of one vehicle.
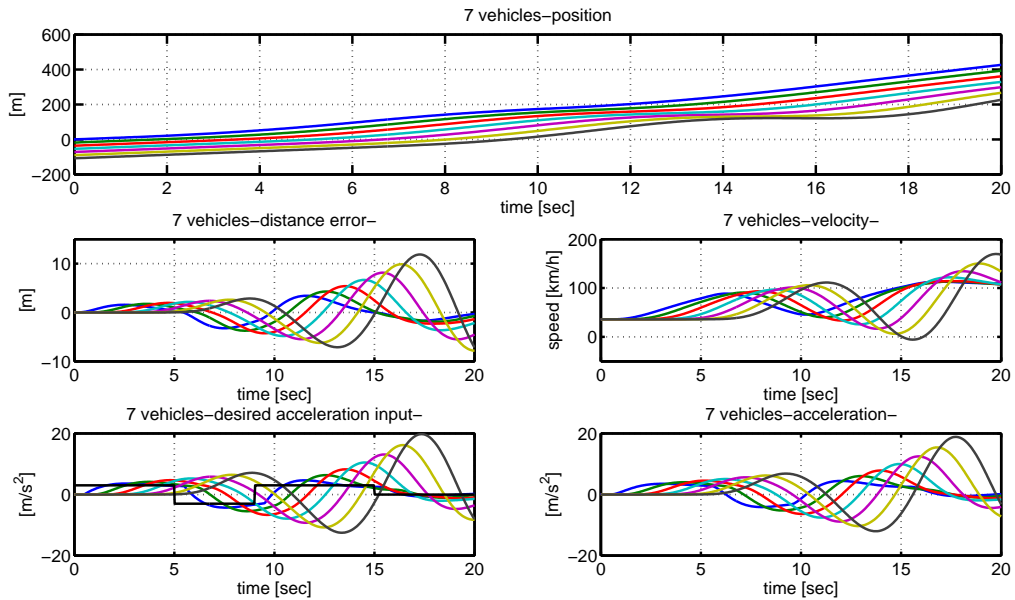
Figure 2.9: Vehicle string with 7 homogenous vehicles performing an acceleration/deceleration maneuver and CACC design that violates $\mathscr{L}_\infty$ strict string stability. Each line represents the motion of one vehicle.

CHAPTER 3

LANE CHANGE MANEUVERS IN VEHICLE STRINGS

This chapter considers the different phases during a lane change. Section 3.1 gives a general description of lane change maneuvers. The completion of a lane change and initiation of a lane change are addressed in Section 3.2 and 3.3, respectively. A first result regarding the effect of multiple lane changes is derived in Section 3.4.

3.1 Lane Change Maneuver Description

The main motivation of this part of the thesis is the combination of results on string-stability and the possibility of lane changes. To this end, we developed a protocol for lane change between at most 3 vehicles. The basic idea is illustrated in Fig. 3.1.

The lane change maneuver consists of the following sequential steps

1. Request of vehicle B to vehicle A (Fig. 3.1 (a)),

2. Vehicle A generates a sufficient gap for vehicle B (Fig. 3.1 (b)),

3. Vehicle B performs the lateral motion into the gap and notifies vehicle E when the lateral motion is completed (Fig. 3.1 (c)),

4. Vehicle E closes the gap to vehicle D (Fig. 3.1 (d)).

Hereby, it is important to note that steps 1 and 3 require communication among the vehicles and steps 2 and 4 involve changes in the longitudinal motion on different lanes. That is, the planning of the desired vehicle trajectories for these actions without adverse effects on string stability is of utmost importance. Fig. 3.1 (a)-(b)
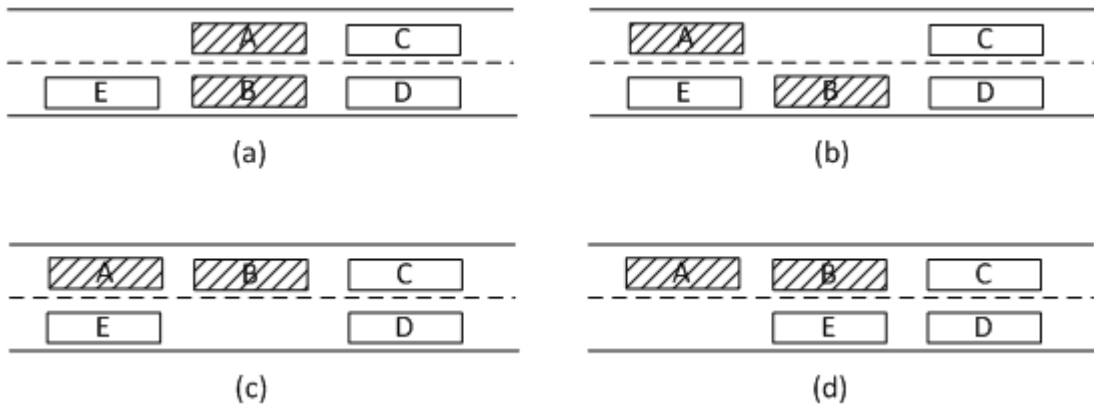
Figure 3.1: Protocol for lane changes: (a) Initial situation, (b) Gap generation,(c) Lane change, (d) Final approach.

describe the phase of initiating a lane change (gap opening). (c) is the phase of completing lane change. Finally, (d) is the phase of final approach (gap closing).

An important topic on multi-lane highways is the possibility of lane changes and their effect on the traffic flow. Usually, lane changing is motivated by merging behavior at on-ramps or off-ramps, bottlenecks and spontaneous driver decision depending on the traffic situation and the desired speed. Throughout our study we have focused on lane changes of particular vehicles, more on the microscopic models. Here, the main idea to study lane-changing behavior is to develop a lane-changing rule set depending on the headway difference, velocity difference, safety distance.

The recent literature [9, 13, 33, 42, 43] considers the longitudinal control of vehicles so as to maintain string-stability of a platoon of vehicles based on CACC. As a result, large fluctuations in the vehicle flow are avoided. As a shortcoming of the approaches on CACC, it has to be noted that these approaches are formulated for car motion on a single lane. That is, lane-changes of vehicles are not captured. This thesis focuses on the effect of lane changes and we have investigated the longitudinal motion during lane changes in detail. The vehicles affected by a lane change maneuver are all the followers.

Moreover, various studies in the literature focus on the effect of lane changes

on multi-lane highways. For example, the works in [44, 45, 46] provide different models of the lane-changing process of human drivers and conduct extensive simulations. The main focus of these studies is the validation of traffic flow models that include lane changing behavior based on empirical data. Although such studies potentially enable the analysis of different traffic situations incorporating human drivers, they do not include possible improvement of traffic flow by control. Research on the control of lane changes is performed for the particular situation of lane changing due to merging at on-ramps [47, 48, 49, 50, 51, 52]. These research works propose different strategies for the pre-computation of vehicle trajectories in order to enable safe merging without collisions. However, none of the existing approaches includes an investigation of string-stability when performing merging maneuvers.

Besides all, safety is the main important fact that after any number of lane changes vehicle following safety margins should not be violated. Therefore, the gap opening, lane change completion and gap closing phase should all be calculated for error accumulations.

3.2 Completing a Lane Change

3.2.1 Maneuver Description

The existing methods in [13, 33] focus on fluctuations in the case where a string is already formed. [53] focuses on CACC based lane change design of interaction protocols, which mimic the driver interactions as much as possible. However, the effect of modifying a vehicle string by adding or removing one or multiple vehicles after a lane change is not included in the discussion. We next consider this problem in the framework developed in this thesis.

To this end, we analyze a lane change maneuver of vehicle i in Fig. 3.2. Before the lane change, vehicle $i+1$ should follow vehicle $i-1$ at a distance $2 d_{i,r}$ in order to provide a sufficient gap for vehicle i to enter the lane. Using the CACC design in Section 2.1, the motion of vehicle $i+1$ depends on the distance measurement $q_{i-1} - q_{i+1} - L_{i+1}$. After the lane change, vehicle $i+1$ should follow vehicle i at
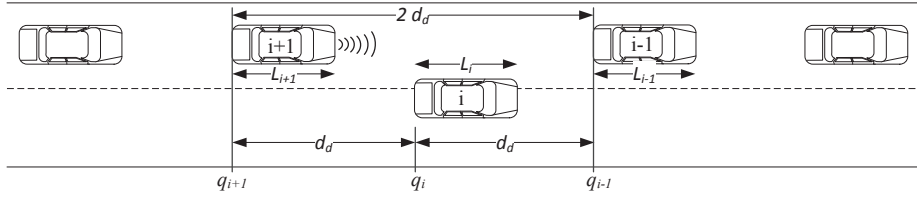
Figure 3.2: Lane change scenario in a vehicle string.

the distance $d_{i,r}$ and now uses the distance measurement $q_i - q_{i+1} + L_{i+1}$. That is, the distance measurement of vehicle $i+1$ switches from vehicle $i-1$ before the lane change to vehicle i after the lane change.

Assuming that vehicle i enters the gap precisely at the desired distance $q_{i-1} - q_i = d_{i,r}$ such that also $q_i - q_{i+1} = d_{i,r}$, the lane change does not generate any disturbance for the motion of the vehicle string. Nevertheless, in practice, an imprecise positioning of vehicle i after the lane change is to be expected. That is, a jump from $2d_{i,r} - (q_{i-1} - q_{i+1})$ to $d_{i,r} - (q_i - q_{i+1})$ in the distance error measurement is observed from the perspective of vehicle $i+1$.

Additionally, in accordance with the model (2.11), there can be jumps in velocity and acceleration also. Vehicles are assumed to be coordinated by intelligent road steering units and as expected from any sensor and control systems, their speed measurement v_i or acceleration a_i control may have errors practically at any time.

3.2.2 Simulation Experiment Validation

Noteworthy is the observation that the main effect of switching is a state jump when a vehicle joins or disappears. This can be modeled by an input impulse $\delta(t)$ with an appropriate input vector. For example, consider a state jump of the error $e_2(t)$ of vehicle 2. This corresponds to an input impulse with input vector $b_2 = \begin{bmatrix} 0 & \cdots 0 & 1 & 0 & \ldots & 0 \end{bmatrix}^T$ where the 1 is at the position of the error state e_2. This means that we want to study the impulse response for each such impulse input and the possible error jumps.

We know that the impulse response can be computed as the inverse Laplace

transform of the corresponding transfer function. Hence, we evaluate the transfer function from the impulse input to the relevant output signals (for example impulse at e_2 and effect on e_2, v_2, a_2, u_2, e_3, v_3, etc.).
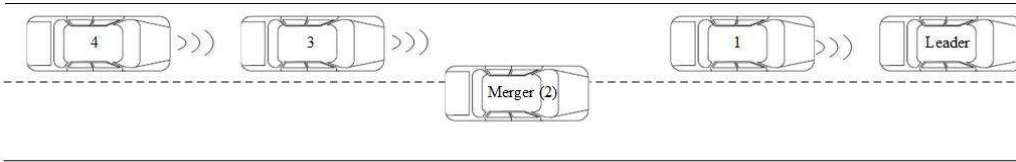
Figure 3.3: Lane change scenario in a vehicle string.

Focusing on a single vehicle merge scenario as illustrated in Fig. 3.3, second vehicle enters in a very aggressive manner such that position error of $3m$, velocity error of $3m/s$ and acceleration error of $1m/s^2$. Initial velocity is $10m/s$ and desired following distance is $v_0 \cdot h + r = 10 \cdot 0.8 + 5 = 13m$. An error of more than $4m$ is observed in Fig. 3.4 such that the safety distance for vehicle following may be violated due to human reaction time in an emergency situation.
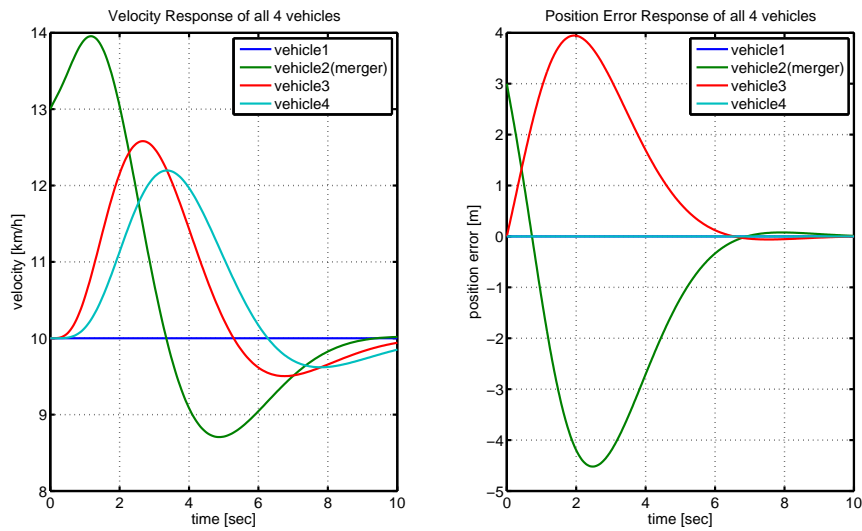
Figure 3.4: Single vehicle merging into second($i = 2$) position with errors.

In another scenario, it is assumed that the merger vehicle enters into the first position following the leader. Selection of first vehicle employing the closed-loop

controller, enables us to observe the worst-case scenario of the whole string.
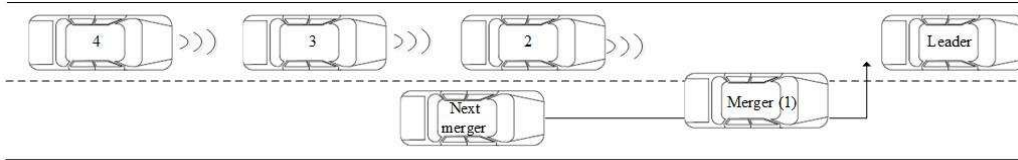
Figure 3.5: Vehicle merge scenario into first ($i = 1$) position of the string.

Then, for our next scenario in Fig. 3.5, merger vehicles enter to the first position of string following each other for a given time interval 10sec, in other words $t = 0, 10, 20, 30, 40, 50$. In each merging maneuver, an acceleration error of $1 m/s^2$ is given and the distance error and acceleration of each vehicle is observed in Fig. 3.6
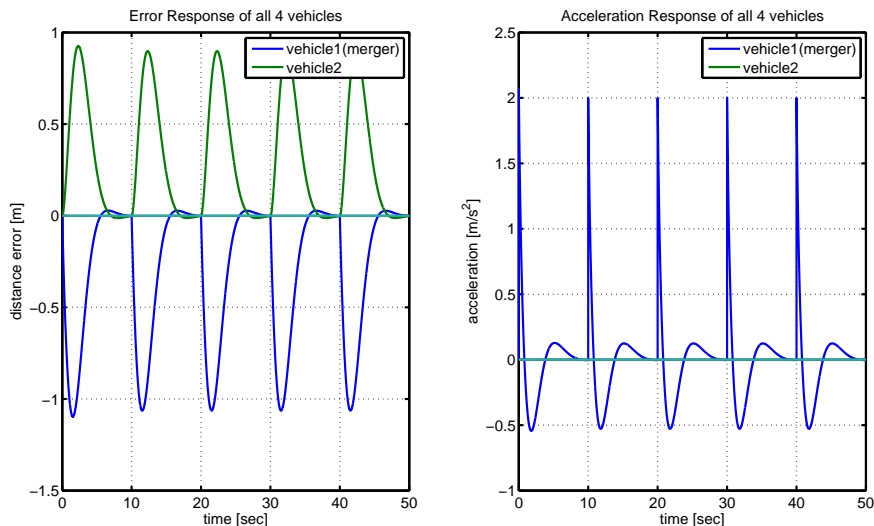
Figure 3.6: Repeated vehicle merging into leader position with 10sec time interval and acceleration errors. The responses of vehicle $3, 4$ and 5 are not illustrated because they are near to zero due to string stable design.

Now, the duration between each merge is shortened as 4sec, in other words for 48sec., at $t = 0, 4, 8, ..., 48$ new vehicle merges into the first position of hte string. The interesting result here is that, even we apply many impulses for very short times, the output signal remains bounded/limited and acceptable in practice.

From the string stability definition, norm of each disturbance might be expected to be added cumulatively, e.g. for a number of k impulse inputs, k times the norm of jump could be expected. However, due to the time evolution of the signals, the superposition of each output is added up after a significant decay of the respective signal. This bound can only be observed after simulation as given in Fig. 3.7 and needs an analytical evaluation.
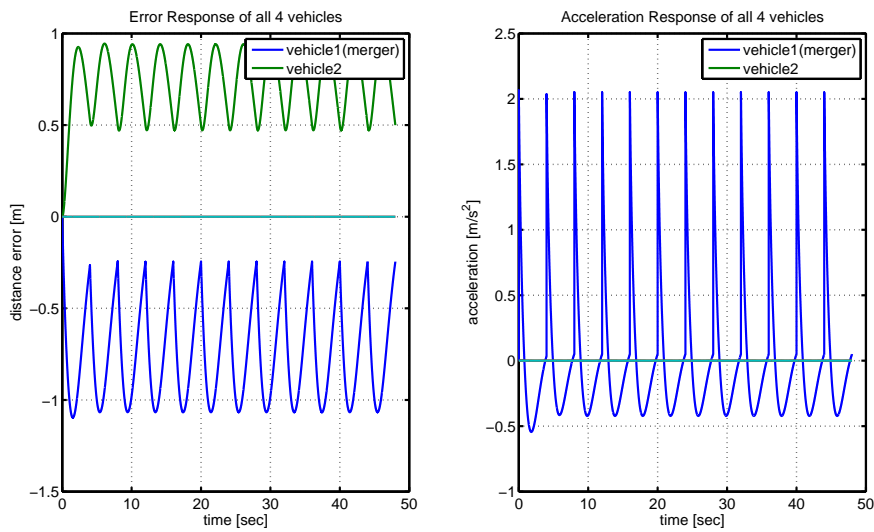
Figure 3.7: Repeated vehicle merging into leader position with 4sec time interval and acceleration errors.

When both Fig. 3.6 and 3.7 are compared, a bound will be computed analytically which we will define in Chapter 4 and 5.

3.2.3 Model

In this section, the particular interconnection structure of the vehicle string is derived. First, we only need to consider vehicles that enter after the leader vehicle $i = r$, illustrated in Fig. 3.5. Hence, we do not need to look at the full model but only the part of the model starting from vehicle $i = 1$. Here, a state jump of any

vehicle and output at any vehicle is modeled as

$$
\begin{bmatrix} \dot{x}_1 \\ \dot{x}_2 \\ x_3 \\ \vdots \\ \dot{x}_{n-1} \\ \dot{x}_n \end{bmatrix} = \begin{bmatrix} A_0 & 0 & 0 & \cdots & 0 & 0 & 0 \\ A_1 & A_0 & 0 & \cdots & 0 & 0 & 0 \\ 0 & A_1 & A_0 & \cdots & 0 & 0 & 0 \\ \vdots & \ddots & \ddots & \ddots & \vdots & \vdots & \vdots \\ 0 & 0 & 0 & \cdots & A_1 & A_0 & 0 \\ 0 & 0 & 0 & \cdots & 0 & A_1 & A_0 \end{bmatrix} x + \begin{bmatrix} B_1 \\ B_2 \\ B_3 \\ \vdots \\ B_{n-1} \\ B_n \end{bmatrix} \delta(t) \qquad (3.1)
$$

$$
y_i = \begin{bmatrix} 0 & C_i & 0 & \cdots & 0 & 0 & 0 \end{bmatrix} x. \qquad (3.2)
$$

We next evaluate the case of more than one input or the combined input scenario which represents a simultaneous or asynchronous error and velocity jump in a single or more than one vehicle. This scenario changes the input matrix B as follows:

$$
\begin{bmatrix} B_1 & 0 & 0 & \cdots & 0 & 0 \\ 0 & B_2 & 0 & \cdots & 0 & 0 \\ 0 & 0 & B_3 & \cdots & 0 & 0 \\ \vdots & \ddots & \ddots & \ddots & \vdots & \vdots & \vdots \\ 0 & 0 & 0 & \cdots & B_{n-1} & 0 \\ 0 & 0 & 0 & \cdots & 0 & B_n \end{bmatrix} \begin{bmatrix} u_1 \\ u_2 \\ u_3 \\ \vdots \\ u_{n-1} \\ u_n \end{bmatrix} \qquad (3.3)
$$

3.2.4 Multiple Lane Changes

We would like to analyze the effect of multiple lane changes of different vehicles in the string. Accordingly, the jump in any parameter error after a lane change at a time can be represented by the impulse input δ. The effect is observed in the output signal $y_i(t)$. Moreover, $k+1$ lane changes in front of vehicle $i+1$ at defined times $t_0, t_1, \ldots, t_k$ in the input directions $v_0, v_1, \ldots, v_k$ are represented by the input signal $\sum_{v=0}^{k} \delta(t - t_v) v_v$. It has to be noted that the removal of a vehicle from a vehicle string follows the same line of argument. That is, we identified the problem of applying repeated impulse inputs to a linear time invariant system in

order to represent the integration of multiple vehicles in or removal of multiple vehicles from a vehicle string.

Assuming that the v-th impulse can be applied in an arbitrary input direction $v_v \in \mathbb{R}^p$, the successive application of input signals $u_v = \delta(t - t_v)v_v$ for a given time sequence $(t_v)_{v=0}^{\infty}$ is represented by the signal

$$u_{(t_v)_{v=0}^{\infty}}(t) = \sum_{v=0}^{\infty} \delta(t - t_v)v_v. \tag{3.4}$$

In this expression, impulse input signal u_v is applied at time t_v.

3.3 Initiating-Preparing Lane Change

3.3.1 Maneuver Description

The vehicle string, CACC, stability and control structure was explained in Chapter 2. In addition to normal driving conditions for the string, it is trivial that some vehicles would like to leave or merge into the string. Then, gaps between vehicles have to be opened or closed if vehicles want to enter or leave an existing platoon as illustrated in Fig. 3.8 (a)-(b). Here, vehicle i at position q_i opens a gap to vehicle $i-1$ such that the new vehicle N can safely enter the platoon.

As discussed in Section 3.2.2, additional maneuvers causing state jumps can have a negative effect on vehicle following. Similarly, it is expected that maneuvers such as opening/closing gaps have an effect on the follower vehicles. Closing gaps in vehicle strings that are already formed are investigated in [54]. They analyzed two controllers, one to manage the approaching maneuver to the leading vehicle and the other to regulate car-following once the vehicle joins the platoon. However, they have not considered a gap opening creating less disturbance for the string. Moreover, [55] explains the effect of opening gaps on traffic flow stability. Analyzing different scenarios for opening multiple gaps in a vehicle string, it is concluded that gaps should not be opened simultaneously in order to avoid traffic breakdown. Hence, they propose a method to schedule the maneuvers for opening gaps while keeping the traffic throughput high. This schedule is directly related
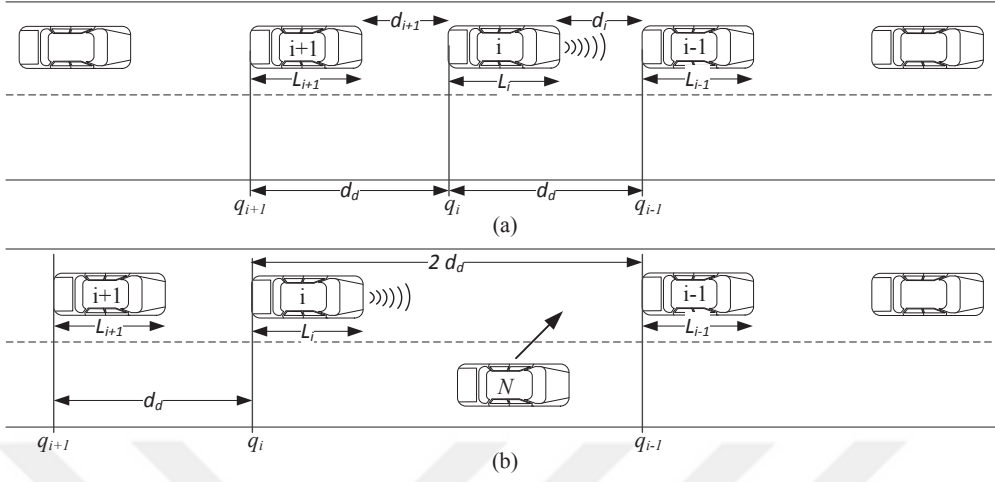
Figure 3.8: Vehicle Platoon: (a) vehicle following; (b) gap opening for preparing a lane change.

with our dwell-time findings for multi-merge and leave scenarios. To the best of our knowledge, [55] is the first method for the feedforward design for opening gaps and the scheduling of lane change maneuvers.

In our setting of initiating or preparing lane changes, we also extend the general design by an additional feedforward input signal as an exogenous input u_i^{ff} similar to [55] as depicted in Fig. 3.9. This input signal provides a means to adjust the vehicle position for opening gaps as described in Fig. 3.9. In order to preserve the possibility of safe following, we also introduce the feedforward reference distance q_i^{ff}, whereby q_i^{ff} and u_i^{ff} are computed such that

$$Q_i^{\mathrm{ff}}(s) = G(s) U_i^{\mathrm{ff}}(s).$$

The feedback loop for vehicle following is not affected by the application of u_i^{ff} since the desired distance signal is adjusted according to the applied input u_i^{ff}. As a consequence, when applying u_i^{ff} for opening a gap, vehicle i keeps following vehicle $i-1$ but at an increasing distance.

Since this input signal is used together with the CACC design for vehicle following, the important property of string stability is preserved. Computation of

29
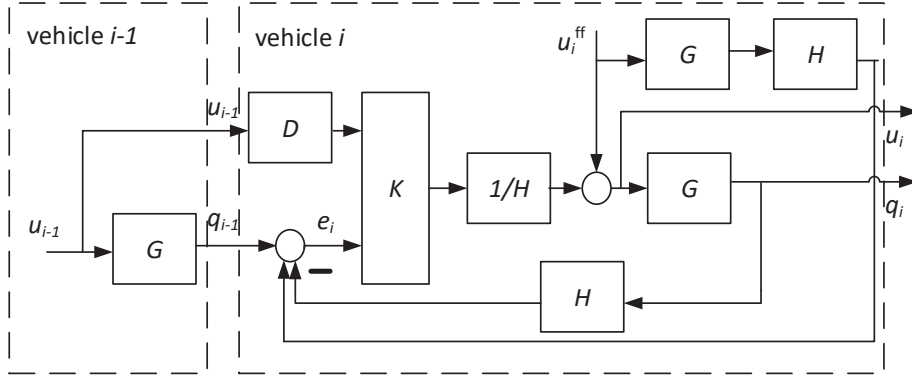
Figure 3.9: Feedforward loop for each vehicle.

feedforward input signal is explicitly defined in [55] and assumed to exist in this study. In summary, gap opening/closing feedforward vehicle following is realized by the CACC architecture of Fig. 3.9

Vehicle $i+1$ follows vehicle i assuming that both vehicles have the same plant transfer function G. Vehicle $i+1$ receives the control signal u_i^{ff} via a filter transfer function K_{ff} from the predecessor vehicle by vehicle-to-vehicle communication. Here, D represents a potential communication delay.

An example signal for closing a gap within 10 s is shown in Fig. 3.10. It has to be noted that, while u_i^{ff} is computed for the maneuver of vehicle i, there is an effect on the distance error e_{i+1} of the follower vehicle $i+1$ via the stable transfer function

$$\frac{E_{i+1}(s)}{U_i^{\text{ff}}(s)} = \frac{G - DK_{\text{ff}}G}{1 + K_{\text{fb}}G}. \tag{3.5}$$

Here, E_{i+1} and U_i^{ff} are the Laplace transforms of e_{i+1} and u_i^{ff}, respectively. This effect is small when closing a single gap as can be seen in Fig. 3.10.

3.3.2 Simulation Experiment Validation

Now, we would like to compare gap opening and closing responses of the vehicle string with and without the feedforward signal. The string is depicted in Fig.
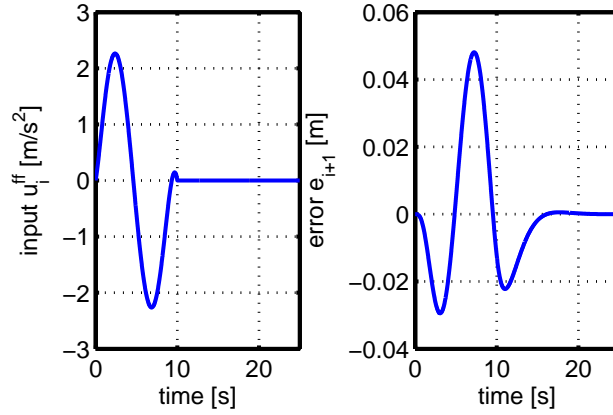
Figure 3.10: Input and error signal when closing a gap.

3.8 where the ith vehicle opens the gap for entrance of vehicle N. In both scenarios, 6 vehicles simulation is given. Initial velocity for the vehicle platoon is 20 m/s. Vehicle lengths are 5 m and the bumper distance is assumed 10 m. Headway constant is taken as 0.8. Thus, the overall following distance evaluates as $0.8 \cdot 20 + 10 + 5 \, \text{m} = 31 \, \text{m}$. In this scenario vehicle $i-1$ is additionally analogous to Vehicle C of 3.1. Entering/Leaving Vehicle is Vehicle B and vehicle i is Vehicle A. The others are successive follower vehicles in the platoon.

Option 1: No feedforward (step reference change)

First, as illustrated in Fig. 3.11, simulation starts with gap generation maneuver of vehicle i. At time=4 sec, a new vehicle (green) enters the string. After that, at time=8 sec, the same vehicle (green) leaves the string and vehicle i starts to close the gap. Just after the gap is closed, a gap open maneuver at time=12sec starts. At time=16sec, the new vehicle once again enters and the string continues to drive.

The simulation is very widely analogous to real life situation that in dense traffic conditions people frequently enter and leave a string. That is, the realistic case of a lane change occurring every 4 sec is simulated. The crucial observation here is that the acceleration maneuvers done by vehicle i is not logical. Accelerations around $20 m/s^2$ with the relevant velocities are not feasible for current

31
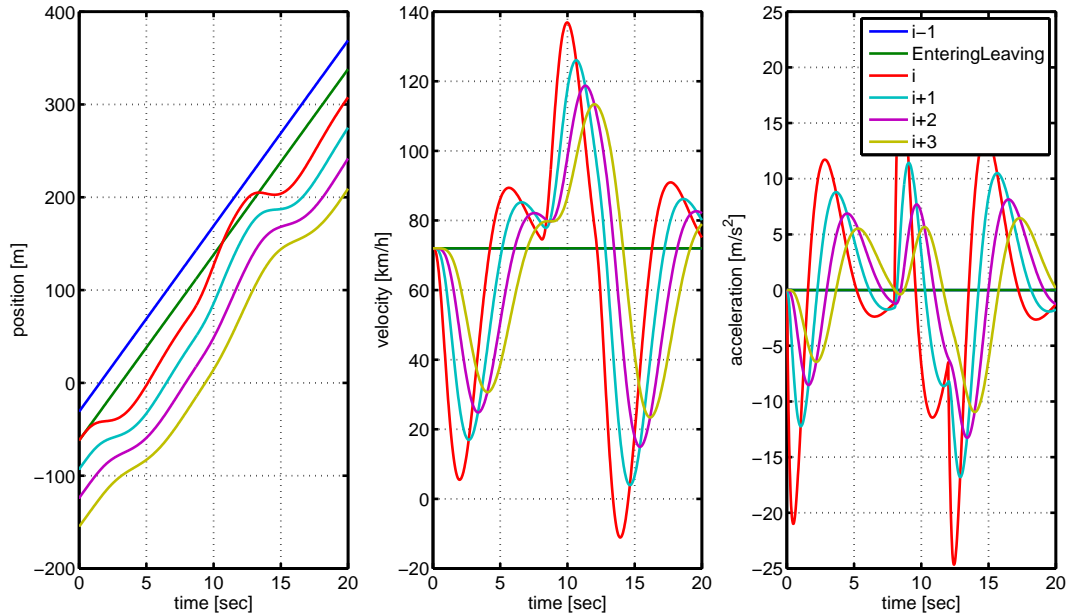
Figure 3.11: Realizations of Gap Opening/Closing without Feedforward Input Signal

vehicles on the road. Physical limitations, e.g. actuator saturation is discussed in [56]. Additionally, as we consider accelerations of about $2-3\,m/s^2$ as comfort limit for human passengers while very sudden jump from $70\,km/h$ velocity reaching $140\,km/h$ is not comfortable, that makes this scenario both not logical and practical. Hence, this fact supports the usage of a feedforward input as will be illustrated next.

Option 2: Computed feedforward signal for Gap Open/Close

Second, as illustrated in Fig. 3.12 we apply the gap opening scenario with feedforward input. Formulation of optimal control problem was addressed explicitly in [57]. In this simulation gap open maneuver starts at $time = 2\,\text{sec}$. This maneuver continues until $time = 12\,\text{sec}$, after then vehicles approach their normal following positions with identical velocities. As observed from acceleration of each vehicle the response of each vehicle is acceptable and comfortable for human passengers.
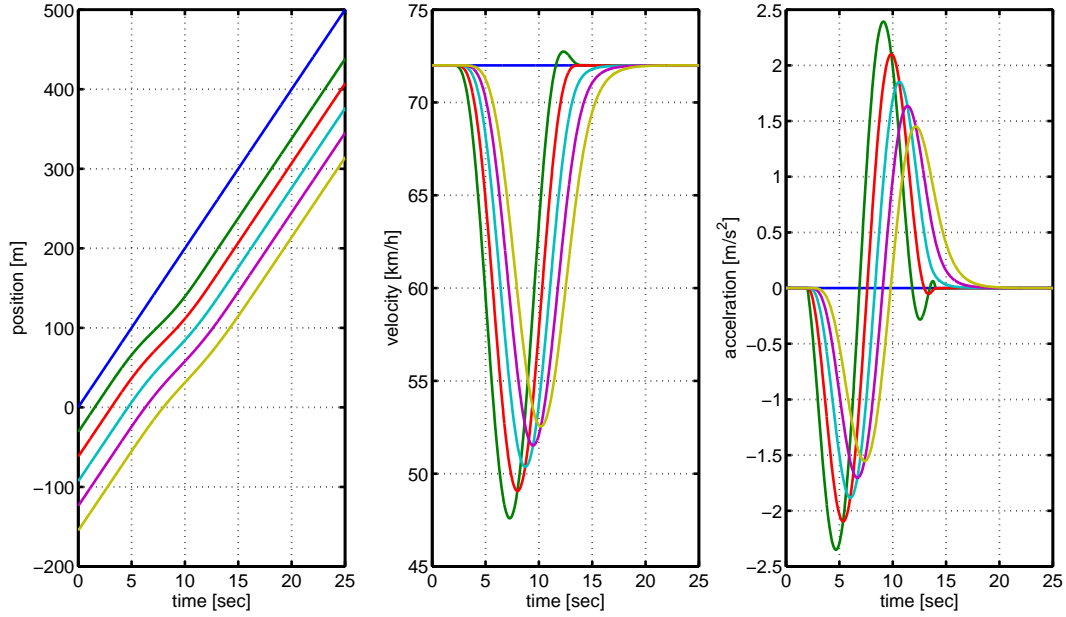
Figure 3.12: Realizations of Gap Opening/Closing with Feedforward Input Signal

3.3.3 Model

The model is the same for *A* matrix of (2.15). Here, gap opening or closing input on any vehicle is selected by B_i and the output at any vehicle is modeled as

$$
\begin{bmatrix} \dot{x}_r \\ \dot{x}_1 \\ \dot{x}_2 \\ x_3 \\ \vdots \\ \dot{x}_{n-1} \\ \dot{x}_n \end{bmatrix} = \begin{bmatrix} A_r & 0 & 0 & 0 & \cdots & 0 & 0 & 0 \\ A_{1,r} & A_0 & 0 & 0 & \cdots & 0 & 0 & 0 \\ 0 & A_1 & A_0 & 0 & \cdots & 0 & 0 & 0 \\ 0 & 0 & A_1 & A_0 & \cdots & 0 & 0 & 0 \\ \vdots & \ddots & \ddots & \ddots & \vdots & \vdots & \vdots & \\ 0 & 0 & 0 & 0 & \cdots & A_1 & A_0 & 0 \\ 0 & 0 & 0 & 0 & \cdots & 0 & A_1 & A_0 \end{bmatrix} x + \begin{bmatrix} B_r \\ B_1 \\ B_2 \\ B_3 \\ \vdots \\ B_{n-1} \\ B_n \end{bmatrix} u(t) \quad (3.6)
$$

$$
y_i = \begin{bmatrix} 0 & C_i & 0 & \cdots & 0 & 0 & 0 \end{bmatrix} x. \quad (3.7)
$$

We next evaluate more than one input or combined input scenario which represents simultaneous or succeeding gap open or close maneuvers for single or more

33

than one vehicle. This scenario changes the input vector B as follows:

$$
\begin{bmatrix}
B_1 & 0 & 0 & \cdots & 0 & 0 \\
0 & B_2 & 0 & \cdots & 0 & 0 \\
0 & 0 & B_3 & \cdots & 0 & 0 \\
\vdots & \ddots & \ddots & \ddots & \vdots & \vdots \\
0 & 0 & 0 & \cdots & B_{n-1} & 0 \\
0 & 0 & 0 & \cdots & 0 & B_n
\end{bmatrix}
\begin{bmatrix}
u_1 \\
u_2 \\
u_3 \\
\vdots \\
u_{n-1} \\
u_n
\end{bmatrix}
\tag{3.8}
$$

3.3.4 Multiple Gap OpeningClosing

Single vehicle and reference vehicle models are given in (2.11)-(2.12). Vehicle string was, in lumped form, denoted by (2.15) with $A \in \mathbb{R}^{n \times n}$ state matrix and $n = N \times 8 + 3$ due to our specific plant model and controller synthesis, $B \in \mathbb{R}^{n \times k}$ input matrix having k inputs. $C_i \in \mathbb{R}^{q \times n}$ output matrix having q outputs.

Since (2.15) describes a controlled system, the matrix A_0 is typically Hurwitz. However, this may not be the case for the matrix A_r, related to the leader reference vehicle in case of vehicle following. As indicated by (2.12), for instance, A_r has a marginally stable mode associated with v_0. Hence, the system matrix A in (2.11) is not Hurwitz. For our analysis, we remove the poles at zero (marginally stable modes) by a specific choice of similarity transformation by $T^{-1}AT$, $T^{-1}B$, CT for A, B and C respectively where system transfer function remains unchanged. After the transform, now state matrix has two less states where we can call as $n - 2$.

We next evaluate the scenario of more than one input or multiple inputswhich may be due to dynamic conditions of the string where several vehicles may enter and exit consecutively.

We formally introduce the set of input signals with time-limit $t_1 < \infty$ as

$$
\mathscr{U}_{t_1} = \{u : \mathbb{R} \to \mathbb{R}^p | u(t) = 0 \text{ for } t < 0 \text{ and } t > t_1\}. \tag{3.9}
$$

Then, the successive application of an input signal $u \in \mathscr{U}_{t_1}$ for a given time
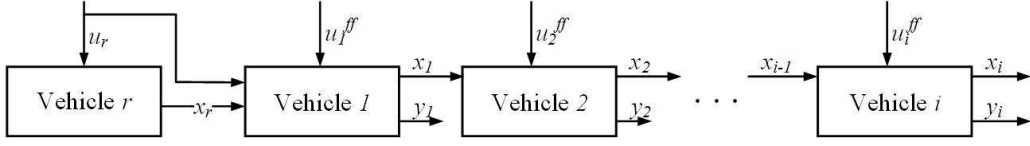
Figure 3.13: Vehicle String with additional exogenous inputs

sequence is represented by the signal

$$u_{(t_v)_{v=0}^{\infty}}(t) = \sum_{v=0}^{\infty} u(t - t_v).$$ (3.10)

3.4 Extended String Stability

String stability notion is first explained in Section 2.3. When a disturbance occurs at the beginning of the string it should not grow or amplify while propagating through the string. In the extended case now, there are exogenous input signals from any vehicle in addition to impulses (state jumps) which should not be amplified along the string.

As described in (3.4), the error introduced when switching between leader vehicles affects the motion of the follower vehicles and needs to be quantified. Hereby, the impulse signal is assumed to be composed of multiple impulses in the following form

$$w_i = \sum_{j=1}^{N_i} r_{ij} \delta(t - t_{ij})$$ (3.11)

r_{ij} represents the weight of the $j-$th impulse and t_{ij} represents the time of the $j-$th impulse applied to vehicle $i = 1, \ldots, N$. Note that an initial condition $x_{i,0}$ of vehicle i can be represented by an impulse input with weight $r_{i0} = x_{i,0}$ and at the time $t_{i1} = 0$.

Using the control architecture in Fig. 3.9, we extend the string stability conditions in Definition 1 to the case of vehicle strings with additional exogenous inputs and error impulses as depicted in Fig. 3.13. In this system, each vehicle is affected by maneuvers of all its predecessor vehicles. To this end, we reformulate

35

the state space model in (2.18) to (2.21) using u_i^{ff} and w_i for $i = 1, \ldots, N$:

$$\dot{x}_1 = f_1(x_1, u_1^{\text{ff}}) + w_1, \tag{3.12}$$

$$\dot{x}_i = f_i(x_i, x_{i-1}, u_i^{\text{ff}}) + w_i, i = 2, 3, \ldots, N, \tag{3.13}$$

$$y_i = h(x_i). \tag{3.14}$$

Definition 2. *Consider the vehicle string in Fig. 3.13 with the exogenous inputs u_i^{ff} and error impulses w_i for $i = 1, \ldots, N$ and the corresponding state space model in (3.12) to (3.14). Let $x = \begin{bmatrix} x_r^T & x_1^T & \cdots & x_N^T \end{bmatrix}^T$ be the lumped state vector and let $\bar{x} = \begin{bmatrix} \bar{x}_r^T & \bar{x}_1^T & \cdots & \bar{x}_N^T \end{bmatrix}^T$ denote the constant equilibrium solution for $u_r = 0$. Then, the system fulfills*

1. *extended $\mathscr{L}_p$ string stability if there exist class $\mathscr{K}$ functions α, β such that for all input signals $u_j^{ff} \in \mathscr{L}_p$, $j = 1, \ldots, N$ and $i \in \{1, \ldots, N\}$ and all error signals w_i in (3.11) such that $||r_{ij}|| < \infty$, it holds that*

$$||y_i(t) - C_i \bar{x}||_{\mathscr{L}_p} \le \alpha \left(\sum_{k=1}^{i} ||u_i^{ff}(t)||_{\mathscr{L}_p} \right) + \beta \left(\sum_{k=1}^{i} \sum_{j=1}^{N_i} ||r_{k,j} - \bar{x}_i|| \right) \tag{3.15}$$

2. *Extended strict $\mathscr{L}_p$ string stability if 1) is fulfilled and for all $i = 2, \ldots, N$, it holds that*

$$||y_i(t) - C_i \bar{x}||_{\mathscr{L}_p} \le ||y_{i-1}(t) - C_{i-1} \bar{x}||_{\mathscr{L}_p}. \tag{3.16}$$

That is, extended string stability requires that the output deviation (in terms of the $\mathscr{L}_p$-norm) of each follower is bounded by the size of the predecessor inputs (in terms of $\mathscr{L}_p$-norm). Extended strict string stability requires the additional condition that the output deviation (in terms of the $\mathscr{L}_p$-norm) of each follower is bounded by the size of the output deviation of its predecessor vehicles (in terms of the $\mathscr{L}_p$-norm) as in the previous Definition 1.

The conditions for extended string stability in Definition 2 are formulated for general interconnected nonlinear systems represented by a state-space model. We

next derive the relevant conditions for the case of linear systems according to the control architecture in Fig. 3.9. Here, the relevant transfer functions are

$$\frac{Y_i(s)}{U_j(s)} = P_{y_i,u_j}(s), \quad i \in \mathbb{N}, j \leq i \tag{3.17}$$

$$\frac{Y_i(s)}{Y_{i-1}(s)} = \Gamma_{y_i}(s) = P_{y_i,u_1}(s)P_{y_{i-1},u_1}(s)^{-1}, \quad i \in \mathbb{N}, \tag{3.18}$$

$$\frac{Y_i(s)}{Y_j(s)} = \Theta_{y_i,y_j}(s) = P_{y_i,u_1}(s)P_{y_j,i_1}^{-1}(s) = \Gamma_{y_i}\cdots\Gamma_{y_{j+1}}, \quad i \in \mathbb{N}, j < i. \tag{3.19}$$

Using these transfer functions, two theorems for extended string stability of vehicle strings with linear vehicle models are derived for the case of the $\mathscr{L}_2$ norm and the case of the $\mathscr{L}_\infty$ norm.

3.4.1 Conditions for Extended String Stability and the $\mathscr{L}_2$ Norm

Theorem 3. *Consider the control architecture in Fig. 3.9 with the exogenous inputs u_i^{ff} for $i = 1,\ldots,N$. The system fulfills extended string stability if and only if*

$$\max_{i,j\leq i}||P_{y_i,u_j}||_\infty < \infty. \tag{3.20}$$

and extended strict $\mathscr{L}_2$ string stability if and only if

$$||P_{y_i,u_i}||_\infty < \infty \text{ for } i = 1,\ldots,N, \tag{3.21}$$

$$||\Gamma_{y_i}||_\infty \leq 1, \quad i = 2,\ldots,N. \tag{3.22}$$

Proof. Extended string stability: (IF) Assume that (3.20) holds and let $p_{\max} := \max_{i,j\leq i}||P_{y_i,u_j}||_\infty$, $\theta_{\max} := \max_{i,j\leq i}||\Theta y_i,y_j||_\infty$ and $a_{\max} := \max_i||(sI-A_i)^{-1}||_\infty$, A_i represents the dynamics matrix of the state space model of vehicle i. Note that $p_{\max}$ exists by assumption in (3.23), $\theta_{\max}$ exists because of (3.23) and (3.19) and $a_{\max}$ exists since $(sI-A_i)^{-1}$ is a stable and proper transfer matrix for all $i = 1,\ldots,N$. It has to be shown that 1. in Theorem 3 is fulfilled. We know from Fig. 3.9 and (3.17) that

$$Y_i(s) = P_{y_i,u_i}(s) U_i^{\text{ff}}(s) + \cdots + P_{y_i,u_1}(s) U_1^{\text{ff}}(s) + C_i (sI - A_i)^{-1} W_i$$
$$+ \Gamma_i C_{i-1} (sI - A_{i-1})^{-1} W_{i-1} + \cdots + \Gamma_i \cdots \Gamma_2 C_1 (sI - A_1)^{-1} W_1.$$

Then,

$$||y_i(t) - C_i \bar{x}||_{\mathscr{L}_2} \leq p_{\max} ||u_1^{\text{ff}}||_{\mathscr{L}_2} + \cdots + p_{\max} ||u_i^{\text{ff}}||_{\mathscr{L}_2} + ||C_i|| a_{\max} \sum_{j=1}^{N_i} ||r_{ij}||$$
$$+ ||C_{i-1}|| \theta_{\max} a_{\max} \sum_{j=1}^{N_{i-1}} ||r_{i-1j}|| + \cdots + ||C_1|| \theta_{\max} a_{\max} \sum_{j=1}^{N_2} ||r_{2j}||.$$

(3.23)

Choosing the class $\mathscr{K}$ functions $\alpha(z) = p_{\max} z$ and $\beta(z) = \max\{1, \theta_{\max}\} a_{\max} z$, (3.15) directly follows.

(ONLY IF) Assume that there exists a $j \in \{1, \ldots, i\}$ such that $||P_{y_i,u_j}||_\infty$ does not exist. Then, (3.23) directly implies that there is no class $\mathscr{K}$ function to fulfill (3.15). Hence, extended strict string stability is violated. Hence, (3.20) is the necessary and sufficient condition for extended string stability in the case of linear models.

Extended strict string stability: (IF) Assume that (3.21) and (3.22) hold. It has to be shown that (3.15) and (3.16) are fulfilled. First note that $P_{y_i,u_j} = \Gamma_{y_i} \cdots \Gamma_{y_{j+1}} P_{y_j,u_j}$. Hence, $||P_{y_i,u_j}||_\infty \leq ||\Gamma_{y_i}||_\infty \cdots ||\Gamma_{y_{j+1}}||_\infty ||P_{y_j,u_j}||_\infty \leq ||P_{y_j,u_j}||_\infty < \infty$ for all $i = 1, \ldots, N$ and $j \leq i$ with (3.21). That is, $\max_{i,j \leq i} ||P_{y_i,u_j}||_\infty < \infty$, which implies that (3.15) is fulfilled. In addition, (3.16) directly follows from (3.22).

(ONLY IF) Assume that (3.21) is violated. In that case (3.20) is violated and also (3.15) is violated according to the proof for extended string stability. Now assume that (3.22) is violated. This directly implies that (3.16) is violated. Hence, (3.21) and (3.22) are the necessary and sufficient conditions for extended strict string stability in the case of linear models. $\qquad\square$

We finally show that a successful controller design satisfying the conditions in Section 2.3 directly implies extended strict string stability if the output signals

$y_i = u_i$ or $y_i = a_i$ are chosen. Considering the vehicle model in (2.5), it holds for each $i = 1, \ldots, N$ that

- $||P_{i,i}(s)||_\infty = ||1||_\infty = 1$ if $y_i = u_i$,

- $||P_{i,i}(s)||_\infty = ||\dfrac{1}{1 + s\,\tau_i}||_\infty = 1$ if $y_i = a_i$.

In addition, $||\Gamma_{y_i}(s)||_\infty \leq 1$ for all $i = 2, \ldots, N$ by design. That is, the control architecture in Fig. 3.9 directly supports the achievement of extended strict string stability with the suitable design method according to Section 2.3. Hence, we can conclude that the signal norms of follower vehicles are bounded.

3.4.2 Conditions for Extended String Stability and the $\mathscr{L}_\infty$ Norm

The conditions in Section 3.4.1 are formulated for the case of L_2 string stability, which is concerned with the energy dissipation along the string. In this section, we derive conditions for L_∞ string stability, which captures the maximum overshoot.

Theorem 4. *Consider the control architecture in Fig. 3.9 with the exogenous inputs u_i^{ff} for $i = 1, \ldots, N$ and the error signals w_i in (3.11). The system fulfills extended $\mathscr{L}_\infty$ string stability if and only if*

$$\max_{i,j \leq i} ||p_{y_i, u_j}||_1 < \infty. \tag{3.24}$$

and extended strict $\mathscr{L}_2$ string stability if and only if

$$||p_{y_i, u_i}||_1 < \infty \text{ for } i = 1, \ldots, N, \tag{3.25}$$

$$||\gamma_{y_i}||_1 \leq 1, \quad i = 2, \ldots, N. \tag{3.26}$$

Proof. Extended $\mathscr{L}_\infty$ string stability: (IF) Assume that (3.24) holds and let $p_{\max} :=$ $\max_{i,j \leq i} ||p_{y_i, u_j}||_1$, $\theta_{\max} := \max_{i,j \leq i} ||\theta y_i, y_j||_1$ and $a_{\max} := \max_i ||\mathscr{L}^{-1}\big((sI - A_i)^{-1}\big))||_1$, A_i represents the dynamics matrix of the state space model of vehicle i and $\mathscr{L}^{-1}(\bullet)$ represents the inverse Laplace transform. Note that $p_{\max}$ exists by assumption in (3.27), $\theta_{\max}$ exists because of (3.27) and (3.19) and $a_{\max}$ exists since $(sI - A_i)^{-1}$

is a stable and proper transfer matrix for all $i = 1, \ldots, N$. It has to be shown that 1. in Theorem 4 is fulfilled. We know from Fig. 3.9 and (3.17) that

$$
\begin{aligned}
Y_i(s) =& P_{y_i,u_i}(s) U_i^{\text{ff}}(s) + \cdots + P_{y_i,u_1}(s) U_1^{\text{ff}}(s) + C_i (sI - A_i)^{-1} W_i \\
& + \Gamma_i C_{i-1} (sI - A_{i-1})^{-1} W_{i-1} + \cdots + \Gamma_i \cdots \Gamma_2 C_1 (sI - A_1)^{-1} W_1.
\end{aligned}
$$

Using Young's inequality for convolutions, it follows that

$$
\begin{aligned}
||y_i(t) - C_i \bar{x}||_{\mathscr{L}_\infty} \leq\ & p_{\max} ||u_1^{\text{ff}}||_{\mathscr{L}_\infty} + \cdots + p_{\max} ||u_i^{\text{ff}}||_{\mathscr{L}_\infty} + ||C_i|| a_{\max} \sum_{j=1}^{N_i} ||r_{ij}|| \\
& + ||C_{i-1}|| \theta_{\max} a_{\max} \sum_{j=1}^{N_{i-1}} ||r_{i-1\,j}|| + \cdots + ||C_1|| \theta_{\max} a_{\max} \sum_{j=1}^{N_2} ||r_{2\,j}||.
\end{aligned}
$$

$$(3.27)$$

Choosing the class $\mathscr{K}$ functions $\alpha(z) = p_{\max} z$ and $\beta(z) = \max\{1, \theta_{\max}\} a_{\max} z$, (3.15) directly follows.

(ONLY IF) Assume that there exists a $j \in \{1, \ldots, i\}$ such that $||p_{y_i,u_j}||_1$ does not exist. Then, (3.27) directly implies that there is no class $\mathscr{K}$ function to fulfill (3.15). Hence, extended strict L_∞ string stability is violated. Hence, (3.24) is the necessary and sufficient condition for extended string stability in the case of linear models.

Extended strict string stability: (IF) Assume that (3.25) and (3.26) hold. It has to be shown that (3.15) and (3.16) are fulfilled. First note that $P_{y_i,u_j} = \Gamma_{y_i} \cdots \Gamma_{y_{j+1}} P_{y_j,u_j}$. Hence, $||p_{y_i,u_j}||_1 \leq ||\gamma_{y_i}||_1 \cdots ||\gamma_{y_{j+1}}||_1 ||p_{y_j,u_j}||_1 \leq ||p_{y_j,u_j}||_\infty < \infty$ for all $i = 1, \ldots, N$ and $j \leq i$ with (3.25). That is, $\max_{i,j \leq i} ||p_{y_i,u_j}||_1 < \infty$, which implies that (3.15) is fulfilled. In addition, (3.16) directly follows from (3.26).

(ONLY IF) Assume that (3.25) is violated. In that case (3.20) is violated and also (3.15) is violated according to the proof for extended string stability. Now assume that (3.26) is violated. This directly implies that (3.16) is violated. Hence, (3.25) and (3.26) are the necessary and sufficient conditions for extended strict string stability in the case of linear models. $\qquad \square$

We finally show that a successful controller design according to Section 2.3
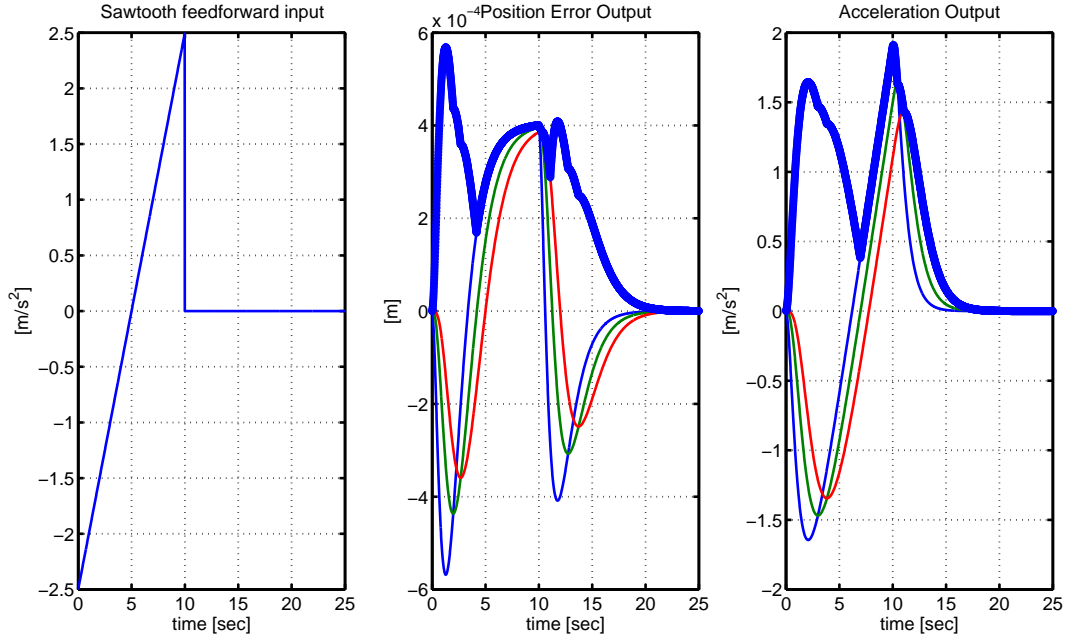
Figure 3.14: Gap Opening Simulation Satisfying Extended String Stability

can be used to address extended strict string stability if the output signals $y_i = u_i$ or $y_i = a_i$ are chosen and the additional condition of $\gamma(t) \geq 0$ is fulfilled. It is a general fact [40] that

$$||\Gamma||_\infty \leq 1 \text{ and } \gamma(t) \geq 0 \Rightarrow ||\gamma||_1 \leq 1. \tag{3.28}$$

Considering the vehicle model in (2.5), it holds for each $i = 1, \ldots, N$ that

- $||p_{i,i}(s)||_1 = ||1||_1 = 1$ if $y_i = u_i$,

- $||p_{i,i}(s)||_1 = ||\frac{1}{1 + s\,\tau_i}||_1 = 1$ if $y_i = a_i$.

In addition, $||\gamma_{y_i}(s)||_1 \leq 1$ for all $i = 2, \ldots, N$ because of (3.28). That is, the control architecture in Fig. 3.9 directly supports the achievement of extended strict string stability with the suitable design method in Section 2.3 and the additional condition that $\gamma(t) \geq 0$.

3.4.3 Simulation Experiment and Discussion

An illustrative practical scenario is simulated for both $\mathcal{L}_2$ and $\mathcal{L}_\infty$ cases of extended string stability. A sawtooth signal for opening a gap within 10s is applied

41
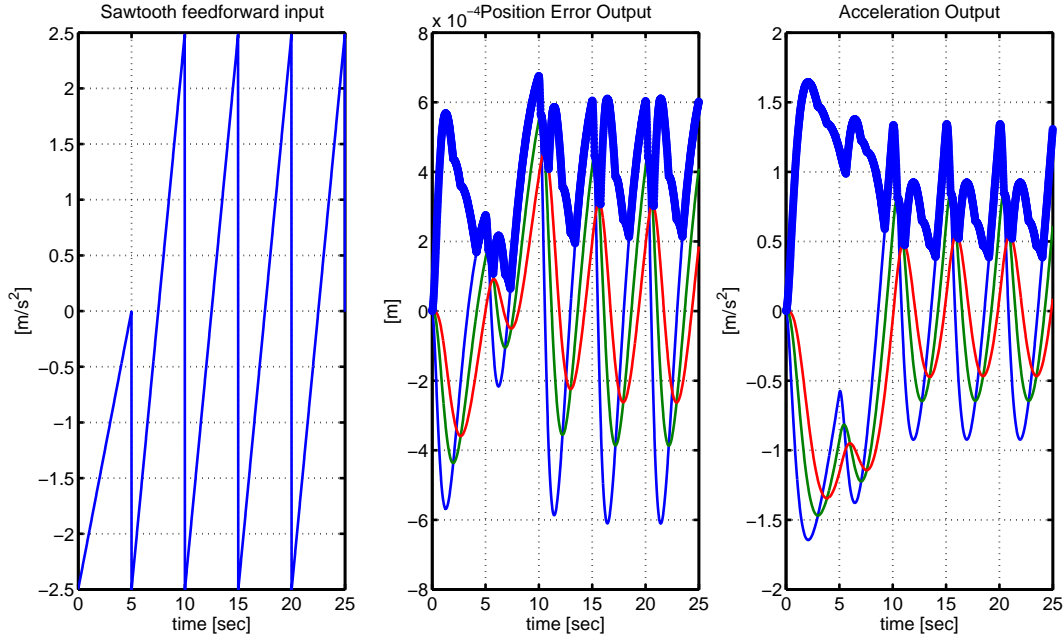
Figure 3.15: Gap Opening Simulation with 5times Repeated Sawtooth Input Satisfying Extended String Stability

to vehicle i as shown in Fig. 3.14. The effect on the physically relevant distance error and acceleration to follower vehicle $i+1$ is observed in the same Fig. 3.14. In numerical comparison terms, then the computed norm values are tabulated in Table 3.1.

Table 3.1: $\mathscr{L}_2$ and $\mathscr{L}_\infty$ norm comparison for input output signals of platoon

	$\mathscr{L}_2$ Norm	$\mathscr{L}_\infty$ Norm
Sawtooth Input	45.58	2.5
Distance Error	0.01	0.0006
Acceleration	38.85	1.91

Let class-$\mathscr{K}$ term coefficient is $\alpha(z) = z$ for being simple, then the difference in the left and right hand-side of equation is $45.58 - 0.01 = 45.57$ and $2.5 - 0.0006 = 2.4994$ for $\mathscr{L}_2$ and $\mathscr{L}_\infty$ cases respectively. In summary, the energy and maximal values of both signals for vehicle $i+1$ is bounded by the input sawtooth signal in the same figure, that conforms to (3.15), it is shown that extended string stability satisfied. Next, we run the same input repeated five times within 5sec as shown in Fig. 3.15.

42

In numerical comparison terms, then the computed norm values are tabulated in Table 3.2.

Table 3.2: $\mathscr{L}_2$ and $\mathscr{L}_\infty$ norm comparison for 5times repeated input output signals of platoon

	$\mathscr{L}_2$ Norm	$\mathscr{L}_\infty$ Norm
Sawtooth Input	72.02	2.5
Distance Error	0.02	0.0007
Acceleration	44.67	1.64

It can be observed that numeric difference or ratio of input to output is getting higher (from single input to five times repeated input case, 45.58/38.85=1.17 to 72.02/44.67=1.61) when the repetition of input signal increased. It is clear that superposition of repeated inputs makes the difference higher depending on the number of feedforward inputs applied, which is practically foreseen in big traffic platoons. Then it is evaluated as using only (3.15) is insufficient for the calculation of a bound. Besides that, it is observed in the simulations that there should be a computed bound which we will elaborate in the Chapter 5.

CHAPTER 4

GENERAL BOUND COMPUTATION

We briefly addressed vehicle strings and their internal effects in Chapter 3. We discussed maneuvers, had simulations and confirmed the string stability notion. We have observed the simulation of multiple lane changes and gap open or close maneuvers. Intuitively, we observed a bound for each scenario instead of an accumulation of the output signals then applying repeated maneuvers.

Oriented from LTI vehicle models we will analytically compute LTI signal bounds and first establish existence results and then compute numeric bound values in the forthcoming sections. In Section 4.1 we look at impulses which would be related to completing lane changes and in Section 4.2, a similar task will be related to gap open-close maneuvers. Since these two scenarios only study individual systems (single vehicle), we will extend the results to cover multiple interconnected systems in analogy to general strings with multiple vehicles in Section 4.3.

4.1 Impulse Input Repetitions

In this section, we consider the case of repeated input impulses for the case of completing lane changes as discussed in Section 3.2. We first provide a general development for LTI systems and then show how the developed results can be applied to lane changes of vehicles.

44

4.1.1 Notation and Problem Statement

We focus on LTI systems with the parameters in Table 4.1 and the state space representation

$$
\begin{aligned}
\dot{x} &= Ax + Bu \\
y &= Cx.
\end{aligned}
\tag{4.1}
$$

Table 4.1: Relevant parameters and functions of the linear system in (4.1).

$A \in \mathbb{R}^{n \times n}$	dynamics matrix
$B \in \mathbb{R}^{n \times p}$	input matrix
$C \in \mathbb{R}^{q \times n}$	output matrix
$x(t) \in \mathbb{R}^n$	system state
$u(t) \in \mathbb{R}^p$	input signal
$y(t) \in \mathbb{R}^q$	output signal
$\Gamma(s) = C(sI - A)^{-1}B$	transfer matrix
$\gamma(t) = Ce^{At}B$	impulse response matrix
$\mathscr{L}$	subspace of stable LTI systems

In addition, we use the notation in Table 4.2 for matrices $A \in \mathbb{R}^{n \times n}$, vectors $v \in \mathbb{R}^n$ and functions $f : \mathbb{R} \to \mathbb{R}$.

Table 4.2: Notation for matrices, vectors and functions.

a_{ij}	entry of A in row i and column j
$spec(A)$	set of eigenvalues of matrix A
$\sigma_{\max}(A)$	maximum singular value of matrix A
$\alpha(A) := \max\{\text{Re}\lambda \,|\, \lambda \in \text{spec}(A)\}$	spectral abscissa of matrix A
v_i	i-th entry of vector v
$\|v\|_2 = \sqrt{\sum_{i=1}^n |v_i|^2}$	vector 2-norm of vector v
$\|f\|_{L_\infty} = \sup_{t>0} |f(t)|$	L_∞-norm of function f

4.1.2 Norm Definition and Verification of Norm Properties

Norms for the impulse response of the LTI system in (4.1) are considered in [58, 59, 60]. Specifically, [58] introduces

$$||\Gamma||_{L_\infty} = \sup_{t \geq 0}\{\sigma_{\max}(\gamma(t))\} = \sup_{t \geq 0}\{\sigma_{\max}(C\,e^{At}\,B)\}. \tag{4.2}$$

as the maximum excursion of the impulse response matrix of the LTI system in (4.1).

In this section, we study the case where repeated impulses that are separated by a *dwell-time* $\Delta > 0$ are applied to the LTI system in (4.1).[1] We write $(t_\nu)_{\nu=0}^N = (t_0, t_1, \ldots, t_N)$ for a sequence with $N+1$ terms and introduce the set Q_Δ^N of monotonically increasing finite time sequences with dwell-time Δ

$$Q_\Delta^N = \{(t_\nu)_{\nu=0}^N | t_0 \geq 0, t_{\nu+1} - t_\nu \geq \Delta, \forall \nu = 0, \ldots, N-1\}. \tag{4.3}$$

Then, the set of monotonically increasing infinite time sequences with dwell-time Δ is

$$Q_\Delta = \{(t_\nu)_{\nu=0}^\infty | t_0 \geq 0, t_{\nu+1} - t_\nu \geq \Delta, \forall \nu = 0, 1, \ldots\}. \tag{4.4}$$

We assume that the ν-th impulse can be applied in an arbitrary input direction $v_\nu \in \mathbb{R}^p$ and define

$$||\Gamma||_{L_\infty, \Delta} = \sup_{(t_\nu)_{\nu=0}^\infty \in Q_\Delta, t \geq 0} \left(\frac{\sigma_{\max}\left(\sum_{\nu=0}^\infty \gamma(t - t_\nu)\,v_\nu\right)}{\max_\nu ||v_\nu||_2} \right)$$

$$= \sup_{(t_\nu)_{\nu=0}^\infty \in Q_\Delta, t \geq 0, ||v_\nu||_2 \leq 1} \left(\sigma_{\max}\left(\sum_{\nu=0}^\infty \gamma(t - t_\nu)\,v_\nu\right)\right). \tag{4.5}$$

In words, $||\Gamma||_{L_\infty, \Delta}$ quantifies the maximum amplification of an input signal in the form of an arbitrary number of repeated impulses, that is applied to the LTI system in (4.1). Hereby, impulses of the form $v_\nu\,\delta(t - t_\nu)$ that are separated by

---

[1]The application to the case of vehicle strings is found in 5.1.

at least Δ are applied at times t_v, $v = 0, 1, \ldots$. Accordingly, the excursion of the output signal $y(t)$ is bounded by the maximum magnitude $\max_v ||v_v||_2$ of the input impulses:

$$||y(t)||_2 \leq ||\Gamma||_{L_\infty,\Delta} \max_v ||v_v||_2. \tag{4.6}$$

The main subject of this chapter is the solution of two problems regarding $||\Gamma||_{L_\infty,\Delta}$ in (4.5). First, it is desired to identify a subspace of LTI systems with transfer matrix Γ such that (4.5) defines a norm. Second, it is intended to compute a close bound for $||\Gamma||_{L_\infty,\Delta}$.

We first present a new result for the summation of right-shifted monotonically decreasing non-negative functions that will be used for the evaluation of $||\Gamma||_{L_\infty,\Delta}$ in (4.5).

Lemma 1. *Let $f : \mathbb{R} \to \mathbb{R}$ be a function with $f(t) = 0$ for $t < 0$, $f(t) \geq 0$ for $t \geq 0$ and $f(t) \geq f(t')$ for all t, t' with $t \leq t'$. Assume that $\Delta > 0$. Then, it holds that*

$$\sup_{(t_v)_{v=0}^\infty \in Q_\Delta, t \geq 0} \sum_{v=0}^\infty f(t - t_v) = \sum_{v=0}^\infty f(v\Delta). \tag{4.7}$$

Proof. We first show that, for any $k \in \mathbb{N}$,

$$\sup_{(t_v)_{v=0}^k \in Q_\Delta^k, t \geq 0} \sum_{v=0}^k f(t - t_v) = \sum_{v=0}^k f(v\Delta). \tag{4.8}$$

It holds that $f(t - t_k)$ assumes its maximum value for $t_k = t$ since $f(t)$ is monotonically decreasing. In addition, since the time instants t_v are separated by the dwell-time Δ for $v = 0, \ldots, k$, the maximum value of $f(t - t_v)$ is obtained for $t_v = t_k - (k - v)\Delta = t - (k - v)\Delta$. That is,

$$\sup_{(t_v)_{v=0}^k \in Q_\Delta^k, t \geq 0} \sum_{v=0}^k f(t - t_v) = \sum_{v=0}^k f(t - t + (k - v)\Delta) = \sum_{v=0}^k f((k - v)\Delta) = \sum_{v=0}^k f(v\Delta).$$

Taking the limit for $k \to \infty$, (4.7) directly follows. □

It is now possible to show that $||\Gamma||_{L_\infty,\Delta}$ constitutes a norm for stable LTI systems in $\mathscr{L}$.

Theorem 5. *Assume that the LTI system in (4.1) belongs to $\mathscr{L}$ and let $\Delta > 0$. Then $||\Gamma||_{L_\infty,\Delta}$ is bounded and $||\Gamma||_{L_\infty,\Delta}$ is a norm for $\mathscr{L}$.*

The proof of Theorem 5 uses the following lemma that is adapted from [61].

Lemma 2. *Consider the LTI system in (4.1) and write $\mu = -\alpha(A)$. Then, for all $\varepsilon > 0$, there exists an $m > 0$ such that for all $t \geq 0$,*

$$\sigma_{max}(\gamma(t)) \leq m e^{-(\mu-\varepsilon)t}. \tag{4.9}$$

We next prove Theorem 5.

Proof. We first show that there exists a $K < \infty$ such that $||\Gamma||_{L_\infty,\Delta} \leq K$. Using (4.5), the triangle inequality for σ_{max} and $\sigma_{max}(v_v) = ||v_v||_2 \leq 1$ for $v = 0, 1, \ldots,$ it holds that

$$\begin{aligned}
||\Gamma||_{L_\infty,\Delta} &= \sup_{(t_v)_{v=0}^\infty \in Q_\Delta, t \geq 0, ||v_v||_2 \leq 1} \left(\sigma_{max} \left(\sum_{v=0}^\infty \gamma(t - t_v) v_v \right) \right) \\
&\leq \sup_{(t_v)_{v=0}^\infty \in Q_\Delta, t \geq 0} \left(\sum_{v=0}^\infty \sigma_{max} \left(\gamma(t - t_v) \right) \right).
\end{aligned}$$

Additionally, there are $m, \varepsilon > 0$ such that $\sigma_{max}(\gamma(t)) \leq m e^{-(\mu-\varepsilon)t}$ (Lemma 2). Then, $f(t) := m e^{-(\mu-\varepsilon)t}$ fulfills the conditions in Lemma 1. Hence,

$$\sup_{(t_v)_{v=0}^\infty \in Q_\Delta, t \geq 0} \left(\sum_{v=0}^\infty \sigma_{max} \left(\gamma(t - t_v) \right) \right) \leq \sup_{(t_v)_{v=0}^\infty \in Q_\Delta, t \geq 0} \left(\sum_{v=0}^\infty f(t - t_v) \right) = \sum_{v=0}^\infty f(v\Delta).$$

Applying the geometric series, we get

$$||\Gamma||_{L_\infty,\Delta} \leq \sum_{v=0}^\infty f(v\Delta) = \sum_{v=0}^\infty m' e^{-(\mu-\varepsilon)v\Delta} = \frac{m'}{1 - e^{-(\mu-\varepsilon)\Delta}} =: K < \infty. \tag{4.10}$$

We finally show that $||\Gamma||_{L_\infty,\Delta}$ is a norm for $\mathscr{L}$.

Absolute Homogeneity: Let $k \in \mathbb{R}$. Then,

$$||k\Gamma||_{L_\infty,\Delta} = \sup_{(t_v)_{v=0}^\infty \in Q_\Delta, t \geq 0, ||v_v||_2 \leq 1} \left(\sigma_{\max} \left(\sum_{v=0}^\infty k\,\gamma(t-t_v)\,v_v \right) \right)$$

$$= |k| \sup_{(t_v)_{v=0}^\infty \in Q_\Delta, t \geq 0, ||v_v|| \leq 1} \left(\sigma_{\max} \left(\sum_{v=0}^\infty \gamma(t-t_v)\,v_v \right) \right) = |k|\,||\Gamma||_{L_\infty,\Delta}.$$

Triangle Inequality: Let Γ_1, Γ_2 be transfer matrices of stable LTI systems. Then,

$$||\Gamma_1 + \Gamma_2||_{L_\infty,\Delta} = \sup_{(t_v)_{v=0}^\infty \in Q_\Delta, t \geq 0, ||v_v||_2 \leq 1} \left(\sigma_{\max} \left(\sum_{v=0}^\infty \left(\gamma_1(t-t_v) + \gamma_2(t-t_v) \right) v_v \right) \right)$$

$$\leq \sup_{(t_v)_{v=0}^\infty \in Q_\Delta, t \geq 0, ||v_v||_2 \leq 1} \left(\sigma_{\max} \left(\sum_{v=0}^\infty \gamma_1(t-t_v)\,v_v \right) \right)$$

$$+ \sup_{(t_v)_{v=0}^\infty \in Q_\Delta, t \geq 0, ||v_v||_2 \leq 1} \left(\sigma_{\max} \left(\sum_{v=0}^\infty \gamma_2(t-t_v)\,v_v \right) \right)$$

$$= ||\Gamma_1||_{L_\infty,\Delta} + ||\Gamma_2||_{L_\infty,\Delta}.$$

Zero Vector Condition:

$$||\Gamma||_{L_\infty,\Delta} = 0 \Rightarrow \sup_{(t_v)_{v=0}^\infty \in Q_\Delta, t \geq 0, ||v_v||_2 \leq 1} \left(\sigma_{\max} \left(\sum_{v=0}^\infty \gamma(t-t_v)\,v_v \right) \right) = 0$$

$$\Rightarrow \forall t \geq 0, \gamma(t) = 0 \Rightarrow \Gamma(s) = 0.$$

Since we know that $||\Gamma||_{L_\infty,\Delta} \leq \infty$ from before, $||\Gamma||_{L_\infty,\Delta}$ is indeed a norm for $\mathscr{L}$. $\qquad\square$

The theorem states that the vector 2-norm of the output signal remains bounded when applying an arbitrary number of impulses with a bounded magnitude that are separated by a dwell-time Δ to a stable LTI system.

We illustrate Theorem 5 by an LTI system with the impulse response matrix

γ_1 and the state space model

$$
A_1 = \begin{bmatrix} -0.5 & 1 & 0 & -2 \\ 0 & -6.5 & 0 & 5 \\ 4 & 4 & -2.5 & -8 \\ 0 & -2.5 & 0 & 1 \end{bmatrix}, \quad B_1 = I, \quad C_1 = I, \tag{4.11}
$$

whereby I denotes the identity matrix. Considering $spec(A_1) = \{-0.5, -1.5, -2.5, -4\}$, it holds that $\mu = 0.5$. Choosing $\varepsilon = 0.1$, a bound for $\gamma_1(t)$ according to (4.9) is $5\,e^{-(0.5-0.1)t}$ as shown in Fig. 4.1.
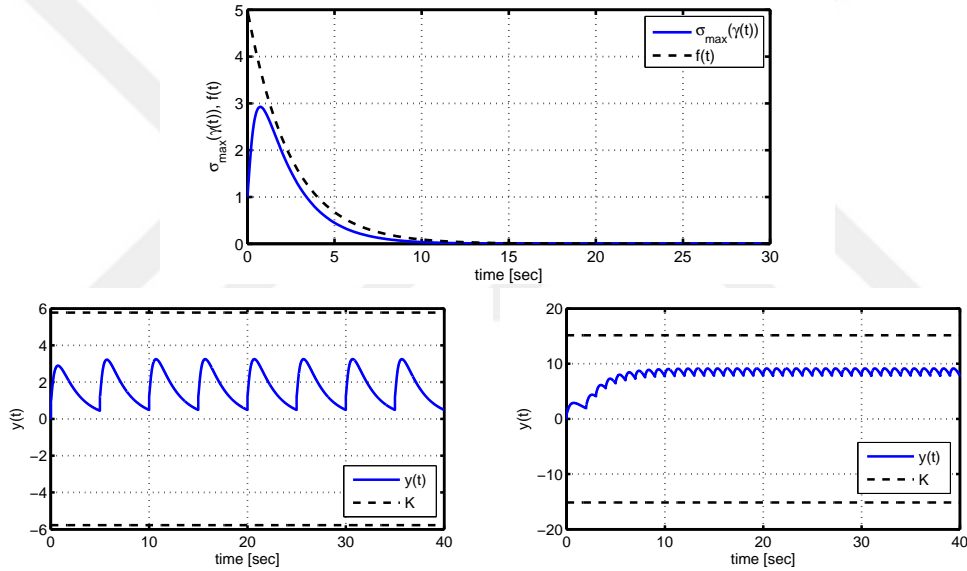
Figure 4.1: Example in (4.11): Comparison of $\sigma_{\max}(\gamma_1(t))$ and exponential bound $f(t)$ (top); comparison of simulated response and K in (4.10) for $\Delta = 5$ (left) and $\Delta = 1$ (right).

We compute $K = \dfrac{5}{1 - e^{-0.4\Delta}}$ in (4.10) such that $K = 5.8$ for $\Delta = 5$ and $K = 15.2$ for $\Delta = 1$. Fig. 4.1 shows a simulation of the LTI system in (4.11) with repeated impulses of magnitude 1 for $\Delta = 5$ and $\Delta = 1$. It can be seen that the maximum value of $||y(t)||_2$ stays well below K, that is, the bound is conservative.[2]

---

[2]Section 4.1.5 shows that the simulation result is close to the actual values of $||\Gamma_1||_{L_\infty,5}$ and $||\Gamma_1||_{L_\infty,1}$.

Second, we consider an LTI system with the transfer function

$$\Gamma_2(s) = \frac{40\,s^6 + 240\,s^5 + 2616\,s^4 + 9632\,s^3 + 46744\,s^2 + 70000\,s + 186120}{(s+5)^2\,(s^2 + 2\,s + 17)^3}.$$

(4.12)

A corresponding bound according to (4.9) has $\mu = 1$, $\varepsilon = 0.3$ and $m' = 50$ (see Fig. 4.2).
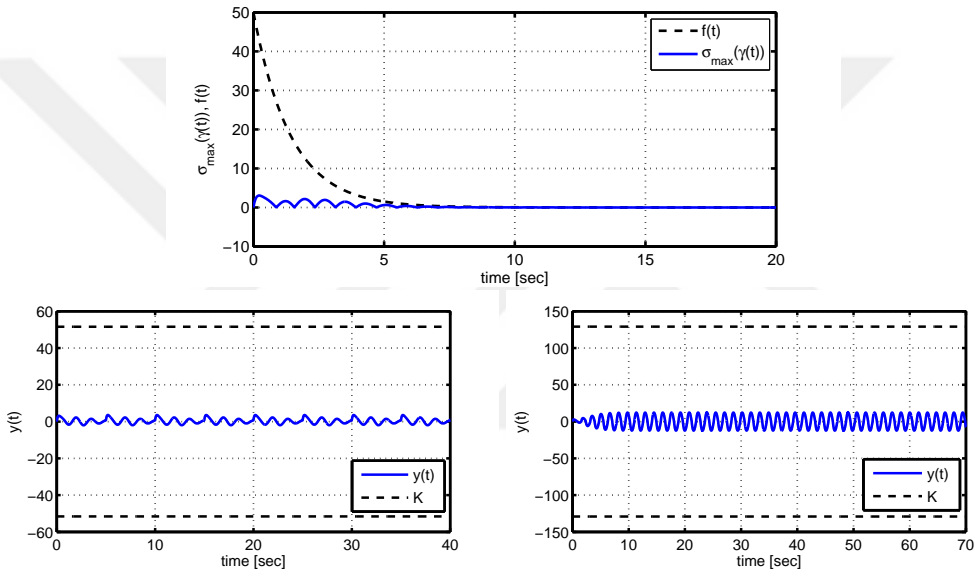
Figure 4.2: Example in (4.12): Comparison of $\gamma_2(t)$ and exponential bound $f(t)$ (top); comparison of simulated response and K in (4.10) for $\Delta = 5$ (left) and $\Delta = 0.7$ (right).

Accordingly, $K = \dfrac{50}{1 - e^{-0.7\Delta}}$ in (4.10) with $K = 51.6$ for $\Delta = 5$ and $K = 129.1$ for $\Delta = 0.7$. Again, the bound is conservative as can be seen in Fig. 4.2.

4.1.3 Exact Bound Computation

We focus on the LTI system in (4.1) with a single input $u(t) \in \mathbb{R}$, a single output $y(t) \in \mathbb{R}$ and a monotonically decreasing impulse response $\sigma_{\max}(\gamma(t)) = |\gamma(t)|$ in order to compute the exact value of $||\Gamma||_{L_\infty,\Delta}$. Then, (4.5) and Lemma 1 imply that

$$
||\Gamma||_{L_\infty,\Delta} = \sup_{(t_v)_{v=0}^\infty \in Q_\Delta, t \geq 0, ||v_v||_2 \leq 1} \left\{ \sum_{v=0}^\infty |\gamma(t-t_v)v_v| \right\} = \sum_{v=0}^\infty |\gamma(v\Delta)|. \quad (4.13)
$$

We use the general representation of $\gamma(t)$ as

$$
\gamma(t) = \sum_{i=1}^k \sum_{j=0}^{l_i} a_{i,j} t^j e^{-\lambda_i t} + \sum_{i=k+1}^K \sum_{j=0}^{l_i} a_{i,j} t^j \cos(\omega_i t + \phi_i) e^{-\lambda_i t} \quad (4.14)
$$

with coefficients $a_{i,j} \in \mathbb{R}$ for $i = 1, \ldots, K$ and $j = 0, \ldots, l_i$, the real poles $-\lambda_i < 0$ for $i = 1, \ldots, k$, the complex poles $-\lambda_i \pm \omega_i j$ and the phase shift $\phi_{i,j}$ for $i = k+1, \ldots, K$ and $j = 0, \ldots, l_i$. Then, the following theorem states sufficient conditions for the exact analytical computation of $||\Gamma||_{L_\infty,\Delta}$.

Theorem 6. *Consider a stable LTI system in (4.1) for $p = q = 1$. If $|\gamma(t)|$ is monotonically decreasing, then*

$$
||\Gamma||_{L_\infty,\Delta} = \Big| \sum_{i=1}^k \sum_{j=0}^{l_i} a_{i,j} \Delta^j (-1)^j \frac{d^j}{d(\lambda_i \Delta)^j} \frac{1}{1 - e^{-\lambda_i,\Delta}}
$$
$$
+ \sum_{i=k+1}^K \sum_{j=0}^{l_i} a_{i,j} \Delta^j (-1)^j \frac{d^j}{d(\lambda_i \Delta)^j} \frac{\cos(\phi_{i,j}) - e^{-\lambda_i \Delta} \cos(\omega_i - \phi_{i,j})}{1 - 2e^{-\lambda_i \Delta} \cos(\omega_i) + e^{-2\lambda_i \Delta}} \Big|.
$$
$$
\quad (4.15)
$$

We use the following general result about exponential series for proving Theorem 6.

Lemma 3. *Let* $\beta, \omega > 0$, $\phi \in \mathbb{R}$ *and* $j \in \mathbb{N}$. *Then, it holds that*

$$\sum_{v=0}^{\infty} v^j e^{-\beta v} = (-1)^j \frac{d^j}{d\beta^j} \frac{1}{1 - e^{-\beta}} \tag{4.16}$$

$$\sum_{v=0}^{\infty} v^j \cos(\omega v + \phi) e^{-\beta v} = (-1)^j \frac{d^j}{d\beta^j} \frac{\cos(\phi) - e^{-\beta} \cos(\omega - \phi)}{1 - 2 e^{-\beta} \cos(\omega) + e^{-2\beta}}. \tag{4.17}$$

We next provide the proof of Theorem 6.

Proof. We use (4.13), (4.14) and Lemma 3:

$$\begin{aligned}
||\Gamma||_{L_\infty,\Delta} &= \sum_{v=0}^{\infty} |\gamma(v\Delta)| = |\sum_{v=0}^{\infty} \gamma(v\Delta)| \\
&= |\sum_{v=0}^{\infty} \sum_{i=1}^{k} \sum_{j=0}^{l_i} a_{i,j} (v\Delta)^j e^{-\lambda_i v\Delta} \\
&\quad + \sum_{v=0}^{\infty} \sum_{i=k+1}^{K} \sum_{j=0}^{l_i} a_{i,j} (v\Delta)^j \cos(\omega_i v\Delta + \phi_{i,j}) e^{-\lambda_i v\Delta}| \\
&= |\sum_{i=1}^{k} \sum_{j=0}^{l_i} a_{i,j} \Delta^j \sum_{v=0}^{\infty} v^j e^{-\lambda_i \Delta v} \\
&\quad + \sum_{i=k+1}^{K} \sum_{j=0}^{l_i} a_{i,j} \Delta^j \sum_{v=0}^{\infty} v^j \cos(\omega_i v\Delta + \phi_{i,j}) e^{-\lambda_i \Delta v}| \\
&= |\sum_{i=1}^{k} \sum_{j=0}^{l_i} a_{i,j} \Delta^j (-1)^j \frac{d^j}{d(\lambda_i\Delta)^j} \frac{1}{1 - e^{-\lambda_i\Delta}} \\
&\quad + \sum_{i=k+1}^{K} \sum_{j=0}^{l_i} a_{i,j} \Delta^j (-1)^j \frac{d^j}{d(\lambda_i\Delta)^j} \frac{\cos(\phi_{i,j}) - e^{-\lambda_i\Delta} \cos(\omega_i - \phi_{i,j})}{1 - 2 e^{-\lambda_i\Delta} \cos(\omega_i) + e^{-2\lambda_i\Delta}}|.
\end{aligned}$$

$\square$

We emphasize that Theorem 6 applies to stable SISO LTI systems with a monotonic impulse response. Examples for such systems are general LTI systems, whose transfer function has alternating negative real poles and zeros [62]. In addition, certain vehicle following applications as described in Section 5.1 have this property.

We consider the example system with the transfer function Γ_3 and the impulse response γ_3:

$$\Gamma_3(s) = \frac{(s+5)(s+10)}{(s+4)(s+8)(s+15)}, \tag{4.18}$$

$$\gamma_3(t) = \frac{3}{22}e^{-4t} + \frac{3}{14}e^{-8t} + \frac{50}{77}e^{-15t}. \tag{4.19}$$

Using (4.15) with $k = 3$, $l_i = 0$ for $i = 1, \ldots, k$ and $a_{1,0} = \frac{3}{22}$, $a_{2,0} = \frac{3}{14}$, $a_{3,0} = \frac{50}{77}$, $\lambda_1 = 4$, $\lambda_2 = 8$, $\lambda_3 = 15$, we obtain

$$||\Gamma_3||_{L_\infty,\Delta} = \frac{3}{22(1 - e^{-4\Delta})} + \frac{3}{14(1 - e^{-8\Delta})} + \frac{50}{77(1 - e^{-15\Delta})}.$$

We compute $||\Gamma_3||_{L_\infty,5} = 1.0$ for $\Delta = 5$ and $||\Gamma_3||_{L_\infty,0.1} = 1.64$ for $\Delta = 0.1$. The exactness of the result is verified by the simulated responses in Fig. 4.3.
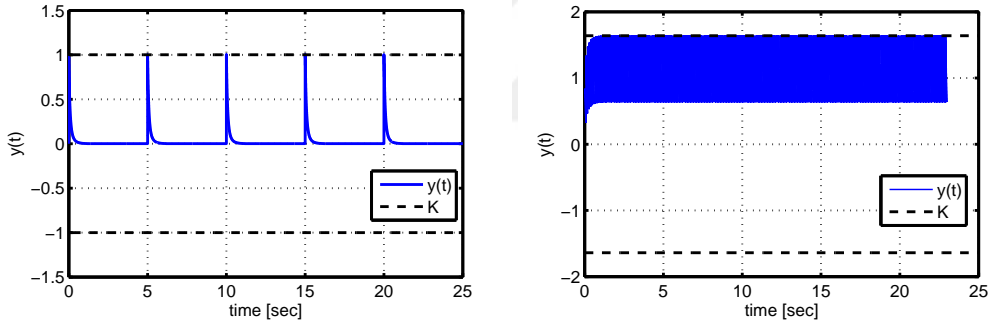
Figure 4.3: Comparison of simulated response and $||\Gamma_3||_{L_\infty,\Delta}$ for $\Delta = 5$ (left) and $\Delta = 0.1$ (right).

4.1.4 Close Bound Computation

We next approximate $||\Gamma||_{L_\infty,\Delta}$ by a close upper bound in the general case of multiple-input multiple-output (MIMO) LTI systems. Referring to Lemma 1, we intend to find such bound by constructing a monotonically decreasing function $f(t)$ such that $f(t) \geq \sigma_{\max}(\gamma(t))$ for all $t \geq 0$. In addition, f must be chosen such that the infinite sum in (4.7) converges. We make use of an impulse response

bound according to [58, 63].

Lemma 4. *Consider the LTI system in* (4.1) *and write* $\mu = -\alpha(A)$. *Then, there exist n and* $a_k > 0$, $k = 0, \ldots, n-1$ *such that for all* $t \geq 0$,

$$\sigma_{max}(\gamma(t)) \leq b(t) := e^{-\mu t}\Big(\sum_{k=0}^{n-1} a_k t^k\Big). \tag{4.20}$$

It is readily observed that $b(t)$ for stable LTI systems has a single maximum for $t \geq 0$ since $\mu > 0$ and $a_k > 0$ for $k = 0, \ldots, n-1$. We denote the maximum value of $b(t)$ as b_{m} and the corresponding time instant as t_{m} such that $b(t_{\mathrm{m}}) = b_{\mathrm{m}}$.

Using (4.16) and (4.20), it follows that the infinite sum in (4.21) converges:

$$\sum_{v=0}^{\infty} b(v\Delta) = \sum_{k=0}^{n-1} a_k \Delta^k (-1)^k \frac{d^k}{d(\mu\Delta)^k} \frac{1}{1 - e^{-\mu\Delta}} < \infty \tag{4.21}$$

Nevertheless, b is not suitable for computing a close bound on $||\Gamma||_{L_\infty, \Delta}$, since it does not fulfill monotonicity in Lemma 1. In addition $b(t)$ is generally very conservative.

In order to circumvent the stated issues, we use a threshold value $\psi > 0$ and define t_ψ as the smallest time instant after t_{m} such that $b(t_\psi)$ remains below ψ:

$$t_\psi = \min_{t \geq t_{\mathrm{m}}, b(t) \leq \psi} t. \tag{4.22}$$

Since $b(t)$ is monotonically decreasing and smaller than ψ after t_ψ, we consider $b(t)$ as a suitable bound for $\sigma_{\max}(\gamma(t))$ after t_ψ.

We further propose to determine a monotonically decreasing bound $a(t) \geq \sigma_{\max}(\gamma(t))$ for $t \in [0, t_\psi)$ by simulation. Consider an impulse response simulation run of the LTI system in (4.1) with the solution values $\hat{\gamma}_i$ at the times τ_i, $i = 1, \ldots, F$ and a maximum simulation error e_{sim} for $\sigma_{\max}(\hat{\gamma}_i)$. Then, we define the bound $a(t)$ for each $t \in [0, t_\psi)$ as

$$a(t) = \max_{i=1,\ldots,F, \tau_i \geq t} \{\hat{\gamma}_i\} + e_{\mathrm{sim}}. \tag{4.23}$$

By construction, it holds that a is a monotonically decreasing staircase function and $a(t) \geq \sigma_{\max}(\gamma(t))$ for all $t \in [0, t_\psi)$. Together, we define the bound

$$c(t) = \begin{cases} a(t) & \text{for } 0 \leq t < t_\psi \\ b(t) & \text{for } t \geq t_\psi. \end{cases} \tag{4.24}$$

We revisit the example in (4.11). Using (4.20) and the definition of a_k in [63], we obtain

$$b(t) = e^{-0.5t}\left(4 + 88.2t + 973t^2 + 7154t^3\right) \tag{4.25}$$

with a maximum value $b_{\mathrm{m}} = b(5.95) = 7.9 \cdot 10^4$ at $t_{\mathrm{m}} = 5.95$ sec. That is, b is indeed very conservative. Using (4.22), we find $t_{0.1} = 45.24\,\mathrm{s} > t_{\mathrm{m}}$ for the threshold $\psi = 0.1$. We further determine $a(t)$ based on a simulation in Matlab/Simulink 2013a (solver `ode45` at a relative tolerance 10^{-3}). $\sigma_{\max}(\gamma(t))$ is shown in Fig. 4.4. Considering that the maximum value is below 3, $e_{\mathrm{sim}} < 0.003$ can be assumed. According to (4.24), $a(t)$ is used as a bound before $t_\psi = 45.24$ sec and $b(t)$ is used afterwards.

Using $c(t)$, the computation of a close bound for $||\Gamma||_{L_{\infty},\Delta}$ is performed as stated in Theorem 7.

Theorem 7. *Assume that the LTI system in (4.1) belongs to $\mathscr{L}$. Let $\Delta > 0$, let $t_\psi > 0$ be computed with (4.22) and let $c(t)$ be given as in (4.24). Write $N = \lfloor \dfrac{t_\psi}{\Delta} \rfloor$. Then, it holds that*

$$||\Gamma||_{L_{\infty},\Delta} \leq \sum_{v=0}^{N-1} a(v\Delta) + e^{-\mu t_\psi} \sum_{k=0}^{n-1} a_k \sum_{i=0}^{k} \binom{k}{i} t_\psi^{k-i} \Delta^i (-1)^i \frac{d^i}{d(\mu\Delta)^i} \frac{1}{1 - e^{-\mu\Delta}} < \infty. \tag{4.26}$$

56
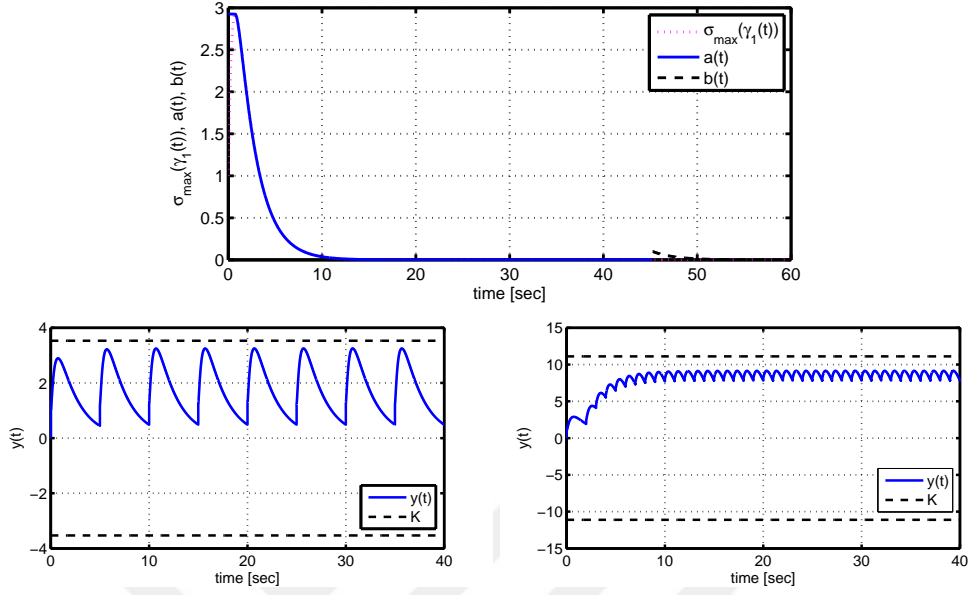
Figure 4.4: Monotonic bound computation for $\sigma_{\max}(\gamma_1(t))$ (top); comparison of simulated response and $||\Gamma_1||_{L_\infty,\Delta}$ for $\Delta = 5$ (left) and $\Delta = 1$ (right).

Proof. By definition,

$$
\begin{aligned}
||\Gamma||_{L_\infty,\Delta} &= \sup_{(t_\nu)_{\nu=0}^\infty \in Q_\Delta, t \geq 0, ||v_\nu||_2 \leq 1} \left(\sigma_{\max}\left(\sum_{\nu=0}^\infty \gamma(t - t_\nu) v_\nu \right) \right) \\
&\leq \sup_{(t_\nu)_{\nu=0}^\infty \in Q_\Delta, t \geq 0} \left(\sum_{\nu=0}^\infty c(t - t_\nu) \right) \\
&= \sup_{(t_\nu)_{\nu=0}^\infty \in Q_\Delta, t \geq 0, t - t_\nu < t_\psi} \left(\sum_{\nu=0}^\infty a(t - t_\nu) \right) + \sup_{(t_\nu)_{\nu=0}^\infty \in Q_\Delta, t \geq 0, t - t_\nu \geq t_\psi} \left(\sum_{\nu=0}^\infty b(t - t_\nu) \right).
\end{aligned}
$$

Considering that $t_{\nu+1} - t_\nu \geq \Delta$ for all $\nu = 0, 1, \ldots,$, there can be at most $N = \lfloor \frac{t_\psi}{\Delta} \rfloor$ values such that $t - t_\nu < t_\psi$. Recalling that a is monotonically decreasing, (4.8) in the proof of Lemma 1 shows that

$$
\sup_{(t_\nu)_{\nu=0}^\infty \in Q_\Delta, t \geq 0, t - t_\nu < t_\psi} \left(\sum_{\nu=0}^\infty a(t - t_\nu) \right) = \sup_{(t_\nu)_{\nu=0}^{N-1} \in Q_\Delta^{N-1}, t \geq 0} \left(\sum_{\nu=0}^{N-1} a(t - t_\nu) \right) = \sum_{\nu=0}^{N-1} a(\nu\Delta).
$$

In addition, since $b(t)$ is monotonically decreasing for $t \geq t_\psi$, $\hat{b}(t) := b(t + t_\psi)$ is

57

monotonically decreasing for $t \geq 0$. Using Lemma 1, we compute

$$\sup_{(t_v)_{v=0}^{\infty} \in Q_\Delta, t \geq 0, t - t_v \geq t_\psi} \left(\sum_{v=0}^{\infty} b(t - t_v) \right) = \sup_{(t_v)_{v=0}^{\infty} \in Q_\Delta, t - t_v \geq 0} \left(\sum_{v=0}^{\infty} \hat{b}(t - t_v) \right)$$

$$= \sum_{v=0}^{\infty} \hat{b}(v\Delta) = \sum_{v=0}^{\infty} b(t_\psi + v\Delta).$$

Hence,

$$||\Gamma||_{L_\infty,\Delta} \leq \sum_{v=0}^{N-1} a(v\Delta) + \sum_{v=0}^{\infty} b(t_\psi + v\Delta)$$

$$= \sum_{v=0}^{N-1} a(v\Delta) + \sum_{v=0}^{\infty} e^{-\mu(t_\psi + v\Delta)} \sum_{k=0}^{n-1} a_k (t_\psi + v\Delta)^k =$$

$$= \sum_{v=0}^{N-1} a(v\Delta) + e^{-\mu t_\psi} \sum_{k=0}^{n-1} a_k \sum_{i=0}^{k} \binom{k}{i} t_\psi^{k-i} \Delta^i \sum_{v=0}^{\infty} v^i e^{-\mu v\Delta} =$$

$$= \sum_{v=0}^{N-1} a(v\Delta) + e^{-\mu t_\psi} \sum_{k=0}^{n-1} a_k \sum_{i=0}^{k} \binom{k}{i} t_\psi^{k-i} \Delta^i (-1)^i \frac{d^i}{d(\mu\Delta)^i} \frac{1}{1 - e^{-\mu\Delta}}.$$

In this computation, we used the binomial theorem and Lemma 3. Considering that all summations in the above expression are finite, it follows that $||\Gamma||_{L_\infty,\Delta} < \infty$. $\square$

Theorem 7 divides the computation of a bound on $||\Gamma||_{L_\infty,\Delta}$ into the finite sum $S_1 := \sum_{v=0}^{N-1} a(v\Delta)$ and the infinite sum $S_2 := \sum_{v=0}^{\infty} b(t_\psi + v\Delta)$. Here, the close monotonic bound $a(t)$ can be easily found by simulation for $t \in [0, t_\psi)$. Moreover, the infinite sum S_2 can be evaluated analytically based on the monotonic bound $b(t_\psi + t)$. Its contribution to $S_1 + S_2$ is small when choosing ψ small enough as is justified by the subsequent examples.

4.1.5 Academic Examples

Using (4.26) for the example in (4.11) with the bounds in Fig. 4.4, we find $||\Gamma_1||_{L_\infty,5} \leq 3.53$ for $\Delta = 5$ and $||\Gamma_1||_{L_\infty,1} \leq 11.1$ for $\Delta = 1$. The simulation in Fig. 4.4 also shows that the 2-norm of the output signal remains below the bound, whereas the bounds are much closer than the bounds in Fig. 4.1.

We next evaluate the example in (4.12). Using (4.20), we obtain

$$b(t) = e^{-t} (6 + 418t + 14 \cdot 10^3 t^2 + 33 \cdot 10^4 t^3 + 58 \cdot 10^5 t^4 + 80 \cdot 10^6 t^5$$
$$+ 92 \cdot 10^7 t^6 + 91 \cdot 10^8 t^7).$$

with $t_{\mathrm{m}} = 6.99$ and $t_{\psi} = 53.0 > t_{\mathrm{m}}$ for $\psi = 0.1$. We further obtain $a(t)$ by simulation with $e_{\mathrm{sim}} < 0.01$. $\gamma_2(t)$ and the resulting bounds $a(t)$ and $b(t)$ are shown in Fig. 4.5.
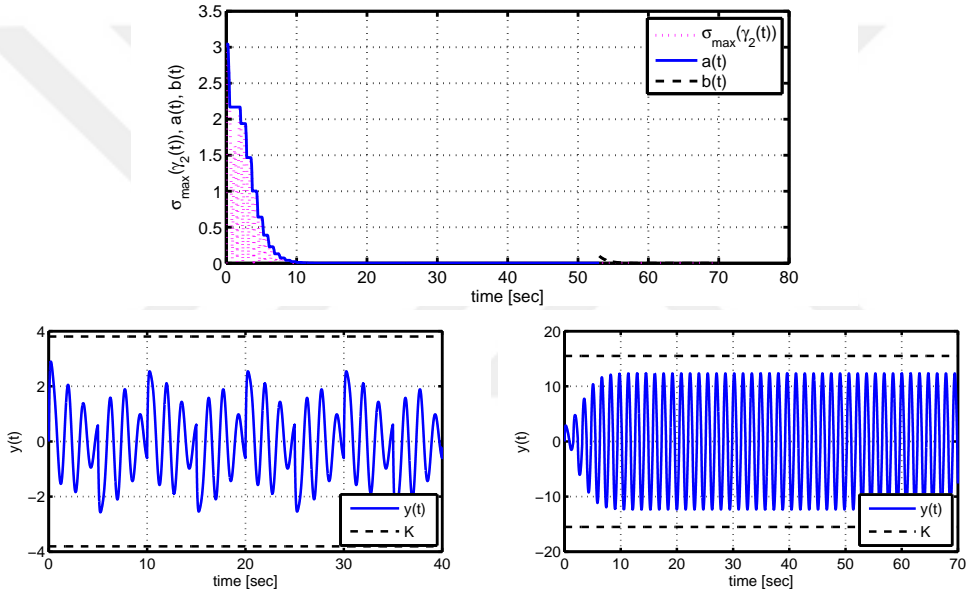
Figure 4.5: Monotonic bound computation for $\sigma_{\max}(\gamma_2(t))$ (top); comparison of simulated response and $||\Gamma_2||_{L_\infty, \Delta}$ for $\Delta = 5$ (left) and $\Delta = 1$ (right).

Using (4.26), $||\Gamma_2||_{L_\infty,5} \leq 3.8$ for $\Delta = 5$ and $||\Gamma_2||_{L_\infty,0.7} \leq 15.5$ for $\Delta = 0.7$. The simulation in Fig. 4.5 again confirms a close bound that is much less conservative than the bound in Fig. 4.2.

4.2 Time-Limited Input Repetitions

Different from the previous section, this section considers the case of repeatedly applying time-limited input signals to an LTI system. As discussed in Section 3.3,

such signals are used when opening/closing gaps in a vehicle string.

4.2.1 Notation and Problem Statement

We focus on LTI systems with the state space model

$$
\begin{aligned}
\dot{x} &= Ax + Bu \\
y &= Cx.
\end{aligned}
\tag{4.27}
$$

$A \in \mathbb{R}^{n \times n}$ is the *dynamics matrix*, $B \in \mathbb{R}^{n \times p}$ is the *input matrix* and $C \in \mathbb{R}^{q \times n}$ is the output matrix, $x(t) \in \mathbb{R}^n$ is the *system state*, $u(t) \in \mathbb{R}^p$ is the *input signal* and $y(t) \in \mathbb{R}^q$ is the *output signal*. We further write γ for the *impulse response matrix* of the system in (4.27).

Regarding matrices, we use the same notation as in Section 4.1.1. $A \in \mathbb{R}^{n \times n}$, we write $spec(A)$ for the *set of eigenvalues* of A, $\sigma_{\max}(A)$ for the *maximum singular value* of A, $\alpha(A) := \max\{\mathrm{Re}\lambda \,|\, \lambda \in \mathrm{spec}(A)\}$ for the *spectral abscissa* of A and $A = Q(D+N)Q^{-1}$ for the Schur decomposition of A with the unitary matrix $Q \in \mathbb{R}^{n \times n}$, the diagonal matrix $D \in \mathbb{R}^{n \times n}$ and the upper triangular matrix $N \in \mathbb{R}^{n \times n}$. For vectors $v \in \mathbb{R}^n$, we write v_i for the i-th entry and use the *vector 2-norm* $||v|| = \sqrt{\sum_{i=1}^{n} |v_i|^2}$.

As described in our motivating example in Section 3.3, we consider stable LTI systems with repeated time-limited input signals that are separated by a minimum *dwell-time* Δ. Using a bound $u_{\max}$, we formally introduce the set of bounded input signals with time-limit $t_l < \infty$ as

$$
\begin{aligned}
\mathscr{U}_{u_{\max},t_l} = \{u : \mathbb{R} \to \mathbb{R}^p \,|\, u(t) = 0 \text{ for } t < 0 \text{ and } t > t_l, ||u(t)|| \\
\leq u_{\max} \text{ for } 0 \leq t \leq t_l\}.
\end{aligned}
\tag{4.28}
$$

In order to formulate the successive application of input signals in $\mathscr{U}_{u_{\max},t_l}$, we define the set Q_Δ of monotonically increasing infinite time sequences with dwell-time Δ as

$$
Q_\Delta = \{(t_v)_{v=0}^{\infty} \,|\, t_0 \geq 0, t_{v+1} - t_v \geq \Delta, \forall v = 0, 1, \ldots\}.
\tag{4.29}
$$

Then, the successive application of input signals $u_v \in \mathscr{U}_{u_{\max},t_1}$ for a given sequence $(t_v)_{v=0}^{\infty} \in Q_\Delta$ is represented by the signal

$$u_{(t_v)_{v=0}^{\infty}}(t) = \sum_{v=0}^{\infty} u_v(t - t_v). \tag{4.30}$$

In this expression, the time-limited input signal u_v is applied at time t_v.

Using the notions introduce above, the aim of this chapter is to determine a bound on the output signal norm $||y(t)||$ over time when applying a repeated input signal $u_{(t_v)_{v=0}^{\infty}}(t)$ to the LTI system in (4.27) for arbitrary input signals $u_v \in \mathscr{U}_{u_{\max},t_1}$ and sequence $(t_v)_{v=0}^{\infty} \in Q_\Delta$. This aim is formalized in Problem 1.

Problem 1. *Consider a stable LTI system with the impulse response matrix γ and let $u \in \mathscr{U}_{u_{max},t_1}$. Determine a bound $K_y < \infty$ such that*

$$\sup_{(t_v)_{v=0}^{\infty} \in Q_\Delta, t \geq 0} ||y(t)|| = \sup_{(t_v)_{v=0}^{\infty} \in Q_\Delta, t \geq 0} ||\gamma(t) \star u_{(t_v)_{v=0}^{\infty}}(t)|| < K_y, \tag{4.31}$$

whenever such bound exists.

4.2.2 Bound Existence

In this section, we show that the bound $K_y < \infty$ in (4.31) exists for any $u \in \mathscr{U}_{u_{\max},t_1}$ and any stable LTI system.

Theorem 8. *Consider a stable LTI system with the impulse response matrix γ. Let $\Delta > 0$, $t_l > 0$ and $u_v \in \mathscr{U}_{u_{max},t_l}$ for some t_l. Then, there exists a bound $K_y < \infty$ such that* (4.31) *holds.*

Proof. We first show that the input signal $u_{(t_v)_{v=0}^{\infty}}(t)$ is bounded, that is, $||u_{(t_v)_{v=0}^{\infty}}(t)|| \leq K_u < \infty$ for some constant K_u. Consider a time instant t and define $N_\Delta = \lceil \frac{t_1}{\Delta} \rceil$. If $t \geq t_1$, it holds that $||u_{(t_v)_{v=0}^{\infty}}(t)|| \leq N_\Delta u_{\max}$ since at most N_Δ successive input signals can be non-zero and the norm of all input signals is bounded by $u_{\max}$. If $t < t_1$, less than N_Δ successive input signals can be non-zero such that $||u_{(t_v)_{v=0}^{\infty}}(t)|| < N_\Delta u_{\max}$. Together, it is true that $||u_{(t_v)_{v=0}^{\infty}}(t)|| \leq N_\Delta u_{\max}$ for all t,

that is, $||u_{(t_v)_{v=0}^\infty}(t)||$ is bounded. Since the LTI system is stable, this implies that also $\sup_{(t_v)_{v=0}^\infty \in Q_\Delta, t \geq 0} ||y(t)||$ is bounded such that (4.31) holds. $\qquad\square$

4.2.3 General Bound Computation

In this section, we propose a method for computing a bound K_y in (4.31). To this end, we develop a new result that allows determining a bound of the output response for any input signal in $\mathscr{U}_{u_{max},t_l}$ depending on a bound on the impulse response of the LTI system.

Lemma 5. *Consider a stable LTI system with the impulse response matrix γ and let $c(t)$ be a function that is zero for $t < 0$ and non-negative monotonically decreasing for $t \geq 0$ such that $||\gamma(t)|| \leq c(t)$ for all $t \in \mathbb{R}$. Then, it holds for any input signal $u \in \mathscr{U}_{u_{max},t_l}$ that the output signal norm is bounded by*

$$||y(t)|| \leq u_{max} \int_0^{t_l} c(t-\tau)\,d\tau \qquad (4.32)$$

Furthermore, the bound in (4.32) is zero for $t < 0$, has a maximum at $t = t_l$ and non-negative monotonically decreasing for $t \geq t_l$.

Proof. It holds that

$$||y(t)|| = ||\gamma(t) \star u(t)|| = ||\int_0^t \gamma(t-\tau)\,u(\tau)\,d\tau|| \leq \int_0^t ||\gamma(t-\tau)||\,||u(\tau)||\,d\tau$$

$$\leq \int_0^{t_l} c(t-\tau)\,u_{max}\,d\tau = u_{max} \int_0^{t_l} c(t-\tau)\,d\tau.$$

In addition, it holds that $\int_0^{t_l} c(t-\tau)\,d\tau = 0$ for $t < 0$ since $c(t) = 0$ for $t < 0$. Considering $t \leq t_l$, it holds that $\int_0^{t_l} c(t-\tau)\,d\tau = \int_0^t c(t-\tau)\,d\tau$. That is, since $c(t)$ is non-negative, $\int_0^{t_l} c(t-\tau)\,d\tau \leq \int_0^{t_l} c(t_l-\tau)\,d\tau$ for any $t \leq t_l$. In addition, $c(t)$ being monotonically decreasing implies that $\int_0^{t_l} c(t'-\tau)\,d\tau \geq \int_0^{t_l} c(t-\tau)\,d\tau$ for any $t' \geq t \geq t_l$. That is, $\int_0^{t_l} c(t-\tau)\,d\tau$ indeed has a maximum at $t = t_l$ and is monotonically decreasing for $t \geq t_l$. $\qquad\square$

Respecting the result in Lemma 5 it is now possible to define a non-negative

and monotonically decreasing bound for $||y(t)||$ as

$$||y(t)|| \le f(t) := u_{\max} \begin{cases} \int_0^{t_1} c(t_1 - \tau)\,d\tau & \text{for } t \le t_1 \\ \int_0^{t_1} c(t - \tau)\,d\tau & \text{otherwise.} \end{cases} \tag{4.33}$$

Using Lemma 1 and (4.33) and writing $N_0 = \lceil \frac{t_1}{\Delta} \rceil$, it is now possible to evaluate (4.31). It holds that

$$\sup_{(t_v)_{v=0}^{\infty} \in Q_\Delta, t \ge 0} ||y(t)|| = \sup_{(t_v)_{v=0}^{\infty} \in Q_\Delta, t \ge 0} ||\gamma(t) \star u_{(t_v)_{v=0}^{\infty}}(t)||$$

$$= \sup_{(t_v)_{v=0}^{\infty} \in Q_\Delta, t \ge 0} \left\| \sum_{v=0}^{\infty} \gamma(t) \star u_v(t) \right\|$$

$$\le \sup_{(t_v)_{v=0}^{\infty} \in Q_\Delta, t \ge 0} \sum_{v=0}^{\infty} ||\gamma(t) \star u_v(t)||$$

$$\le \sup_{(t_v)_{v=0}^{\infty} \in Q_\Delta, t \ge 0} \sum_{v=0}^{\infty} u_{\max} \int_0^{t_1} c(t - \tau)\,d\tau \tag{4.34}$$

$$\le \sup_{(t_v)_{v=0}^{\infty} \in Q_\Delta, t \ge 0} \sum_{v=0}^{\infty} f(t) \tag{4.35}$$

$$= u_{\max} \left(N_0 \cdot \int_0^{t_1} c(t_1 - \tau)\,d\tau + \sum_{v=N_0}^{\infty} \int_0^{t_1} c(v\Delta - \tau)\,d\tau \right). \tag{4.36}$$

Here, (4.34) follows from Lemma 5, (4.35) follows from Lemma 1 and (4.36) follows from (4.33).

In order to ensure that the bound in (4.36) is finite, it is required to find a function $c(t) \ge ||\gamma(t)||$ such that the infinite sum $\sum_{v=N_0}^{\infty} \int_0^{t_1} c(v\Delta - \tau)\,d\tau$ converges. According to Lemma 5, $c(t)$ needs to be zero for $t < 0$, non-negative and monotonically decreasing for $t \ge 0$. In addition, it is desired that $c(t)$ constitutes a close bound for $||\gamma(t)||$ such that the bound in (4.36) is as well close.

In the literature [58, 63], analytical bounds for $||\gamma(t)||$ exist in the form

$$||\gamma(t)|| \le b(t) := ||C|| \, ||B|| \, e^{-\mu t} \left(\sum_{k=0}^{n-1} a_k t^k \right), \tag{4.37}$$

whereby a_k depends on the system matrices A, B, C in (4.27) and n depends on the bounding method which we will elaborate based on matrix exponential in Chapter 6. Such bound is non-negative, monotonically decreasing and close for large enough values of t. Accordingly, we suggest to select a threshold value θ and employ the bound $b(t)$ for times $t \geq t_\mathrm{f}$, whereby $b(t) \leq \theta$ for $t \geq t_\mathrm{f}$. In the remaining bounded interval $[0, t_\mathrm{f}]$, we find a monotonic bound $a(t) \geq ||\gamma(t)||$ by simulation similar to [64]. We perform a simulation run of $||\gamma(t)||$ for $t \in [0, t_\mathrm{f}]$ and determine a bounding function $a(t) \geq ||\gamma(t)||$ for $t \in [0, t_\mathrm{f}]$ with $a(t_\mathrm{f}) = b(t_\mathrm{f})$. In this work, we use a bounding function of the type

$$a(t) = m e^{-\eta t}. \tag{4.38}$$

As a result, $a(t)$ is non-negative and monotonically decreasing and $a(t) \geq ||\gamma(t)||$ for all $t \in [0, t_\mathrm{f})$. The overall bound for all $t \geq 0$ is then

$$c(t) := \begin{cases} 0 & \text{for } t < 0 \\ a(t) & \text{for } 0 \leq t \leq t_\mathrm{f} \\ b(t) & \text{for } t > t_\mathrm{f}. \end{cases} \tag{4.39}$$

By construction, $c(t)$ is zero for $t < 0$ and non-negative monotonically decreasing for $t \geq 0$. It remains to show that the infinite sum in (4.36) is bounded. This is shown in the following theorem.

Theorem 9. *Consider a stable LTI system with the set of input signals $\mathscr{U}_{u_{max}, t_l}$ and the impulse response bound $c(t)$ in (4.39). Let $\Delta > 0$ and $t_f > 0$. Write $N_0 = \lceil \frac{t_l}{\Delta} \rceil$, $N_1 = \lceil \frac{t_f}{\Delta} \rceil$ and $N_2 = \lfloor \frac{t_f + t_l}{\Delta} \rfloor$. Then, it holds for any $u \in \mathscr{U}_{u_{max}, t_l}$ that a suitable bound in (4.31) is given by*

$$K_y = u_{max} \frac{m}{\eta} \left(N_0 \left(1 - e^{-\eta t_l} \right) + \left(e^{\eta t_l} - 1 \right) \sum_{v=N_0+1}^{N_2} e^{-\eta v \Delta} \right)$$

$$+ u_{max} e^{-\mu N_1 \Delta} \sum_{l=0}^{n-1} c_l \sum_{i=0}^{l} \binom{l}{i} (N_1 \Delta)^{l-i} (-\Delta)^i \frac{d^i}{d(\mu \Delta)^i} \frac{1}{1 - e^{-\mu \Delta}}, \quad (4.40)$$

whereby c_l is computed with (4.41) *for $l = 0, \ldots, n-1$.*

$$c_l = \sum_{j=0}^{n-1-l} a_{l+j} \binom{l+j}{j} \int_0^{t_l} \tau^j e^{\mu \tau} d\tau. \tag{4.41}$$

Proof. It has to be shown that

$$\sup_{(t_\nu)_{\nu=0}^\infty \in Q_\Delta, t \geq 0} \left\| y(t) \right\| \leq K_y < \infty$$

for all possible input signals in $\mathscr{U}_{u_{\max}, t_1}$. Using (4.36), we compute

$$\sup_{(t_\nu)_{\nu=0}^\infty \in Q_\Delta, t \geq 0} \left\| y(t) \right\| \leq u_{\max} \left(N_0 \int_0^{t_1} c(t_1 - \tau) d\tau + \sum_{\nu=N_0}^\infty \int_0^{t_1} c(\nu \Delta - \tau) d\tau \right)$$

$$= u_{\max} \left(N_0 \int_0^{t_1} c(t_1 - \tau) d\tau + \sum_{\nu=N_0}^{N_1-1} \int_0^{t_1} a(\nu \Delta - \tau) d\tau + \right.$$

$$\tag{4.42}$$

$$+ \sum_{\nu=N_1}^{N_2} \left(\int_0^{\nu \Delta - t_f} b(\nu, \Delta - \tau) d\tau + \int_{\nu \Delta - t_f}^{t_1} a(\nu \Delta - \tau) d\tau \right)$$

$$\left. + \sum_{\nu=N_2+1}^\infty \int_0^{t_1} b(\nu \Delta - \tau) d\tau \right)$$

This computation considers that the convolution integral is applied to $a(t)$ before $t = t_f$ (until $\nu = N_1 - 1$), to $a(t)$ and $b(t)$ for $t_f \leq t \leq t_f + t_1$ ($N_1 \leq \nu \leq N_2$) and to $b(t)$ for $t \geq t_f + t_1$ ($\nu > N_2$). Further noting that $a(t)$ and $b(t)$ are non-negative, it also holds that

$$\sup_{(t_\nu)_{\nu=0}^\infty \in Q_\Delta, t \geq 0} \left\| y(t) \right\| \leq u_{\max} \left(N_0 \int_0^{t_1} a(t_1 - \tau) d\tau + \sum_{\nu=N_0}^{N_2} \int_0^{t_1} a(\nu \Delta - \tau) d\tau \right.$$

$$\tag{4.43}$$

$$\left. + \sum_{\nu=N_1}^\infty \int_0^{t_1} b(\nu \Delta - \tau) d\tau \right). \tag{4.44}$$

It can be directly computed for $t \geq t_1$ that

$$\int_0^{t_1} a(t_1 - \tau) \, d\tau = \frac{m}{\eta} (1 - e^{-\eta t_1}) \text{ and } \int_0^{t_1} a(t - \tau) \, d\tau = \int_0^{t_1} m e^{-\eta (t-\tau)} \, d\tau = \frac{m}{\eta} (e^{\eta t_1} - 1) e^{-\eta t}.$$
(4.45)

In order to evaluate $\int_0^{t_1} b(v\Delta - \tau) \, d\tau$, we use (4.37) and the binomial theorem and write

$$\int_0^{t_1} b(v\Delta - \tau) \, d\tau = \int_0^{t_1} \sum_{k=0}^{n-1} a_k (t - \tau)^k e^{-\mu (t-\tau)} \, d\tau$$

$$= e^{-\mu t} \int_0^{t_1} \sum_{k=0}^{n-1} a_k \sum_{i=0}^{k} \binom{k}{i} t^{k-i} (-\tau)^i e^{\mu \tau} \, d\tau.$$

Re-organizing the summations and the integral according to powers of t leads to

$$\int_0^{t_1} b(t - \tau) \, d\tau = e^{-\mu t} \sum_{l=0}^{n-1} t^l \sum_{j=0}^{n-1-l} a_{l+j} \binom{l+j}{j} \int_0^{t} (-\tau)^j e^{\mu \tau} \, d\tau \|$$

$$\overset{t \geq t_1}{=} e^{-\mu t} \sum_{l=0}^{n-1} t^l \sum_{j=0}^{n-1-l} a_{l+j} \binom{l+j}{j} \int_0^{t_1} (-\tau)^j e^{\mu \tau} \, d\tau$$

$$\leq e^{-\mu t} \sum_{l=0}^{n-1} t^l \underbrace{\sum_{j=0}^{n-1-l} a_{l+j} \binom{l+j}{j} \int_0^{t_1} \tau^j e^{\mu \tau} \, d\tau}_{=: \, c_l} = e^{-\mu t} \sum_{l=0}^{n-1} c_l t^l.$$

Then, the infinite sum in (4.43) results in

$$\sum_{v=N_1}^{\infty} \int_0^{t_1} b(v\Delta - \tau)\,d\tau = \sum_{v=N_1}^{\infty} e^{-\mu v\Delta} \sum_{l=0}^{n-1} c_l (v\Delta)^l$$

$$= e^{-\mu N_1 \Delta} \sum_{v=0}^{\infty} e^{-\mu v\Delta} \sum_{l=0}^{n-1} c_l (N_1\Delta + v\Delta)^l$$

$$= e^{-\mu N_1 \Delta} \sum_{l=0}^{n-1} c_l \Delta^l \sum_{v=0}^{\infty} e^{-\mu v\Delta}(N_1 + v)^l$$

$$= e^{-\mu N_1 \Delta} \sum_{l=0}^{n-1} c_l \Delta^l \sum_{i=0}^{l} \binom{l}{i} N_1^{l-i} \sum_{v=0}^{\infty} v^i e^{-\mu v\Delta}$$

$$= e^{-\mu N_1 \Delta} \sum_{l=0}^{n-1} c_l \Delta^l \sum_{i=0}^{l} \binom{l}{i} N_1^{l-i} (-1)^i \frac{d^i}{d(\mu\Delta)^i} \frac{1}{1 - e^{-\mu\Delta}}$$

$$(4.46)$$

Here, the last two identities are derived based on the binomial theorem and the geometric series. Using (4.45) and (4.46), the result in (4.40) directly follows. Since all the summations in (4.40) are finite, $K_y < \infty$. □

4.2.4 Illustrative Example

We illustrate the bound computation in Section 4.2.3 by a small example system with the matrices

$$A = \begin{bmatrix} 1 & 0 & 1 \\ 1 & -1 & 1 \\ -32 & 16 & -7 \end{bmatrix}, \quad B = \begin{bmatrix} 4 \\ 0 \\ 0 \end{bmatrix}, \quad C = \begin{bmatrix} 1 & 2 & 1 \end{bmatrix}$$

and the eigenvalues $\lambda_1 = -5$ and $\lambda_{2,3} = -1 \pm 2i$. Fig. 4.6 (a) shows the impulse response norm and the corresponding bound $c(t)$ in (4.39). Hereby, $a(t) = 3e^{-t}$ in (4.38) and $b(t) = 9.8e^{-t} \sum_{k=0}^{2} \frac{36^k t^k}{k!}$ in (4.37) are found suitable using $\theta = 10^{-9}$ and $t_f = 35$. In addition, Fig. 4.6 (b) and (c) show the bound in (4.32) and the corresponding function $f(t)$ in (4.33) for $t_1 = 4$ and $t_1 = 8$, respectively. For comparison, these figures also show example input responses for the time-limited

input signals in $\mathscr{U}_{1,t_1}$

$$u_1(t) = -\text{square}(2\pi/3t), \quad u_2(t) = -\text{triang}(2\pi/3t), \quad u_3(t) = -\cos(2\pi/3t).$$

Hereby, square(t), triang(t) and sin(t) denote the square wave, triangular wave and sine wave with period 2π, respectively. It can be seen that the corresponding output signals all stay below the computed bound.
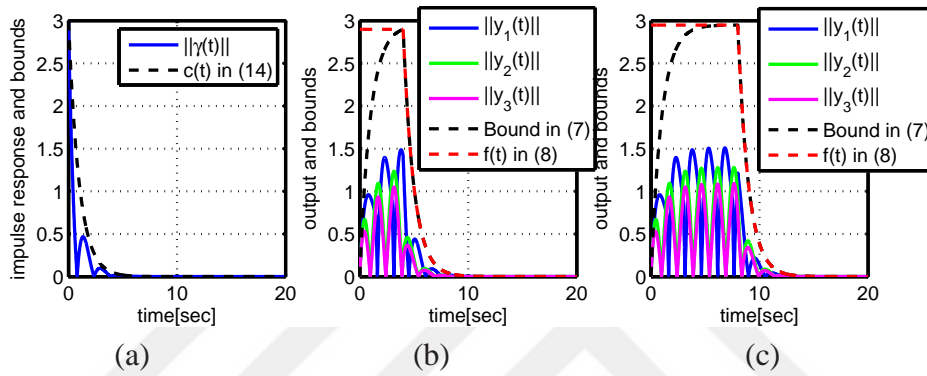
Figure 4.6: Bounds: (a) Impulse response; (b) $f(t)$ for $t_1 = 4$; (c) $f(t)$ for $t_1 = 8$.

Using $f(t)$, it is possible to evaluate the bound in (4.40). Example results for different combinations of t_1 and Δ are shown in Table 4.3. It is readily observed

Table 4.3: Bound K_y for different values of t_1 and Δ

$t_1 = 4, \Delta = 2$	$t_1 = 4, \Delta = 5$	$t_1 = 4, \Delta = 10$	$t_1 = 8, \Delta = 5$	$t_1 = 8, \Delta = 2$	$t_1 = 8, \Delta = 10$
9.3	4.0	3.0	15.2	6.3	3.3

that the bounds decrease when increasing Δ and when decreasing t_1. This is expected from the computation in (4.40). In addition, we compare a simulation with the repeated input $u_1(t) \in \mathscr{U}_{1,t_1}$ for different combinations of t_1 and Δ with the respective bound K_y as shown in Fig. 4.7.

It can be seen that a valid bound is obtained in all cases. Moreover, it can be observed that the bound appears closer in cases where $\Delta > t_1$. This can be explained by the conservativeness of the bound $f(t)$ for $t \leq t_1$ as can be seen in Fig. 4.6.
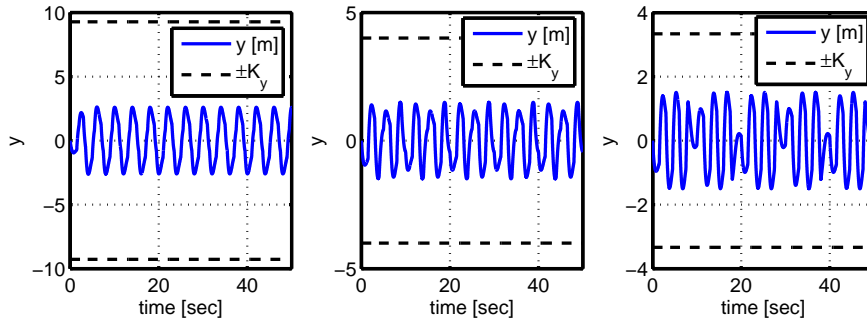
Figure 4.7: Comparison of repeated input response and close bound K_y: (a) $t_1 = 4$, $\Delta = 2$; (b) $t_1 = 4$, $\Delta = 5$; (c) $t_1 = 8$, $\Delta = 10$.

4.3 Input Repetitions for Distributed Interconnected Systems

The case of repeated input signals for general LTI systems is investigated in Section 4.1.1 and 4.2.1. Motivated by the vehicle string scenario, we next consider the case of interconnected systems. The basic block diagram of such distributed interconnected system is shown in Fig. 4.8.
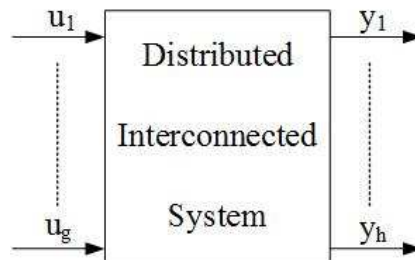
Figure 4.8: Distributed interconnected system

Here, the LTI system defined in Section 4.1.1 and 4.2.1 is extended as a system with g inputs, $u_i \in \mathbb{R}^{p_i}$ and h outputs, $y_j \in \mathbb{R}^{q_j}$. In view of the vehicle string application, the input signals can represent the impulse input signals in case of lane change completion (Section 4.1 or the feedforward input signals in case of opening/closing gap maneuvers (Section 4.2). From the application perspective, we are interested in the effect of repeated lane changes on the relevant signals such as distance errors of a vehicle string. Accordingly, we consider the effect of apply-

69

ing repeated inputs (impulses or time-limited input signals) to the interconnected system in Fig. 4.8. The main result is given in Theorem 10.

Theorem 10. *Consider a stable distributed interconnected system with the input signal vector $u = [u_1 u_2 \cdots u_g]^T$ and the impulse responses $\gamma_{i,j}(t)$ where $i \in \{i \in \mathbb{N} | 1 \le i \le g\}$ and $j \in \{j \in \mathbb{N} | 1 \le j \le h\}$. Here, assume $||\gamma_{i,j}(t)||_2 \le b_{i,j}(t)$, whereby*

$$b_{i,j}(t) := e^{-\alpha_{i,j} t} \left(\sum_{k=0}^{n_{i,j}-1} \frac{H_{i,j}^k t^k}{k!} \right). \tag{4.47}$$

Here, $n_{i,j}$ and $H_{i,j}$ depend on the respective bounding method. Then, for each $\psi, \exists t_\psi$ and H, α, n such that with

$$c(t) = \begin{cases} a(t) & \text{for } 0 \le t < t_\psi \\ b(t) = e^{-\alpha t} \left(\sum_{k=0}^{n-1} \frac{H^k t^k}{k!} \right) & \text{for } t \ge t_\psi. \end{cases} \tag{4.48}$$

$||\gamma_{i,j}(t)||_2 \le c(t)$ *for all $i \in \{i \in \mathbb{N} | 1 \le i \le g\}$ and $j \in \{j \in \mathbb{N} | 1 \le j \le h\}$.*

Proof. Choose

$$H = \max_{i,j} ||H_{i,j}||_2$$

$$n = \max_{i,j} n_{i,j}$$

$$\alpha = \min_{i,j} \alpha_{i,j}$$

Together all of the above taken into computation, since H, n and α is chosen accordingly, $b(t) \ge b_{i,j}(t) \forall i, j$

Moreover, we choose t_ψ in the same way as (4.22), such that $b(t) \le \psi$ for $t \ge t_\psi$. For $a(t)$, we simulate all $\gamma_{i,j}(t)$ until t_ψ. Take $\hat{a}(t) = \max_{i,j} \gamma_{i,j}(t) \forall t \le t_\psi$ and determine a monotonically decreasing bound $a(t) \ge \hat{a}(t)$ for $t \in [0, t_\psi)$ in analogy to (4.23). $\qquad \square$

In words, Theorem 10 states that the impulse response norm between each in-

put/output pair of an LTI system with multiple inputs and outputs can be bounded by a single monotonically decreasing function $c(t)$ in (4.48). This bound is again suitable for the application of Lemma 1.

Specifically, for the case of input impulses and time-limited inputs, the following corollaries are obtained.

Corollary 2. *Assume that the LTI system illustrated in Fig. 4.8 belongs to $\mathscr{L}$. Let the input u_i be given in (3.4), let $\Delta > 0$, let $t_\psi > 0$ be computed and let $c(t)$ be given as in (4.48). Write $N = \lfloor \frac{t_\psi}{\Delta} \rfloor$. Then, $\forall j \in 1,...,h$, it holds that*

$$
||y_j(t)||_2 \leq \sum_{\nu=0}^{N-1} a(\nu\Delta) + e^{-\alpha t_\psi} \sum_{k=0}^{n-1} \frac{H^k}{k!} \sum_{i=0}^{k} \binom{k}{i} t_\psi^{k-i} \Delta^i (-1)^i \frac{d^i}{d(\alpha\Delta)^i} \frac{1}{1-e^{-\alpha\Delta}}
$$
$$
< \infty. \tag{4.49}
$$

similar to Theorem 7.

That is, (4.49) represents an analytical bound for the norm of any output signal, when applying repeated impulse signals to any of the inputs.

Corollary 3. *Consider a stable LTI system with the set of input signals u_i as given in (3.10) in $\mathscr{U}_{u_{max},t_l}$ and the impulse response bound $c(t)$ in (4.48). m and η are defined depending on $a(t)$ of (4.48) with the bounding function logic of (4.38). Let $\Delta > 0$ and $t_\psi > 0$. Write $N_0 = \lceil \frac{t_l}{\Delta} \rceil$, $N_1 = \lceil \frac{t_\psi}{\Delta} \rceil$, $N_2 = \lfloor \frac{t_\psi + t_l}{\Delta} \rfloor$ and $a_k = \frac{H^k}{k!}$. Then, it holds for any $u \in \mathscr{U}_{u_{max},t_l}$ that a suitable bound $\forall j \in 1,...,h$ is given by*

$$
||y_j(t)||_2 \leq u_{max} \frac{m}{\eta} \left(N_0 \left(1 - e^{-\eta t_l}\right) + (e^{\eta t_l} - 1) \sum_{\nu=N_0+1}^{N_2} e^{-\eta \nu \Delta} \right)
$$
$$
+ u_{max} e^{-\alpha N_1 \Delta} \sum_{l=0}^{n-1} c_l \sum_{i=0}^{l} \binom{l}{i} (N_1\Delta)^{l-i} (-\Delta)^i \frac{d^i}{d(\alpha\Delta)^i} \frac{1}{1-e^{-\alpha\Delta}}, \tag{4.50}
$$

whereby c_l is computed with (4.51) for $l = 0,\dots,n-1$.

$$c_l = \sum_{j=0}^{n-1-l} a_{l+j} \binom{l+j}{j} \int_0^{t_l} \tau^j e^{\alpha \tau} d\tau. \qquad (4.51)$$

similar to Theorem 9.

That is, (4.50) represents an analytical bound for the norm of any output signal, when applying repeated time-limited signals to any of the inputs.

As an interesting point, we determine the case of $\Delta \to \infty$ for both (4.49) and (4.50). In the first case, it holds that

$$\lim_{\Delta \to \infty} ||y_j(t)||_2 \le a(0) = \max_t \gamma(t)$$

since $N_0 = 0$ and in the second case, we get

$$\lim_{\Delta \to \infty} ||y_j(t)||_2 \le u_{\max} \frac{m}{\eta}(1 - e^{-\eta t_1})$$

since $N_0 = 1$. That is, in both cases, the resulting bound corresponds to the application of a single input signal.

4.4 Summary and Discussion

The thesis study is motivated by lane changes in vehicle strings. The vehicle strings could for example be traveling on a highway, where each vehicle would move on its way and could perform lane changes at different time instants. Lane changes require opening/closing gap maneuvers and are associated to potential measurement errors and the corresponding jumps in state variables as discussed in Section 3.2 and 3.3. The main interest of the thesis is the existence and computation of bounds for the output signal norm when repeatedly applying the mentioned types of input signals. Finding such bounds allows quantifying the effect of lane changes on the longitudinal vehicle motion in strings and hence is important for the analysis of driving safety.

This chapter addresses the stated issues for both impulse inputs and time-

limited input signals. Bound existence is shown for both cases if the LTI system under consideration is linear.

Bounds for the lane change completion are computed based for arbitrary output signal and repeated impulses in Section 4.1. These results are then extended to the case of repeated impulses of systems with multiple inputs/outputs in Section 4.3. That is, the thesis provides an effective method for computing output bounds in the case of vehicle strings with many vehicles and lane change completions at different positions and times.

Results regarding opening/closing gaps for lane changes are obtained with a general formulation using the set of time-limited inputs. A bound for the output signal norm for repeated inputs is derived in Section 4.2. This scenario is extended to the case of repeated inputs of systems with multiple inputs/outputs in Section 4.3. As a result, thesis proposes an effective method for computing output bounds in the case of vehicle string with many vehicles and opening/closing gap maneuvers at different positions and times.

The closeness of bound is related with selection of Δ. That is to say, the $a(t)$ term of (4.48) add the contribution from the values where time is equal to Δ multiples. In practice, the simple observation is that if Δ is sufficiently bigger than the point where $a(t)$ is sufficiently small and converging to 0, then the bound computed remains to be convergent for increasing Δ.

Up to now, the two different cases of lane change completion and opening/closing gaps were investigated separately. Similar to the combination of both maneuvers in the definition of extended string stability in Section 3.4, we now combine the bound for both maneuvers in order to properly capture the practical CACC vehicle string lane change scenario. In doing so, we focus on the case of distributed interconnected systems since the vehicle string scenario will be special case of this concept.

Corollary 4. *Consider a stable LTI system with the set of input signals $u_1, \ldots, u_g$ as given in (3.10) in $\mathscr{U}_{u_{max}, t_l}$ and in (3.4). Let $\Delta > 0$ and $t_\psi > 0$. Let $c(t)$ be given as in (4.48). Combining the bounds computed separately in (4.49), (4.50) and (4.51), it holds that*

$$\|y_j(t)\|_2 \leq \sum_{v=0}^{N-1} a(v\Delta) + e^{-\alpha t_\psi} \sum_{k=0}^{n-1} a_k \sum_{i=0}^{k} \binom{k}{i} t_\psi^{k-i} \Delta^i (-1)^i \frac{d^i}{d(\alpha\Delta)^i} \frac{1}{1-e^{-\alpha\Delta}}$$

$$+ u_{max} \frac{m}{\eta} \left(N_0 (1-e^{-\eta t_l}) + (e^{\eta t_l} - 1) \sum_{v=N_0+1}^{N_2} e^{-\eta v\Delta} \right)$$

$$+ u_{max} e^{-\alpha N_1 \Delta} \sum_{l=0}^{n-1} c_l \sum_{i=0}^{l} \binom{l}{i} (N_1\Delta)^{l-i} (-\Delta)^i \frac{d^i}{d(\alpha\Delta)^i} \frac{1}{1-e^{-\alpha\Delta}}$$

$$\text{(4.52)}$$

That is, an analytical bound for the output signal norm in the case of repeated lane changes is given by (4.52). This bound combines the effect of opening/closing gaps and the lane change completion. An experimental evaluation of the presented results by simulation will be given in Chapter 5.

As an interesting point for future study, we note that the current formulation considers the case of impulse inputs and time-limited inputs separately. Nevertheless, it has to be noted that both formulations are based on impulse trains (repeated impulse inputs in Corollary 2) or convolutions with impulse trains (repeated time-limited inputs in Corollary 3). Hence, it would be interesting to determine a unified representation based on convolutions with impulse trains for the bound computation.

CHAPTER 5

LONGITUDINAL MANEUVER INPUTS TO VEHICLE STRINGS

The previous sections of the thesis provide new results for LTI systems that are subject to repeated input signals. Specifically, bounds for the output signal norm of LTI systems with repeated input impulses and time-limited input signals are determined in Section 4.1 and 4.2, respectively. Moreover, these results are extended to the case of LTI systems with multiple inputs and outputs in Section 4.3 and a combination of all results is achieved in Section 4.4.

Although these general results for LTI systems are motivated by performing lane change maneuvers in vehicle strings, they were not directly applied to vehicle strings up to now. This chapter shows that these results are indeed suitable for quantifying the effect of repeated lane changes of multiple vehicles in a string. Section 5.1 and 5.2 illustrate the case of applying repeated impulses and repeated time-limited input signals, respectively, to a single vehicle. The general case of a vehicle string with many vehicles and different repeated input signals is considered in Section 5.3

5.1 Application Example with Input Impulses for a Single Vehicle

5.1.1 Motivation and Description

We consider the scenario in Fig. 5.1 with a string of autonomous vehicles that follow each other in dense traffic. Each vehicle i has a length L_i, a position q_i, a velocity v_i and a distance $q_{i-1} - q_i$ to its predecessor vehicle. Introducing the desired distance $d_{i,r}$, the distance error e_i is

$$e_i = d_{i,r} - (q_{i-1} - q_i). \tag{5.1}$$
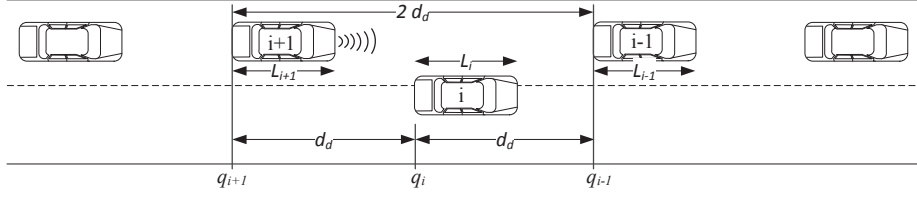
Figure 5.1: Lane change scenario in a vehicle string.

In this scenario, the vehicle spacing $q_{i-1} - q_i$ should be small in order to increase the traffic capacity. On the other hand, a sufficient vehicle spacing must be guaranteed for driving safety. This task can be accomplished by using *cooperative adaptive cruise control* (CACC) with the property of *string stability* that ensures the attenuation of fluctuations in the motion of a leader vehicle along the vehicle string [8, 26, 27]. In particular, bounds for the L_2-norm or the L_∞-norm of the distance error e_i can be established as described in Section 2.3.

The existing methods focus on fluctuations in the case where a string is already formed. However, the effect of modifying a vehicle string by adding or removing one or multiple vehicles after a lane change is not included in the discussion. This problem is investigated in the framework developed in this thesis.

To this end, we consider a lane change maneuver of vehicle i in Fig. 5.1. We use the CACC design in [8] to model the described scenario for vehicle $i+1$. The closed-loop system is represented by the state space model

$$
\dot{x} = \begin{bmatrix} 0 & -1 & -h & 0 \\ 0 & 0 & 1 & 0 \\ 0 & 0 & -\frac{1}{\tau} & \frac{1}{\tau} \\ \frac{K_p}{h} & -\frac{K_d}{h} & -K_d & -\frac{1}{h} \end{bmatrix} x + \begin{bmatrix} 1 \\ 0 \\ 0 \\ 0 \end{bmatrix} u(t)
$$

$$
y(t) = Cx. \tag{5.2}
$$

The state vector is $x = \begin{bmatrix} e_{i+1} & v_{i+1} & a_{i+1} & u_{i+1} \end{bmatrix}^T$ with the distance error e_{i+1}, velocity v_{i+1}, acceleration a_{i+1} and controller state u_{i+1}. τ is a plant parameter and K_d, K_p are the controller parameters. According to Section 3.2, the jump in the

distance error e_{i+1} after a lane change at a time t_v can be represented by an impulse input $u(t) = v\,\delta(t - t_v)$ with the maximum level v of the distance measurement error. Example output signals that are affected by the jump in the distance error measurement are e_{i+1} with $C = \begin{bmatrix} 1 & 0 & 0 & 0 \end{bmatrix}$ for driving safety or a_{i+1} with $C = \begin{bmatrix} 0 & 0 & 1 & 0 \end{bmatrix}$ for driving comfort. We write $\Gamma_e(s)$ and $\Gamma_a(s)$ for the respective transfer functions. Moreover, $k+1$ lane changes in front of vehicle $i+1$ at times t_v for $v = 0, 1, \ldots, k$ are represented by the input signal $u(t) = \sum_{v=0}^{k} v_v\,\delta(t - t_v)$, $v_v \leq v$. Assuming that different lane changes are separated by at least Δ in time, the effect of an arbitrary number of lane changes on the error signal e_{i+1} is bounded by $v\,\|\Gamma_e\|_{L_\infty,\Delta}$, whereas the effect on the acceleration signal a_{i+1} is bounded by $v\,\|\Gamma_a\|_{L_\infty,\Delta}$. Hereby, $\|\bullet\|_{L_\infty,\Delta}$ denotes the norm defined in Section 4.1.2.

5.1.2 Evaluation

We first consider $y(t) = e_{i+1}(t)$ using the parameters in Table 5.1. The corre-

Table 5.1: Parameters of the example system [8].

$L_{i+1} = 5\,\text{m}$	$r_{i+1} = 5\,\text{m}$	$h = 0.7\,\text{sec}$	$\tau = 0.1\,\text{sec}$	$K_d = 1.0$	$K_p = 0.25$

sponding impulse response

$$\gamma_e(t) = 0.004\,e^{-8.91t} - 1.73\,e^{-0.68t} + 2.72\,e^{-0.42t}$$

is positive and monotonically decreasing as can also be seen in Fig. 5.2. That is, (4.15) with $k = 3$, $l_i = 0$ for $i = 1, \ldots, k$, $a_{1,0} = 0.004$, $a_{2,0} = -1.73$, $a_{3,0} = 2.72$, $\lambda_1 = 8.91$, $\lambda_2 = 0.68$, $\lambda_3 = 0.42$ gives the exact bound

$$\|\Gamma_e\|_{L_\infty,\Delta} = \frac{0.004}{1 - e^{-8.91\Delta}} + \frac{-1.73}{1 - e^{-0.68\Delta}} + \frac{2.72}{1 - e^{-0.42\Delta}}.$$

For example, $\|\Gamma_e\|_{L_\infty,4} = 1.51$ (for $\Delta = 4$) and $\|\Gamma_e\|_{L_\infty,10} = 1.04$ (for $\Delta = 10$). That is, even in the (unrealistic) case of a lane change occurring every 4 sec with a measurement error of $v = 2\,\text{m}$, the distance error is bounded by $2 \cdot 1.51\,\text{m} = 3.02\,\text{m}$. Considering that $d_{i,r} = 5\,\text{m} + 5\,\text{m} + 0.7\text{sec} \cdot 20\,\text{m/sec} = 24\,\text{m}$ for a reference speed

of 20 m/sec, driving safety is ensured for an arbitrary number of lane changes. The exactness of the computed bound is further verified by the simulation in Fig. 5.2.
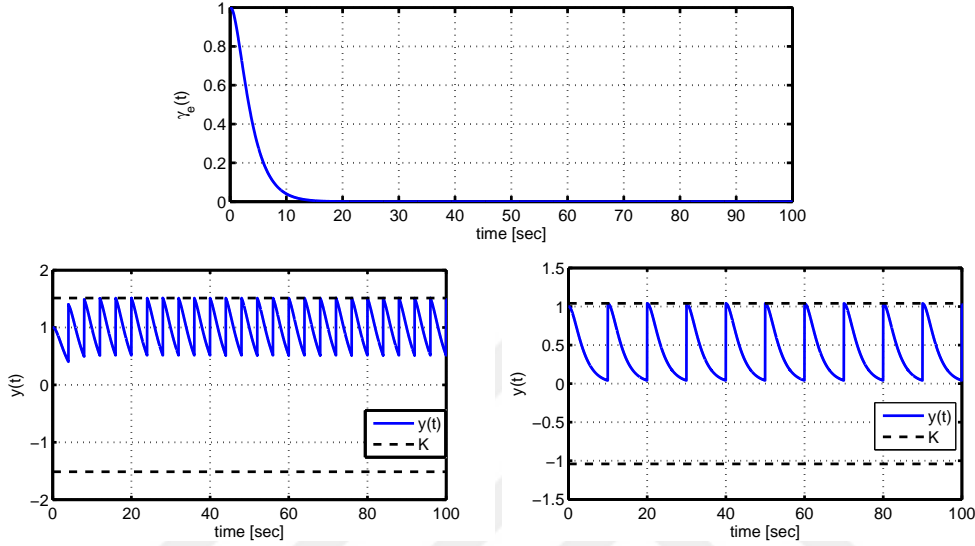
Figure 5.2: Monotonic impulse response $\gamma_e(t)$ (top); comparison of simulated response and $||\Gamma_e||_{L_\infty,\Delta}$ for $\Delta = 4$ (left) and $\Delta = 10$ (right).

We finally consider $y(t) = a_{i+1}(t)$. Here, the impulse response is not monotonic such that the bounding method in Section 4.1.4 is applied. We first obtain

$$b(t) = e^{-0.42t}\left(1 + 10.92t + 59.7t^2 + 217.3t^3\right)$$

and $a(t)$ in Fig. 5.3 by simulation. Choosing $\psi = 0.005$, it holds that $t_m = 54.6$ sec.

Using (4.40), we find $||\Gamma_a||_{L_\infty,4} \leq 0.172$ for $\Delta = 4$ and $||\Gamma_a||_{L_\infty,10} \leq 0.125$ for $\Delta = 10$. In both cases, the resulting acceleration bounds are far below the acceleration limit for comfortable driving which is in the range of $2 - 3$ m/s^2 [65]. We further perform a simulation of the system in (5.2) with repeated unit impulses that are separated by $\Delta = 4$ sec and $\Delta = 10$ sec in time as shown in Fig. 5.3. It is readily observed that the computed bound on $||\Gamma_a||_{L_\infty,\Delta}$ is close.
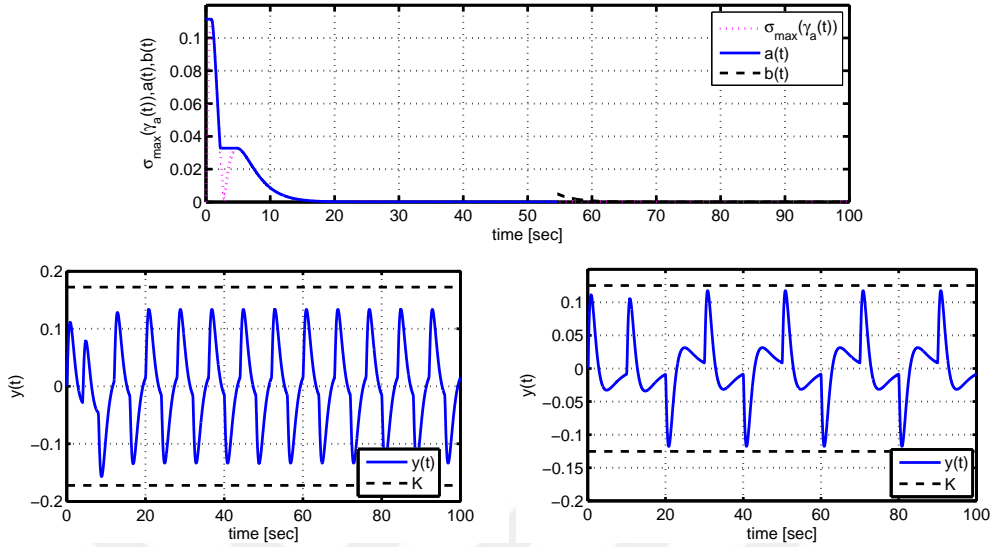
Figure 5.3: Monotonic bound computation for $\sigma_{\max}(\gamma_a(t))$ (top); comparison of simulated response and $||\Gamma_a||_{L_\infty, \Delta}$ for $\Delta = 4$ (left) and $\Delta = 10$ (right).

5.2 Application Example for Repeated Time-Limited Inputs for a Single Vehicle

The plant model, vehicle following, controller design for CACC and the relevant parameters were already described in Chapter 2 and lane change maneuvers in Chapter 3. This section first gives an example for a repetition of the same input signal u. After that, the example will be extended with input signals from a set as defined in Section 3.3.

In order to perform gap opening and closing maneuvers of a vehicle i in the described architecture, we use the feedforward input signal u_i^{ff} and a feedforward reference signal q_i^{ff} for vehicle i as was discussed in Section 3.3. The generation of suitable input signals is discussed in the subsequent section.

5.2.1 Input Signal Generation

If vehicle i opens/closes a gap, it is desired to increase/decrease the vehicle distance d_i by the velocity-dependent value $d_{i,r}$ within a certain time T. This behav-

ior can be formulated in the form of a linear optimal control problem with state constraints

$$\min J = \int_0^T F(z_i, u_i^{\text{ff}}, t)\, dt \tag{5.3}$$

subject to the dynamic plant constraints

$$\dot{q}_i = v_i; \quad \dot{v}_i = a_i; \quad \dot{a}_i = \frac{-1}{\tau} \cdot a_i + \frac{1}{\tau} \cdot u_i^{\text{ff}} \tag{5.4}$$

initial and terminal conditions

$$q_i(0) = 0, \quad v_i(0) = v, \quad a_i(0) = 0, \quad q_i(T) = d_{i,r}, \quad v_i(T) = v, \quad a_i(T) = 0 \tag{5.5}$$

additional constraints

$$v_{\min} \leq v_i(t) \leq v_{\max}, \quad a_{\min} \leq a_i(t) \leq a_{\max} \tag{5.6}$$

(5.4) is a state space realization of that plant transfer function $G(s)$ for vehicle i with the state $z_i = \begin{bmatrix} q_i & v_i & a_i \end{bmatrix}'$, T is the terminal time, J denotes the objective function and it is assumed that the vehicle string travels at a constant velocity v. In addition, in order to maintain driver comfort, the acceleration and velocity variation during such maneuver is limited using (5.6). Depending on the desired maneuver, different objective functions can be used. In this paper, we use $F_1(z_i, u_i^{\text{ff}}, t) = 1$ in order to minimize the maneuver time and $F_2(z_i, u_i^{\text{ff}}, t) = (u_i^{\text{ff}})^2$ in order to minimize the accumulated input signal. Example input signals for opening gaps at different velocities and with different objective functions are generated using the PROPT solver [66] according to Table 5.2 and are shown together with the created gap and acceleration in Fig. 5.4. Note that the same signals can be used for closing gaps when multiplying by -1.

It can be seen from the figure that the considered gap opening/closing scenario requires input signal levels that are bounded by ± 2.5 m/sec and their duration is

Table 5.2: Input signals for different velocities and objective functions

$v = 10\,\text{m/sec},\ F_1$	$v = 20\,\text{m/sec},\ F_1$	$v = 30\,\text{m/sec},\ F_1$
u_1	u_2	u_3
$v = 10\,\text{m/sec},\ F_2$	$v = 20\,\text{m/sec},\ F_2$	$v = 30\,\text{m/sec},\ F_2$
u_4	u_5	u_6
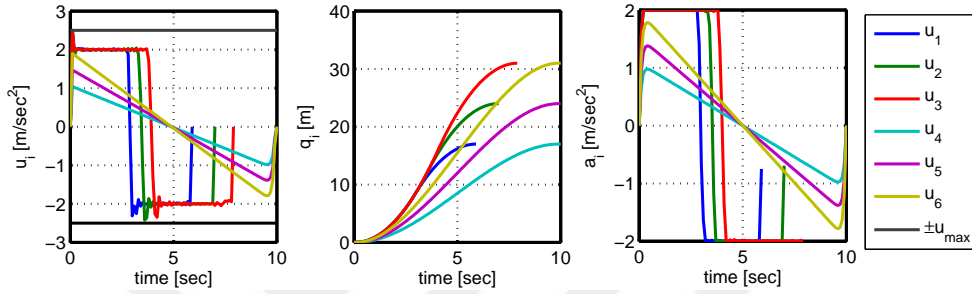
Figure 5.4: Different input signals for $T \leq 10$.

below 10 sec. That is, it is possible to employ the set of input signals $\mathscr{U}_{2.5,10}$.

5.2.2 Repeated Application of the Same Input Signal

We apply the obtained bound computation in Section 4.2 to the platooning example with the feedback loop in Fig. 3.9, the input signal $u_1 \in \mathscr{U}_{2.5,10}$ and output signal e_{i+1} in Fig. 3.10 for opening a gap.

Using the controller design of [33], the bound $c(t)$ in (4.39) has the coefficients in Table 5.3. The last maximum of $c(t)$ is at $t_\text{m} = 3.2$ s. Choosing $\psi = 0.01$, we obtain $t_\text{f} = 180.7$ s in (4.39).

Table 5.3: Coefficients of $c(t)$.

c_0	c_1	c_2	c_3
$6.1 \cdot 10^{35}$	$4.8 \cdot 10^{35}$	$1.6 \cdot 10^{35}$	$2.7 \cdot 10^{34}$

c_4	c_5	c_6	μ
$2.7 \cdot 10^{33}$	$1.5 \cdot 10^{32}$	$3.1 \cdot 10^{30}$	0.55

We further perform a simulation of the output response in Matlab/Simulink

81

with a simulation error $e_{\text{sim}} \approx 0.001$ to determine the bound $a(t)$ for $t < t_{\text{f}}$. The bounds $a(t)$ and $c(t)$ are shown in Fig. 5.5.
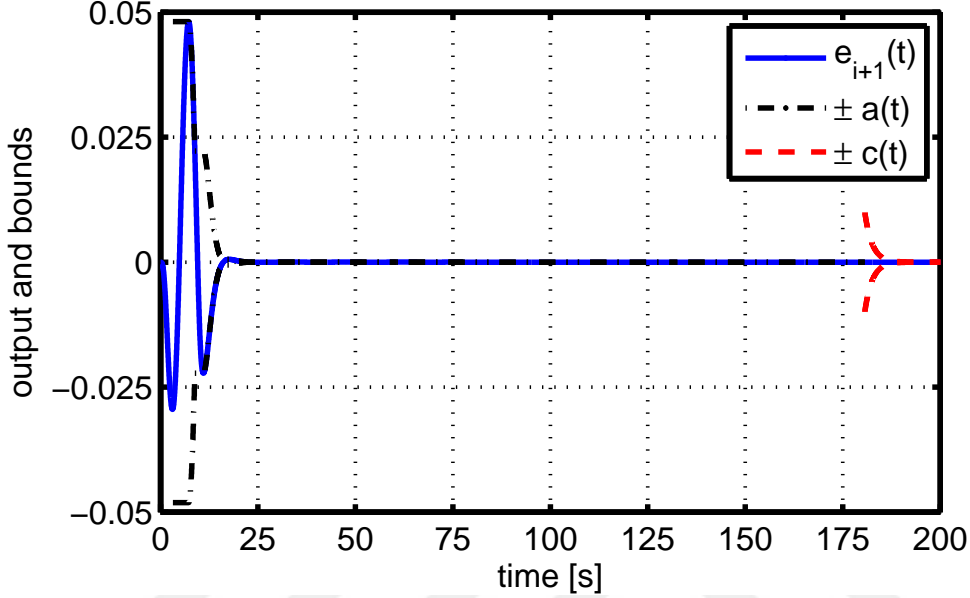
Figure 5.5: Bounds for the platooning example.

Choosing $\Delta = 6\,\text{s}$, we compute $K_u = 0.125\,\text{m}$ and choosing $\Delta = 20\,\text{s}$, we compute $K_u = 0.058\,\text{m}$. We further compare the bounds with a simulation of the system where gaps are repeatedly opened by vehicle i with a dwell-time of $\Delta = 6\,\text{s}$ and $\Delta = 20\,\text{s}$. The results are shown in Fig. 5.6. It can be seen that the computed bound is close, especially for large values of Δ. The conservativeness for small values of Δ can be explained by inspecting the bound $a(t)$ and the actual output signal e_{i+1} in Fig. 5.5. Here, repeated "open gap" maneuvers do not lead to an accumulation in the error signal due to the sign change in e_{i+1}.

In contrast, an accumulation of the error can be observed when alternating 'open gap' and 'close gap' maneuvers. Since the input signal $\hat{u}_i^{\text{ff}}$ for closing a gap fulfills $|\hat{u}_i^{\text{ff}}(t)| = |u_i^{\text{ff}}(t)|$ for all $t \geq 0$, the same bound $f(t)$ is valid in both cases. That is, the same bound K_u is obtained when alternating u_i^{ff} and $\hat{u}_i^{\text{ff}}$ according to Theorem 9. Fig. 5.7 shows a simulation where 'open gap' and 'close gap' maneuvers are alternated for $\Delta = 6\,\text{s}$ and $\Delta = 20\,\text{s}$. In this case, the bound K_u for
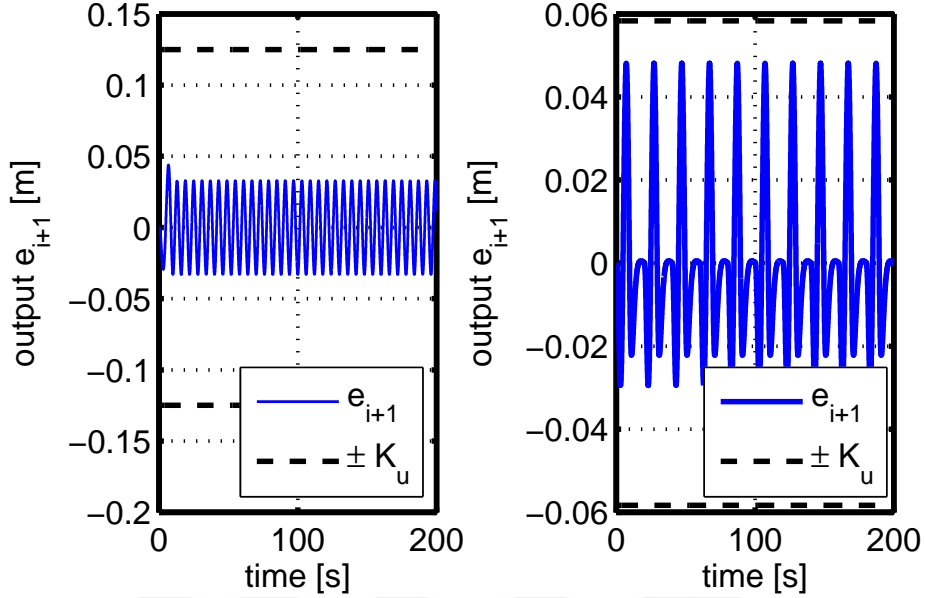
Figure 5.6: Simulation and bound for $\Delta = 6\,\mathrm{s}$ (left) and $\Delta = 20\,\mathrm{s}$ (right).

$\Delta = 6\,\mathrm{s}$ is less conservative.

In summary, it can be confirmed that driving safety is ensured when performing arbitrary 'open gap' and 'close gap' maneuvers. Even in the case where a gap is opened/closed every $\Delta = 6\,\mathrm{s}$, it holds that the accumulated distance error stays below 0.125 m. Considering that the desired distance is $d_{i,r} = 29\,\mathrm{m}$ at a speed of 20 m/s [33], such error is negligible.

5.2.3 Repeated Application of Different Input Signals

We next evaluate the bound in (4.40) for all input signals in $\mathcal{U}_{2.5,10}$. We find $a(t) = 0.016\,e^{-0.33t}$ by simulation and $b(t) = 10.1\,e^{-0.55t} \sum_{k=0}^{8} \dfrac{11.4^k t^k}{k!}$ using a minimal realization of (3.5). Choosing scenarios, where vehicle i potentially has to open a gap every $\Delta = 10\,\mathrm{sec}$ and $\Delta = 20\,\mathrm{sec}$ and using $\theta = 10^{-5}$ ($t_\mathrm{f} = 135$), the bounds $K_y = 0.25\,\mathrm{m}$ and $K_y = 0.13\,\mathrm{m}$ are obtained, respectively. Fig. 5.8 shows a comparison of the bounds with a simulation of different repeated input signals.

It can be seen that the computed bound is valid for the repeated input signals
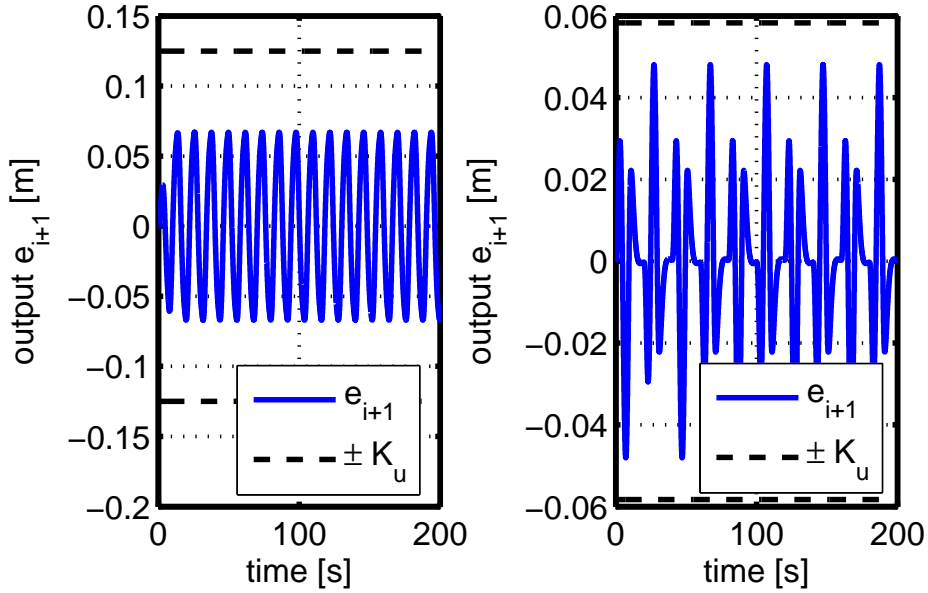
Figure 5.7: Simulation and bound for $\Delta = 6\,\mathrm{s}$ (left) and $\Delta = 20\,\mathrm{s}$ (right).

chosen from $\mathscr{U}_{2.5,10}$. In addition, it can be concluded that the error signal of vehicle i (follower vehicle of predecessor vehicle on which feedforward signals are applied) remains below $0.25\,\mathrm{m}$ even if the predecessor vehicle i performs gap opening maneuvers in $\mathscr{U}_{2.5,10}$ every $10\,\mathrm{sec}$ in the described setting. Considering that the desired distance at a speed of $v = 10\,\mathrm{m/sec}$ is $d_{r,i} = 17\,\mathrm{m}$, this does not cause a violation of driving safety.

5.2.4 Discussion

After demonstrating the proposed bound computation by means of the application example, we next discuss the obtained results.

First, we note that the evaluation of the bound in (4.40) has two addends. The first addend is computed based on the bound $a(t)$ in (4.38) that is obtained using simulation. It determines a bound for up to N_2 repetitions of input signals in $\mathscr{U}_{u_{\max},t_1}$. The second addend depends on the bound $b(t)$ in (4.37) and captures the effect of applying an arbitrary number of input signals.
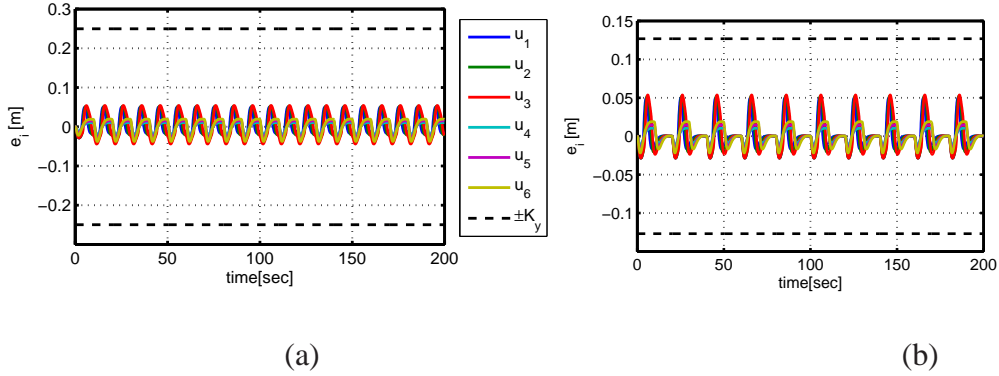
Figure 5.8: Comparison of bound and simulation for repeated inputs: (a) $\Delta = 10\,\mathrm{sec}$; (b) $\Delta = 20\,\mathrm{sec}$.

In principle, it could be argued that the rather intricate second addend can be avoided if it is ensured that the input signal is repeated no more than N_2 times. Nevertheless, such assumption poses a restriction on the possible system behavior. In our application example, this would mean that only a limited number of N_2 opening/closing gap maneuvers is permitted while guaranteeing the bound on the error signal. Precisely, the advantage of the bound in (4.40) including the second addend is that a bound is obtained for any number of input signal repetitions. In addition, the evaluation of (4.40) is an offline computation that only depends on the range of the possible input signals in $\mathscr{U}_{u_{\max},t_1}$ and the impulse response bound of the LTI system in (4.39). Furthermore, choosing θ small enough (and hence t_{f} large enough) always ensures that the contribution of the second addend in (4.40) is small. For example, when computing the bound $K_y = 0.25\,\mathrm{m}$ for the input signal u_3 and $\Delta = 10\,\mathrm{sec}$ in Section 5.2.1, the first addend amounts to $0.249\,\mathrm{m}$ and the second addend is $0.001\,\mathrm{m}$.

Finally, we recall that the set $\mathscr{U}_{u_{\max},t_1}$ is obtained by inspecting the expected input signals to be applied to the LTI system as illustrated in Section 5.2.3. A benefit of the proposed method is that any new input signal can be applied without violating the computed bound as long as it belongs to $\mathscr{U}_{u_{\max},t_1}$.

5.3 Vehicle String Application

Effects of multiple impulses and time-limited inputs with a sufficient temporal spacing Δ were investigated for a single follower vehicle in Section 5.1 and Section 5.2. Now, we consider the effect of lane change maneuvers on a complete vehicle string composed of N vehicles. The main contributions compared to the previous results of Section 5.1 and 5.2 is that we now compute the bound of impulse and time-limited responses for the whole vehicle string. To this end, Section 5.3.1 identifies a relation among the impulse responses between different vehicles. Then, it is possible to apply the result for LTI systems with multiple inputs and outputs in Section 4.3.

5.3.1 Vehicle Strings Structure

It is important to note that the dynamic matrix of a vehicle string in (3.2) has a special structure. For each transfer function, we use the standard equation from state space to transfer function conversion:

$$\Lambda(s) = C(sI - A)^{-1}B$$

Writing $\Delta(s) = (sI - A_0)$, with the help of the lower triangular matrix structure, we compute

$$(sI - A)^{-1} =$$

$$
\begin{bmatrix}
\Delta^{-1} & 0 & \cdots & 0 & 0 & 0 \\
\Delta^{-1}A_1\Delta^{-1} & \Delta^{-1} & \ddots & 0 & 0 & 0 \\
(\Delta^{-1}A_1)^2\Delta^{-1} & \Delta^{-1}A_1\Delta^{-1} & \ddots & 0 & 0 & \\
\vdots & \ddots & \ddots & \vdots & & \vdots \\
(\Delta^{-1}A_1)^{n-2}\Delta^{-1} & (\Delta^{-1}A_1)^{n-3}\Delta^{-1} & \cdots & (\Delta^{-1}A_1)^1\Delta^{-1} & \Delta^{-1} & 0 \\
(\Delta^{-1}A_1)^{n-1}\Delta^{-1} & (\Delta^{-1}A_1)^{n-2}\Delta^{-1} & \cdots & (\Delta^{-1}A_1)^2\Delta^{-1} & (\Delta^{-1}A_1)^1\Delta^{-1} & \Delta^{-1}
\end{bmatrix}
$$

having the form of a block Toeplitz matrix with identical transfer functions along the diagonals.

That is, the transfer matrix between each vehicle state and the successor vehicle states can be easily computed. Likewise, the transfer matrix between each input signal and output signal can be easily determined. For example using the input vector $\begin{bmatrix} B_1 & 0 & 0 & \vdots & 0 & 0 \end{bmatrix}^T$ and the output vector $\begin{bmatrix} 0 & C_2 & 0 & \cdots & 0 & 0 & 0 \end{bmatrix}$, we get the transfer function

$$\Gamma(s) = C_2 \Delta^{-1} A_1 \Delta^{-1} B_1$$

With the assumption that the string is homogenous and using the transfer matrix representation above, the relation between any vehicle state and successor vehicle states can be generalized.

Proposition 1. *Consider a vehicle string with N vehicles and impulse responses $\gamma_{i,j}$ from the state of vehicle i to the state of successor vehicle $j > i$. Then, it holds that any impulse response $\gamma_{i,j}$ is identical to the impulse response $\gamma_{1,j-i+1}$.*

Proof. We show that, for any $i, j \in \{i, j \in \mathbb{N} | 1 \leq i \leq j \leq N\}$ by using the lower triangular matrix special structure

$$\Gamma_{i,j}(s) = (\Delta^{-1} A_1) \cdots (\Delta^{-1} A_1) \Delta^{-1} = (\Delta^{-1} A_1)^{j-i} \Delta^{-1} = \Gamma_{1,j-i+1}(s).$$

$\square$

Practically this means, as an example, 2nd to 4th vehicle and 3rd to 5th vehicle and 6th to 8th vehicle have the same state-to-state relation. The important consequence of Proposition 1 is that it is only necessary to compute evaluate the impulse response matrices from the first vehicle state to all successor vehicle states, which include the impulse response matrices of the successor vehicles.

Additionally, as was concluded in the Section 3.4, whenever multiple gap/opening or closing maneuvers and different input signals are applied to the system, using the bound of (3.15) a large bound which is practically infeasible. We next compute a new feasible, improved bound for the whole vehicle string.

5.3.2 Multiple Impulse to Vehicle String

We first consider $y(t) = [e_{i+1}(t) \quad e_{i+2}(t) \quad \cdots \quad e_n(t)]$ using the parameters in Table 5.4.

Table 5.4: Parameters of the example system [8].

$L_{i+1} = 5\,\mathrm{m}$	$r_{i+1} = 5\,\mathrm{m}$	$h = 0.8\,\mathrm{sec}$	$\tau = 0.4\,\mathrm{sec}$	K_{ff} by H_∞	K_{fb} by H_∞

For example, $||\Gamma_e||_{L_\infty,7} = 1.02$ (for $\Delta = 7$) as given in the Fig. 5.9.

That is, even in the case of a lane change occurring in the string for every 7 sec with a measurement error of $v = 2\,\mathrm{m}$, the distance error is bounded by $2 \cdot 1.02\,\mathrm{m} = 2.04\,\mathrm{m}$. Considering that $d_{i,r} = 5\,\mathrm{m} + 5\,\mathrm{m} + 0.8\mathrm{sec} \cdot 20\,\mathrm{m/sec} = 26\,\mathrm{m}$ for a reference speed of 20 m/sec, driving safety is ensured for an arbitrary number of lane changes.
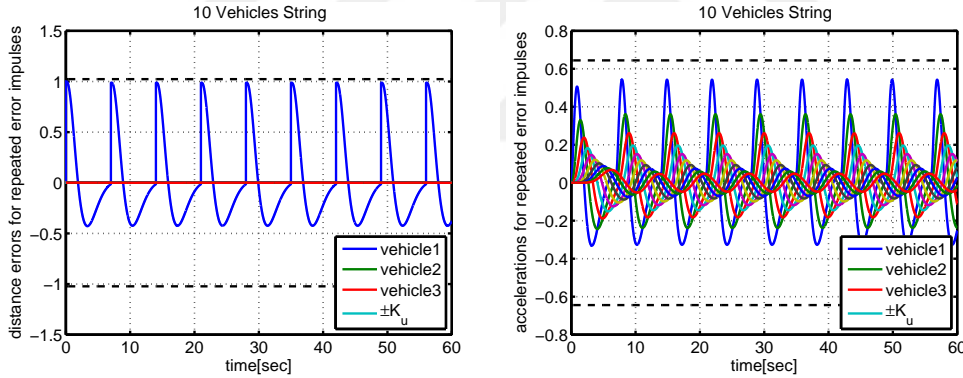
Figure 5.9: Multiple error impulse response of vehicle string: $\gamma_e(t)$ (left) and $\gamma_a(t)$ (right) for $\Delta = 7$

We next consider $y(t) = [a_{i+1}(t) \quad a_{i+2}(t) \quad \cdots \quad a_n(t)]$ using the same parameters of Table 5.4. Using (4.40), we find $||\Gamma_a||_{L_\infty,7} = 0.64$ for $\Delta = 7$. In this case, the resulting acceleration bounds are far below the acceleration limit for comfortable driving which is in the range of $2 - 3\,\mathrm{m/s^2}$ [65]. We further perform a simulation of the system in (5.2) with repeated unit impulses that are separated by $\Delta = 7$ sec in time as shown in Fig. 5.9. It is readily observed that the computed bound on $||\Gamma_a||_{L_\infty,\Delta}$ is close.

5.3.3 Multiple Time-Limited Input to Vehicle String

We apply the results to the platooning example with the feedback loop in Fig. 3.9, the input signal $u_1 \in \mathscr{U}_{2.5,10}$ and output signal $[e_{i+1}(t) \quad e_{i+2}(t) \quad \cdots \quad e_n(t)]$ in Fig. 3.10 and $[a_{i+1}(t) \quad a_{i+2}(t) \quad \cdots \quad a_n(t)]$ in Fig. 3.10 for opening a gap.

Using the H_∞ controller design of Matlab/Simulink, the bound $c(t)$ in (4.39) is computed. Choosing $\psi = 0.005$, we obtain $t_f = 59.94\,\mathrm{s}$ in (4.39).

We first performed a simulation of the output response in Matlab/Simulink with a simulation error $e_{\mathrm{sim}} \approx 0.001$ to determine the bound $a(t)$ for $t < t_f$.

Choosing $\Delta = 5\,\mathrm{s}$, we compute $K_u = 1\,\mathrm{m}$ and $K_u = 6.14\,\mathrm{m/s^2}$ for $e(t)$ and $a(t)$ respectively. We compare the bounds with a simulation of the system where gaps are repeatedly opened by vehicle i with a dwell-time of $\Delta = 5\,\mathrm{s}$. The results are shown in Fig. 5.10. It may be asserted that the computed bound is conservative, due to accumulation of error by repeated exogenous acceleration input. However, for larger values of Δ the bound is quickly getting closer by inspecting the bound $a(t)$ and $e(t)$ in Fig. 5.11. With $\Delta = 15\,\mathrm{s}$, we compute $K_u = 0.0013\,\mathrm{m}$ and $K_u = 2.69\,\mathrm{m/s^2}$ for $e(t)$ and $a(t)$ respectively.
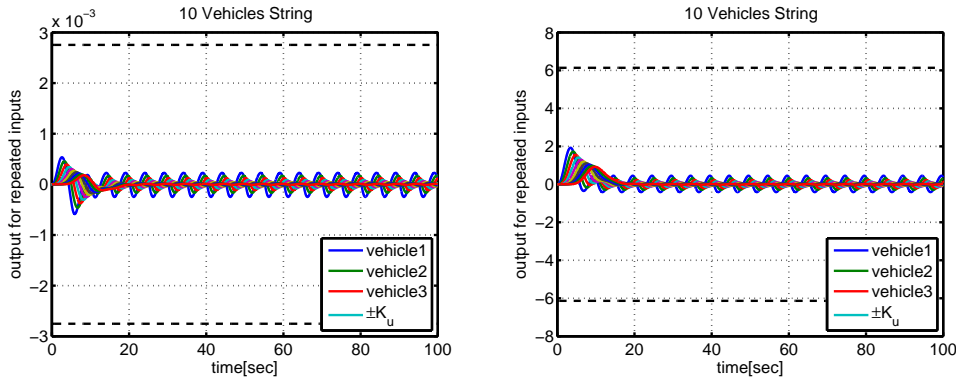
Figure 5.10: Simulation and bound for $\Delta = 5\,\mathrm{s}$ distance error(left) and acceleration (right).

In summary, it can be confirmed that driving safety is ensured when performing arbitrary 'open gap' and 'close gap' maneuvers. Even in the case where a gap is opened/closed every $\Delta = 5\,\mathrm{s}$, it holds that the accumulated distance error stays
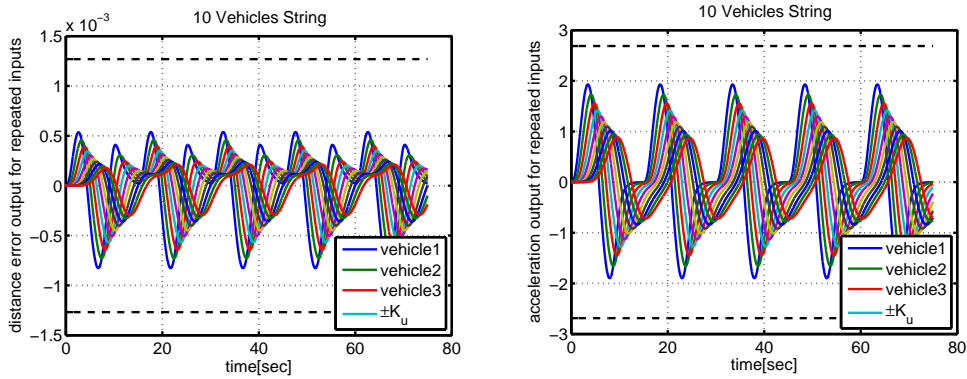
Figure 5.11: Simulation and bound for $\Delta = 15$ s distance error(left) and acceleration (right).

below 0.005 m. Considering that the desired distance is $d_{i,r} = 29$ m at a speed of 20 m/s [33], such error is negligible.

5.4 Summary and Discussion

In summary, the main subject of this chapter is the application of the general results on norm bounds for the output signal of stable LTI systems derived in Chapter 4.

Section 5.1 applies the bound computation for LTI systems with repeated input impulses to the case of lane change completion in vehicle strings. It is shown that suitable analytical bounds for the error signal of successor vehicles are found when realizing vehicle following be cooperative adaptive cruise control (CACC). Moreover, simulations illustrate that the obtained bounds are close especially in case where the repeated input impulses are separated by a sufficiently large dwell-time.

Section 5.2 focuses on the bound computation for LTI systems with repeated time-limited input signals for opening/closing gaps in vehicle strings. Using the analytical bounds derived in Section 4.2, it is shown that very small error signals are encountered when using CACC and the closeness of the analytical bounds is confirmed by simulation experiments.

Finally, Section 5.3 extends the previous studies in this section for the case of vehicle strings with many vehicles. Here, it is possible to employ the general result for LTI systems with multiple inputs and outputs in Section 4.3. It is shown that the special structure of a homogeneous vehicle string makes it sufficient to apply this result to a reduced number of impulse response matrices. Using the analytical bounds, safe driving during lane changes is ensured as long as the dwell-time between lane changes is not too small.

It has to be noted that the analytical bounds in Section 4.1 and 4.2 depend on the evaluation of the impulse response bound $b(t)$ in (4.20). In the course of this thesis study, it turned out that existing methods for computing this bound suffer from numerical problems in case of large systems. Since the thesis focuses on vehicle strings, whose dynamic models have many states, it was necessary to develop an original improved method for the numerical computation of $b(t)$. This additional work is the subject of Chapter 6.

CHAPTER 6

LINEAR ALGEBRAIC COMPUTATIONS FOR BOUNDS DERIVATIONS

The results in the previous chapters are based on the computation of a bound $b(t)$ for the impulse response matrix of LTI systems as in (4.20). Although such bounds have been determined in the existing literature, it turns out that their numerical evaluation becomes infeasible for large LTI systems. Because of this reason, this chapter develops new methods for the numerical evaluation of norm bounds for the impulse response matrix of large LTI systems. Since the obtained method is general and not limited to vehicle applications, it is presented in a separate self-contained chapter.

6.1 Preliminaries

We first introduce the necessary notation in Section 6.1.1. Then, we state several basic results for matrices and block matrices as well as the matrix exponential function in Section 6.1.2. We formalize the Jordan canonical form in Section 6.1.3 and recall the Schur decomposition in Section 6.1.4. Finally, we summarize and discuss existing bounds for the matrix exponential function in Section 6.1.5.

6.1.1 Notation

Consider a quadratic matrix $A \in \mathbb{C}^{n \times n}$. We write a_{ij} for the entry in the i-th row and j-th column of A. The set of eigenvalues of A is denoted as $spec(A)$ and $\alpha(A) = \max\{Re(\lambda) | \lambda \in spec(A)\}$ is the largest real part of any eigenvalue in $spec(A)$. Writing $||A||$ for the induced matrix norm, $\kappa(A) = ||A^{-1}|| \cdot ||A||$ is the condition number of A if A is invertible. Furthermore, using $A^\star$ for the conjugate

transpose of A, $\mu(A) = \max\{\mu \mid \mu \in spec((A + A^\star)/2)\}$ is the logarithmic norm of A [67].

We write I_n for the identity matrix with dimension n, $\mathscr{T}$ for the set of upper triangular matrices such that $a_{i,j} = 0$ for all $1 \leq i, j \leq n$ with $i > j$ if $A \in \mathscr{T}$ and $\mathscr{S} \subset \mathscr{T}$ for the set of strictly upper triangular matrices such that $a_{i,j} = 0$ for all $1 \leq i, j \leq n$ with $i \geq j$ if $A \in \mathscr{S}$. A matrix A is nilpotent if $A^k = 0$ for some index k and the smallest such k is called the nilpotency index of A. Consider a matrix $A \in \mathscr{T}$. We write $A = A_D + A_N$, whereby A_D is the diagonal part of A and $A_N \in \mathscr{S}$ is the strictly upper triangular part of A.

In this chapter, we employ block matrices with quadratic blocks on the main diagonal. In general, we write

$$B = \begin{bmatrix} B_{11} & B_{12} & \cdots & B_{1m} \\ B_{21} & B_{22} & \cdots & B_{2m} \\ \vdots & \vdots & \ddots & \vdots \\ B_{m1} & B_{m2} & \cdots & B_{mm} \end{bmatrix}$$

for an $m \times m$ block matrix, whereby $B_{ii} \in \mathbb{C}^{n_i \times n_i}$ is an $n_i \times n_i$ complex matrix for $1 \leq i \leq m$ and $B_{ij} \in \mathbb{C}^{n_i \times n_j}$ for $1 \leq i, j \leq m$. We use the notation $\mathrm{diag}(B_{11}, \cdots, B_{mm})$ for block diagonal matrices with $B_{ij} = 0$ for $i \neq j$. Additionally, we call a block matrix (strictly) upper triangular if the relevant block matrices are zero.

6.1.2 Basic Results Regarding Matrices, Block Matrices and the Matrix Exponential Function

Lemma 6 summarizes several results regarding matrices and block matrices that are used to prove the main results in this thesis.

Lemma 6. *Consider that $T, U \in \mathscr{T}$ are upper triangular matrices, $S \in \mathscr{S}$ is a strictly upper triangular matrix and R is an invertible diagonal matrix with compatible dimensions. Then,*

1. *$T \cdot U$ and $U \cdot T$ are upper triangular,*

2. $S \cdot T$ and $T \cdot S$ are strictly upper triangular,

3. T^{-1} is upper triangular if T is invertible,

4. $R^{-1} \cdot T \cdot R = R^{-1} \cdot (T_D + T_N) \cdot R = T_D + R^{-1} \cdot T_N \cdot R$.

We study bounds for the norm of the matrix exponential function e^{At} of matrices $A \in \mathbb{R}^{n \times n}$. To this end, we present several relevant results. A possible representation of the matrix exponential function is

$$e^{At} = \sum_{k=0}^{\infty} \frac{A^k t^k}{k!}. \tag{6.1}$$

Then, it holds for the matrix exponential function of a block diagonal matrix that

$$e^{\mathrm{diag}(B_{11},\dots,B_{mm})t} = \mathrm{diag}(e^{B_{11}t},\dots,e^{B_{mm}t}). \tag{6.2}$$

Finally, we state a result that allows evaluating the matrix exponential function of a matrix product with commuting matrices [68, 69].

Proposition 2. *Let $A, B \in \mathbb{R}^{n \times n}$. Then, it holds for all $t \in \mathbb{R}$ that*

$$e^{(A+B)t} = e^{At} e^{Bt} \tag{6.3}$$

if and only if $AB = BA$.

6.1.3 Jordan Canonical Form

We next provide a formal definition of the Jordan canonical form to be used in the remainder of the thesis.

Definition 3. *Let $J \in \mathbb{C}^{n \times n}$ be a matrix. Then, J is a Jordan matrix with eigenvalue λ and Segre characteristic $(d_1, d_2, \dots, d_s)$ if the following conditions hold:*

1. $d_1 + d_2 + \cdots + d_s = n$ is a partition of n with $d_1 \geq d_2 \geq \cdots \geq d_s \geq 1$ and J is an $s \times s$ block matrix with $J_{ii} \in C^{d_i \times d_i}$ for $i = 1, \dots, s$.

2. The main diagonal entries of J_{ii} are all λ for $i = 1, \dots, s$.

3. *The superdiagonal entries of J_{ii} are equal to 1 for $i = 1, \ldots, s$.*

4. *All other blocks of J are zero. That is, $J_{ij} = 0$ if $j \neq i$.*

An example Jordan matrix with eigenvalue λ and Segre characteristic $(4, 4, 2, 1)$ is given in (6.4).

$$
J = \begin{bmatrix}
\lambda & 1 & 0 & 0 & 0 & 0 & 0 & 0 & 0 & 0 & 0 \\
0 & \lambda & 1 & 0 & 0 & 0 & 0 & 0 & 0 & 0 & 0 \\
0 & 0 & \lambda & 1 & 0 & 0 & 0 & 0 & 0 & 0 & 0 \\
0 & 0 & 0 & \lambda & 0 & 0 & 0 & 0 & 0 & 0 & 0 \\
0 & 0 & 0 & 0 & \lambda & 1 & 0 & 0 & 0 & 0 & 0 \\
0 & 0 & 0 & 0 & 0 & \lambda & 1 & 0 & 0 & 0 & 0 \\
0 & 0 & 0 & 0 & 0 & 0 & \lambda & 1 & 0 & 0 & 0 \\
0 & 0 & 0 & 0 & 0 & 0 & 0 & \lambda & 0 & 0 & 0 \\
0 & 0 & 0 & 0 & 0 & 0 & 0 & 0 & \lambda & 1 & 0 \\
0 & 0 & 0 & 0 & 0 & 0 & 0 & 0 & 0 & \lambda & 0 \\
0 & 0 & 0 & 0 & 0 & 0 & 0 & 0 & 0 & 0 & \lambda
\end{bmatrix}
\tag{6.4}
$$

Using the Jordan matrix for a given eigenvalue λ in Definition 3 as the building block, it is possible to define the general Jordan matrix.

Definition 4. *Let $J \in \mathbb{C}^{n \times n}$ be a square matrix with the distinct eigenvalues $\lambda_1, \ldots, \lambda_m$. J is in Jordan canonical form if*

$$
J = \mathrm{diag}(J_1, \ldots, J_m),
\tag{6.5}
$$

whereby $J_i \in \mathbb{C}^{n_i \times n_i}$ is a Jordan matrix with eigenvalue λ_i for $i = 1, \ldots, k$. We write s_i for the number of diagonal blocks of J_i.

It is a well-established result in the literature that any complex matrix can be transformed to its Jordan canonical form.

Proposition 3. *Let $A \in \mathbb{C}^{n \times n}$ be a matrix. Then, there exists an invertible matrix T_J such that $T_J^{-1} A_J T_J = J$, where J is a matrix in Jordan canonical form.*

6.1.4 Schur Decomposition

We further employ the Schur decomposition as formalized in Proposition 4.

Proposition 4. *Let $A \in \mathbb{R}^{n \times n}$ be a matrix. Then, A can be transformed to*

$$S = Q^{-1} A Q, \tag{6.6}$$

where Q is a unitary matrix and $S \in \mathscr{T}$. In that case, S is denoted as a Schur form of A.

6.1.5 Existing Bounds for the Matrix Exponential Function

Various bounds for the matrix exponential function are provided in the literature. In this section, we summarize the most relevant bounds as identified in [63, 69]. Consider a complex matrix $A \in \mathbb{C}^{n \times n}$.

The first bound is derived based on a result on the logarithmic norm of matrices by [67].

Lemma 7. *Assume that T is an invertible matrix and write $E = T^{-1} A T$. Then,*

$$||e^{At}|| \le lb_A(t) := \kappa(T) \cdot e^{\mu(E)t}. \tag{6.7}$$

Also, for each $\varepsilon > 0$, there exists an invertible T such that

$$\mu(E) \le \alpha(A) + \varepsilon. \tag{6.8}$$

The second bound is based on the Jordan canonical form as introduced in Section 6.1.3.

Lemma 8. *Assume that T_J is an invertible matrix such that $J = T_J^{-1} A T_J$ is in Jordan canonical form and let b be the size of the largest Jordan block of J. Then, it holds that*

$$||e^{At}|| \le jb_A(t) := b \cdot \kappa(T_J) \cdot e^{\alpha(A)t} \cdot \max_{0 \le k < b} \frac{t^k}{k!}. \tag{6.9}$$

We denote the bound in (6.9) as the *Jordan bound*.

The third bound is based on a transformation of A to an upper triangular matrix.

Lemma 9. *Let Q be an invertible matrix such that $S = Q^{-1}AQ \in \mathcal{T}$. Write $S = S_D + S_N$. Then,*

$$||e^{At}|| \leq \kappa(Q) \cdot e^{\alpha(A)t} \cdot \sum_{k=0}^{n-1} ||S_N||^k \frac{t^k}{k!}. \tag{6.10}$$

In particular, if a Schur decomposition of A is used such that $\kappa(Q) = 1$, the following corollary is obtained.

Corollary 5. *Let $S = Q^{-1}AQ$ be a Schur form of A and write $S = S_D + S_N$. Then,*

$$||e^{At}|| \leq \mathrm{sb}_A(t) := e^{\alpha(A)t} \cdot \sum_{k=0}^{n-1} ||S_N||^k \cdot \frac{t^k}{k!}. \tag{6.11}$$

We denote the bound in (6.11) as the *Schur bound*.

The bounds introduced in this section show different properties and it is argued in [63] that the effectiveness of each bound depends on A and the relevant time instances t. If all the eigenvalues of A are in the left half complex plane, the bound in (6.7) can ensure a monotonically decreasing exponential decay that is slower than $e^{\alpha(A)t}$. The speed of the decay can be adjusted by a similarity transformation as in (6.8). Here, increasing the speed of the decay such that $\mu(E) \approx \alpha(A)$ generally has the effect that the maximum value $\kappa(T)$ of the bound at $t = 0$ becomes very large.

The bounds in (6.9) and (6.11) both constitute the product of a decaying exponential with exponent $\alpha(A)t$ and an increasing polynomial in t with positive coefficients. That is, the exponential decay is faster compared to the bound in (6.7). On the other hand, the bounds in (6.9) and (6.11) generally show a hump [70] (maximum) such that the exponential decay is dominant only for large enough times. Here, the size of the hump depends on the growth of the polynomial in (6.9) and (6.11), which is determined by the polynomial coefficients and the polynomial order.

In (6.9), the polynomial coefficients are always equal to one and the polynomial order only depends on the size b of the largest Jordan block in (6.9) and not on the size of A. A disadvantage of the bound in (6.9) is the requirement of obtaining the Jordan canonical form of A, which is generally not possible in floating point arithmetic [71, 72]. In addition, the condition number $\kappa(T_J)$ can be arbitrarily large [70].

On the other hand, the bound in (6.11) depends on the Schur decomposition, which can be obtained in a stable way using the QR algorithm [73, 74]. Moreover, since Q is a unitary matrix, it is ensured that the bound is equal to one for $t = 0$ and hence close for very small times. Nevertheless, the polynomial coefficients in (6.11) are given by the norm $||S_N||$ and the polynomial order grows with the size n of A in (6.11). That is, a large maximum is commonly observed before the bound exponentially decays to zero unless $||S_N||$ and/or n are sufficiently small.

In summary, all bounds have to be considered as conservative. Although the bounds in (6.9) and (6.11) ensure exponential decay with $\alpha(A)$ for large enough times, they can assume a very large maximum especially for large and ill-conditioned matrices A, which impairs the numerical bound computation.

The subject of this chapter is the computation of bounds on the matrix exponential function that can be better evaluated for large and not well-conditioned matrices A. Hereby, the main focus is on obtaining bounds with a fast decay and a maximum value that can be evaluated numerically. To this end, Section 6.2 derives new bounds based on the Jordan canonical form and Section 6.3 proposes a new method that is based on the Schur decomposition.

6.2 Improved Bounds for the Matrix Exponential Function Using the Jordan Canonical Form

This section focuses on computing bounds for the matrix exponential function using the Jordan canonical form. Section 6.2.1 states several relevant properties of the Jordan canonical form and Section 6.2.2 determines a general result that slightly improves the bound in (6.9). A method for obtaining a faster decay of the bound is developed in Section 6.2.3 and an evaluation and comparison of the

presented results is given in Section 6.2.4.

6.2.1 Properties of the Jordan Canonical Form

We next state several basic results for matrices in Jordan canonical form.

Proposition 5. *Let $J = \mathrm{diag}(J_1,\ldots,J_m) \in \mathbb{C}^{n \times n}$ be a matrix in Jordan canonical form with Jordan matrices $J_i \in \mathbb{C}^{n_i \times n_i}$ with eigenvalue λ_i and Segre characteristic $(d_{i,1},\ldots,d_{i,s_i})$ for $i = 1,\ldots,m$. Then, it holds that*

1. *J can be written as*

$$J = J_D + J_N = \mathrm{diag}(\lambda_1 I_{n_1},\ldots,\lambda_m I_{n_m}) + \mathrm{diag}(N_1,\ldots,N_m), \qquad (6.12)$$

   where N_i is a nilpotent Jordan matrix with the same Segre characteristic as J_i for $i = 1,\ldots,m$.

2. *$||J_N|| = 1$,*

3. *J_D and J_N commute,*

4. *the nilpotency index of J_N is $b := \max_{i=1,\ldots,m} d_{i,1}$.*

Proof.   1. Directly follows from Definition 4.

2. Since $J_N = \mathrm{diag}(N_1,\ldots,N_m)$, it holds that

$$||J_N|| = \max_{1 \leq i \leq m} ||N_i||.$$

   Considering that the structure of N_i implies $||N_i|| = 1$ for $i = 1,\ldots,m$, the assertion directly follows.

3. It holds that

$$J_D \cdot J_N = \mathrm{diag}(\lambda_1 I_{n_1} \cdot N_1,\ldots,\lambda_m I_{n_m} \cdot N_m)$$
$$= \mathrm{diag}(N_1 \cdot \lambda_1 I_{n_1},\ldots,N_m \cdot \lambda_m I_{n_m}) = J_N \cdot J_D.$$

99

4. It holds that

$$J_N^k = \mathrm{diag}(N_1^k, \ldots, N_m^k)$$

and the nilpotency index of N_i is equal to $d_{i,1}$ according to [75]. That is, for $k < b$, there exists an i such that $N_i^k \neq 0$ and hence $J_N^k \neq 0$. However for $k = b$, it follows that $N_i^b = 0$ for all $i = 1, \ldots, m$, implying that also $J_N^b = 0$.

□

6.2.2 Bound Derivation for the Jordan Canonical Form

Using the properties in Proposition 5, it is now possible to determine an improved bound for the matrix exponential function based on the Jordan canonical form.

Theorem 11. *Assume that $A \in \mathbb{C}^{n \times n}$ is a matrix. Let $J = T_J^{-1} A T_J = \mathrm{diag}(J_1, \ldots, J_m) \in \mathbb{C}^{n \times n}$ be the Jordan canonical form of A with Jordan matrices $J_i \in \mathbb{C}^{n_i \times n_i}$ with eigenvalue λ_i and Segre characteristic $(d_{i,1}, \ldots, d_{i,s_i})$ for $i = 1, \ldots, m$. Write $b = \max_{1 \leq i \leq m} d_{i,1}$. Then,*

$$||e^{At}|| \leq \kappa(T_J) \cdot e^{\alpha(A)t} \cdot \sum_{k=0}^{b-1} \frac{t^k}{k!}. \tag{6.13}$$

Proof. We first compute

$$||e^{At}|| = ||T_J e^{T_J^{-1} A T_J} T_J^{-1}|| \leq \kappa(T_J) ||e^{Jt}||.$$

Considering Proposition 5 item 3., it holds that $J_D \cdot J_N = J_N \cdot J_D$. That is, Proposition 2 implies that

$$e^{Jt} = e^{(J_D + J_N)t} = e^{J_D t} e^{J_N t}.$$

We further know from Proposition 5 item 4. that $J_N^b = 0$. Using the representation of $e^{J_N t}$ according to (4.16) and noting that $||J_N|| = 1$ from Proposition 5 item 2.,

we obtain

$$||e^{At}|| \leq \kappa(T_J) \cdot ||e^{(J_D + J_N)t}|| = \kappa(T_J) \cdot ||e^{J_D t} \cdot e^{J_N t}|| \leq \kappa(T_J) \cdot ||e^{J_D t}|| \cdot ||e^{J_N t}||$$

$$= \kappa(T_J) \cdot e^{\alpha(A)t} \cdot ||\sum_{k=0}^{\infty} \frac{J_N^k t^k}{k!}|| = \kappa(T_J) \cdot e^{\alpha(A)t} \cdot ||\sum_{k=0}^{b-1} \frac{J_N^k t^k}{k!}||$$

$$\leq \kappa(T_J) \cdot e^{\alpha(A)t} \cdot \sum_{k=0}^{b-1} \frac{||J_N||^k t^k}{k!} = \kappa(T_J) \cdot e^{\alpha(A)t} \cdot \sum_{k=0}^{b-1} \frac{t^k}{k!}$$

$\square$

It is readily observed that the bound in (6.13) is smaller than the bound in (6.9) since

$$\sum_{k=0}^{b-1} \frac{t^k}{k!} \leq b \cdot \max_{0 \leq k < b} \frac{t^k}{k!}.$$

Of course, it has to be noted that the difference between the two bounds need not be significant. Nevertheless, as will be shown in the subsequent section, the bound formulation in (6.13) allows for a straightforward improvement of the bound especially for sufficiently small times.

6.2.3 Adjusting the Bounds for Sufficiently Small Times

The bound in (6.13) is the product of $e^{-\alpha(A)t}$ (monotonically decreasing) and the polynomial $\sum_{k=0}^{b-1} \frac{t^k}{k!}$ (monotonically increasing). Hereby, the polynomial coefficients are determined by the fact that $||J_N|| = 1$. Accordingly, depending on the value of $\alpha(A)$, the bound in (6.13) shows a large maximum (hump) and slow decay. In this section, an additional transformation with a matrix $R \in \mathbb{R}^{n \times n}$ is introduced in order to decrease this hump and to achieve faster decay to zero. To this end, we use the properties stated in the following proposition.

Proposition 6. *Let $J = \mathrm{diag}(J_1, \ldots, J_m) \in \mathbb{C}^{n \times n}$ be a matrix in Jordan canonical form with Jordan matrices $J_i \in \mathbb{C}^{n_i \times n_i}$ with eigenvalue λ_i and Segre characteristic $(d_{i,1}, \ldots, d_{i,s_i})$ for $i = 1, \ldots, m$. Write $b = \max_{1 \leq i \leq m} d_{i,1}$. Let $r < 1$ and define $R_{i,j} = \mathrm{diag}(r^0, \ldots, r^{d_{i,j}-1})$ for $i = 1, \ldots, m$ and $j = 1, \ldots, s_i$. Let $R_i =$*

$\operatorname{diag}(R_{i,1},\ldots,R_{i,s_i})$ *for* $i=1,\ldots,m$ *and* $R=\operatorname{diag}(R_1,\ldots,R_m)$. *Write* $\hat{J}=R^{-1}JR=\hat{J}_D+\hat{J}_N$. *Then, it holds that* $\hat{J}_D=J_D$, $\hat{J}_N=rJ_N$ *and* $\kappa(R)=r^{1-b}$.

Proof. First, it holds for $\hat{J}_D$ that

$$\begin{aligned}
R^{-1}J_D R &= \operatorname{diag}(R_1^{-1},\ldots,R_m^{-1})\operatorname{diag}(\lambda_1 I_{n_1},\ldots,\lambda_m I_{n_m})\operatorname{diag}(R_1,\ldots,R_m)\\
&= \operatorname{diag}(\lambda_1 R_1^{-1}I_{n_1}R_1,\ldots,\lambda_m R_m^{-1}I_{n_m}R_m)\\
&= \operatorname{diag}(\lambda_1 I_{n_1},\ldots,\lambda_m I_{n_m}) = J_D.
\end{aligned}$$

Next, we consider $\hat{J}_N$:

$$\begin{aligned}
R^{-1}J_N R &= \operatorname{diag}(R_1^{-1},\ldots,R_m^{-1})\operatorname{diag}(N_1,\ldots,N_m)\operatorname{diag}(R_1,\ldots,R_m)\\
&= \operatorname{diag}(R_1^{-1}N_1 R_1,\ldots,R_m^{-1}N_m R_m).
\end{aligned}$$

We show that $R_i^{-1}N_i R_i = r\cdot N_i$ for $i=1,\ldots,m$. Recall that $R_i=\operatorname{diag}(R_{i,1},\ldots,R_{i,s_i})$ by definition and write $N_i=\operatorname{diag}(N_{i,1},\ldots,N_{i,s_i})$, whereby $N_{i,j}$ represents the nilpotent Jordan block of size $d_{i,j}$. Then,

$$\begin{aligned}
R_i^{-1}N_i R_i &= \operatorname{diag}(R_{i,1}^{-1},\ldots,R_{i,s_i}^{-1})\operatorname{diag}(N_{i,1},\ldots,N_{i,s_i})\operatorname{diag}(R_{i,1},\ldots,R_{i,s_i})\\
&= \operatorname{diag}(R_{i,1}^{-1}N_{i,1}R_{i,1},\ldots,R_{i,s_i}^{-1}N_{i,s_i}R_{i,s_i}).
\end{aligned}$$

Considering that $R_{i,j}=\operatorname{diag}(r^0,\ldots,r^{d_{i,j}-1})$, $R_{i,j}^{-1}=\operatorname{diag}(r^0,\ldots,r^{1-d_{i,j}})$ and $N_{i,j}$ is a matrix where the superdiagonal entries are equal to 1 and all the other entries are zero, it is readily observed that $R_{i,j}^{-1}N_{i,j}R_{i,j}=rN_{i,j}$. Hence, $R_i^{-1}N_i R_i = rN_i$ which implies $\hat{J}_N=rJ_N$.

Finally, since $r<1$, the largest singular value of R is 1 and the smallest singular value of R is r^{b-1}, that is, $\kappa(R)=1/r^{b-1}=r^{1-b}$. $\qquad\square$

Using Proposition 6, it is possible to modify the polynomial coefficients in the bound for the matrix exponential function as shown in Theorem 12.

Theorem 12. *Let A, J, J_i, $i=1,\ldots,m$, b, R be defined as in Theorem 11 and*

Proposition 6. Then, it holds that

$$||e^{At}|| \le \text{ijb}_A(t) := \kappa(T_J \cdot R) \cdot e^{\alpha(A)t} \cdot \sum_{k=0}^{b-1} \frac{r^k \cdot t^k}{k!} \le r^{1-b} \kappa(T_J) \cdot e^{\alpha(A)t} \cdot \sum_{k=0}^{b-1} \frac{r^k \cdot t^k}{k!}.$$

(6.14)

We denote the bound in (6.14) *as* improved Jordan bound.

Proof. In analogy to the proof of Theorem 11, it follows from Proposition 6 that

$$||e^{At}|| \le \kappa(T_J R) \cdot e^{\alpha(A)t} \cdot \sum_{k=0}^{b-1} \frac{||\hat{J}_N||^k t^k}{k!} = \kappa(T_J R) \cdot e^{\alpha(A)t} \cdot \sum_{k=0}^{b-1} \frac{||r \cdot J_N||^k t^k}{k!}$$

$$= \kappa(T_J R) \cdot e^{\alpha(A)t} \cdot \sum_{k=0}^{b-1} \frac{r^k \cdot t^k}{k!} \le r^{1-b} \kappa(T_J) \cdot e^{\alpha(A)t} \cdot \sum_{k=0}^{b-1} \frac{r^k \cdot t^k}{k!}.$$

$\square$

Inspecting (6.14), it is possible to adjust the effect of the polynomial $\sum_{k=0}^{b-1} \frac{r^k \cdot t^k}{k!}$ on the overall bound. In order to achieve fast decay to zero, r should be chosen depending on $\alpha(A)$ in order to decrease the maximum of $e^{\alpha(A)t} \cdot \sum_{k=0}^{b-1} r^k \cdot \frac{t^k}{k!}$. The subsequent section provides several examples for this choice.

6.2.4 Evaluation Examples

We consider two examples for the evaluation of the bound in (6.14). The first example uses the matrix $A_1 = T_{J_1} J_1 T_{J_1}^{-1}$ with

$$J_1 = \begin{bmatrix} -5 & 1 & 0 & 0 & 0 & 0 & 0 \\ 0 & -5 & 1 & 0 & 0 & 0 & 0 \\ 0 & 0 & -5 & 0 & 0 & 0 & 0 \\ 0 & 0 & 0 & -5 & 1 & 0 & 0 \\ 0 & 0 & 0 & 0 & -5 & 1 & 0 \\ 0 & 0 & 0 & 0 & 0 & -5 & 0 \\ 0 & 0 & 0 & 0 & 0 & 0 & -5 \end{bmatrix}$$

and the randomly generated transformation matrix

$$
T_{J_1} = \begin{bmatrix}
3 & 7 & 5 & 7 & 4 & 5 & 4 \\
0.25 & 0.2 & 0.45 & 0.4 & 0.45 & 0.25 & 0 \\
100 & 0 & 0 & 800 & 100 & 100 & 200 \\
6 & 2 & 4 & 0 & 2 & 8 & 1 \\
200 & 900 & 100 & 300 & 100 & 600 & 100 \\
1.8 & 0.3 & 2.7 & 0.6 & 0.3 & 0.9 & 0.6 \\
6 & 8 & 0 & 8 & 8 & 5 & 4
\end{bmatrix}.
$$

That is, A_1 has a single eigenvalue -5 and Segre characteristic $(3,3,1)$ and $\kappa(T_{J_1}) = 4021$. Evaluating the bound in (6.14) for different values of r gives the bounds in Fig. 6.1.
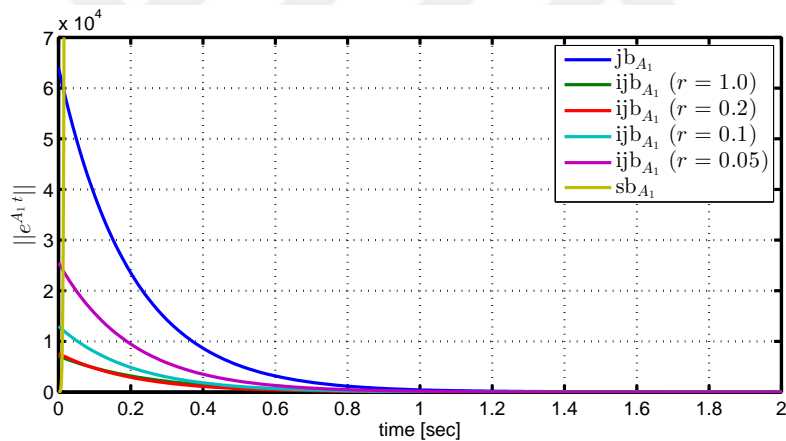
Figure 6.1: Bound computation for the example matrix A_1.

It can be seen in this example that a choice of $r = 0.2$ supports fast convergence to zero. Choosing a smaller value of r increases the condition number $\kappa(T_{J_1} R)$. Hence, the initial value of the bound is significantly increased, whereas the exponential decay is not affected. Fig. 6.1 also confirms that the existing Jordan bound in (6.9) is more conservative than the improved Jordan bound in (6.14).

104

For comparison, we also state the Schur bound according to (6.11) as

$$\text{sb}_{A_1}(t) = e^{-5t} \cdot \sum_{k=0}^{6} \frac{1\,185^k\, t^k}{k!} \tag{6.15}$$

with a maximum at $2.86 \cdot 10^{13}$. That is, the bound in (6.11) is considerably more conservative for this example except for very small times (see Fig. 6.1).

As the second example, we use $A_2 = T_{J_2} J_2 T_{J_2}^{-1}$ with

$$J_2 = \begin{bmatrix} -1 & 1 & 0 & 0 & 0 & 0 & 0 \\ 0 & -1 & 1 & 0 & 0 & 0 & 0 \\ 0 & 0 & -1 & 0 & 0 & 0 & 0 \\ 0 & 0 & 0 & -1 & 1 & 0 & 0 \\ 0 & 0 & 0 & 0 & -1 & 0 & 0 \\ 0 & 0 & 0 & 0 & 0 & -3 & 1 \\ 0 & 0 & 0 & 0 & 0 & 0 & -3 \end{bmatrix}$$

and the randomly generated transformation matrix

$$T_{J_2} = \begin{bmatrix} 600 & 1\,400 & 1\,000 & 1\,400 & 6\,800 & 1\,000 & 800 \\ 1\,000 & 800 & 1\,800 & 1\,600 & 1\,800 & 1\,000 & 0 \\ 200 & 0 & 0 & 1\,600 & 200 & 200 & 400 \\ 0.3 & 0.1 & 0.2 & 0 & 0.1 & 0.4 & 0.1 \\ 0.1 & 0.4 & 0.1 & 0.2 & 0.1 & 0.3 & 0.1 \\ 6 & 1 & 9 & 2 & 1 & 3 & 2 \\ 6 & 8 & 0 & 8 & 865 & 4 \end{bmatrix}.$$

That is, A_2 has a the eigenvalue -1 with Segre characteristic $(3,2)$ and the eigenvalue -3 with Segre characteristic (2). In this example, $\kappa(T_{J_2}) = 3\,086$. Evaluating the bound in (6.14) for different values of r gives the bounds in Fig. 6.2.

In this example, the choice of $r = 0.1$ is most suitable. Here, the hump in the bound can be observed when choosing r too large. It can also be seen that smaller values of r are required compared to the first example due to the slower
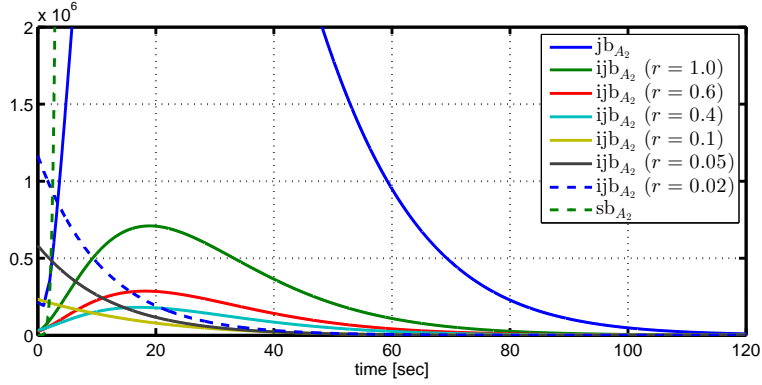
Figure 6.2: Bound computation for the example matrix A_2.

exponential decay with eigenvalue -1. Fig. 6.2 again confirms that the Jordan bound in (6.9) and the Schur bound with

$$\text{sb}_{A_2}(t) = e^{-t} \cdot \sum_{k=0}^{7} \frac{11.9^k t^k}{k!} \tag{6.16}$$

are more conservative than the improved Jordan bound.

6.3 Improved Bound using the Schur Decomposition

It is shown in Section 6.2.4 that the improved Jordan bound can be significantly better than the Schur bound in (6.11) except for very small times. Nevertheless, the bound in (6.14) requires the availability of the Jordan canonical form, whose computation is generally numerically not stable [71, 72]. In this section, we propose an improved bound using the Schur decomposition which can be computed in a stable way. To this end, we address two main reasons for the conservativeness of the bound in (6.11). First, as confirmed by the examples in Section 6.2.4, it holds that the value of $||S_N||$ can be large. Second, the nilpotency index of S_N is generally equal to the dimension n of A, leading to a polynomial degree of $n-1$ in (6.11). Accordingly, the proposed method attempts to reduce the nilpotency index of S_N using a similarity transformation of A to block diagonal form. Then, the norm of the strictly upper triangular part of the resulting matrix is further de-

106

creased with the aim of reducing $||S_N||$.

6.3.1 Bound Derivation

As the first step, we transform the matrix A to block diagonal form. Hereby, similar to [76], we first determine an ordered Schur decomposition, where similar (close) eigenvalues of A are grouped next to each other. Then, we apply a method to eliminate off-diagonal blocks by using a special similarity transform and a Sylvester equation. To this end, we employ the following proposition that is adapted to the notation in this thsis from [76].

Proposition 7. *Let $A \in \mathbb{R}^{n \times n}$ be a matrix and let $\delta > 0$ be a constant. Then, there exists a unitary transformation $U \in \mathbb{R}^{n \times n}$ and a $p \in \mathbb{N}$ such that*

$$S = U^{-1}AU = \begin{bmatrix} S_{11} & S_{12} & \cdots & S_{1p} \\ 0 & S_{22} & \cdots & S_{2p} \\ \vdots & \ddots & \ddots & \vdots \\ 0 & 0 & \cdots & S_{pp} \end{bmatrix} \tag{6.17}$$

and

- *S_{ii} is upper triangular for $i = 1, \ldots, p$,*

- *either λ is the sole eigenvalue of S_{ii} or there exists another eigenvalue λ' of S_{ii} such that $\lambda \neq \lambda'$ and $|\lambda - \lambda'| \leq \delta$,*

- *for all i, j with $i \neq j$, it holds that if λ_i is an eigenvalue of S_{ii} and λ_j is an eigenvalue of S_{jj}, then $|\lambda_i - \lambda_j| > \delta$.*

That is, S in (6.17) is an ordered Schur decomposition of A. On the one hand, each block S_{ii} of S either contains a single eigenvalue or each eigenvalue of S_{ii} has an adjacent eigenvalue with a distance that is bounded by δ. On the other hand, different blocks S_{ii} and S_{jj}, $i \neq j$, have eigenvalues with a distance larger than δ. Hereby, it has to be noted that the unitary transformation U in (6.17) can be computed efficiently. Algorithm 4.1 in [76] allows grouping the eigenvalues of A into

p groups, whereas Algorithm 4.2 in [76] determines a similarity transformation $S = U^{-1}AU$ such that the eigenvalues in each group are adjacent in S.

After obtaining S in (6.17), we transform S to a block diagonal matrix. It is known that such transformation always exists if the diagonal blocks of S have distinct eigenvalues [77, 78].

Proposition 8. *Let S be given as in* (6.17) *such that* $\mathrm{spec}(S_{ii}) \cap \mathrm{spec}(S_{jj}) = \emptyset$ *for all $i \neq j$. Then, S is similar to $\hat{S} = \mathrm{diag}(S_{11}, \ldots, S_{pp})$.*

The computation of $\mathrm{diag}(S_{11}, \ldots, S_{pp})$ is based on the following lemma [79, 75, 78], which establishes such transform for block matrices with two blocks.

Lemma 10. *Let $S = \begin{bmatrix} S_{11} & S_{12} \\ 0 & S_{22} \end{bmatrix}$ and $\mathrm{spec}(S_{11}) \cap \mathrm{spec}(S_{22}) = \emptyset$. Define the transformation matrix $Q = \begin{bmatrix} I & X \\ 0 & I \end{bmatrix}$ such that X is the unique solution of*

$$S_{11}X - XS_{22} + S_{12} = 0. \tag{6.18}$$

Then, $Q^{-1}SQ = \mathrm{diag}(S_{11}, S_{22})$.

The successive application of Lemma 10 leads to the iterative Algorithm 1 for computing $\mathrm{diag}(S_{11}, \ldots, S_{pp})$ for general block matrices.

The algorithm initializes the matrix $\hat{S}$ with the ordered Schur decomposition S and successively applies the similarity transformation in Lemma 10 to make the block (j, i) of $\hat{S}$ zero starting from the block $(p-1, p)$. According to the transformation, all blocks (k, l) with $l > i$ or $k > j$ remain unchanged. In particular, if a block (k, l) has been made zero, it will remain zero in all subsequent iterations.

The resulting matrix $\hat{S} = (U\hat{T})^{-1}A(U\hat{T})$ after applying grouping of eigenvalues as in Proposition 7 and block diagonalization as in Proposition 8 and Algo-

```
input  : S
output: T̂, Ŝ
 1  Initialize T̂ = I and Ŝ = S
 2  for i = p, . . . , 2 do
 3      for j = i − 1, . . . , 1 do
 4          Solve the Sylvester equation
 5              −X S_{ii} + S_{jj} X + S_{ji} = 0
 6          Define the transformation matrix Q = I
 7          Set the block (j, i) of Q to X
 8          Compute Ŝ = Q^{-1} Ŝ Q and T̂ = T̂ Q
 9      end
10  end
```

Algorithm 1: Transformation of a block triangular matrix S to a block diagonal matrix $\hat{S}$.

rithm 1 is a block diagonal matrix

$$
\hat{S} = \begin{bmatrix} \hat{S}_{11} & 0 & \cdots & 0 \\ 0 & \hat{S}_{22} & \ddots & 0 \\ \vdots & \ddots & \ddots & \vdots \\ 0 & 0 & \cdots & \hat{S}_{pp} \end{bmatrix} \tag{6.19}
$$

and can be written as $\hat{S} = \hat{S}_D + \hat{S}_N$, whereby

$$
\hat{S}_D = \begin{bmatrix} \hat{D}_{11} & 0 & \cdots & 0 \\ 0 & \hat{D}_{22} & \ddots & 0 \\ \vdots & \ddots & \ddots & \vdots \\ 0 & 0 & \cdots & \hat{D}_{pp} \end{bmatrix} \text{ and } \hat{S}_N = \begin{bmatrix} \hat{N}_{11} & 0 & \cdots & 0 \\ 0 & \hat{N}_{22} & \ddots & 0 \\ \vdots & \ddots & \ddots & \vdots \\ 0 & 0 & \cdots & \hat{N}_{pp} \end{bmatrix} . \tag{6.20}
$$

For each $i = 1, \ldots, p$, $\hat{D}_{ii}$ is a diagonal matrix with dimension q_i and the eigenvalues of the block $\hat{S}_{ii}$ on the diagonal. $\hat{N}_{ii}$ is a strictly upper triangular matrix with nilpotency index q_i. It further holds that each block $\hat{S}_{ii}$ of $\hat{S}$, $i = 1, \ldots, p$ has similar eigenvalues and different blocks have separated eigenvalues. In the scope of this thesis, the latter fact is particularly useful since it aids in limiting the condition number of the related similarity transformation [77, 80]. Writing

$q = \max_{i=1,\ldots,p} q_i$, the bound for the matrix exponential function after this step is denoted as

$$||e^{At}|| \leq \mathrm{isb1}_A(t) := \kappa(U\hat{T}) e^{\alpha(A)t} \sum_{k=0}^{q-1} \frac{||\hat{S}_N||^k t^k}{k!}, \qquad (6.21)$$

The remaining issue in the bound computation is the dependency on the norm of the strictly upper triangular part $\hat{S}_N$ of $\hat{S}$. In the next step, we propose a method for decreasing $||\hat{S}_N||$.

To this end, we apply a diagonal transformation [81]

$$R_{ii} = \mathrm{diag}(1, r, \ldots, r^{q_i-1}). \qquad (6.22)$$

to decrease the norm of N_{ii} below a desired limit β. Hereby, the value of r in R_{ii} is computed by a bi-section algorithm. Define the upper bound r_u and lower bound r_l such that $||R_{ii}^{-1} N_{ii} R_{ii}|| > \beta$ for $r = r_u$ and $||R_{ii}^{-1} N_{ii} R_{ii}|| < \beta$ for $r = r_l$. Then, Algorithm 2 bisects the interval between r_l and r_u until

$$||R_{ii}^{-1} N_{ii} R_{ii}|| \leq \beta \text{ and } \beta - ||R_{ii}^{-1} N_{ii} R_{ii}|| \leq \theta.$$

That is, the deviation of $||R_{ii}^{-1} N_{ii} R_{ii}||$ from the desired value β is below a given threshold θ. Computing R_{ii} for $i = 1, \ldots, p$, the overall transformation matrix of this step is $R = \mathrm{diag}(R_{11}, \ldots, R_{pp})$.

The result of the computation in this section is a matrix

$$\tilde{S} = T^{-1} A T = \begin{bmatrix} \tilde{S}_{11} & 0 & \cdots & 0 \\ 0 & \tilde{S}_{22} & \ddots & 0 \\ \vdots & \ddots & \ddots & \vdots \\ 0 & 0 & \cdots & \tilde{S}_{pp} \end{bmatrix} = \begin{bmatrix} \tilde{D}_{11} & 0 & \cdots & 0 \\ 0 & \tilde{D}_{22} & \ddots & 0 \\ \vdots & \ddots & \ddots & \vdots \\ 0 & 0 & \cdots & \tilde{D}_{pp} \end{bmatrix} + \begin{bmatrix} \tilde{N}_{11} & 0 & \cdots & 0 \\ 0 & \tilde{N}_{22} & \ddots & 0 \\ \vdots & \ddots & \ddots & \vdots \\ 0 & 0 & \cdots & \tilde{N}_{pp} \end{bmatrix}$$

with the overall similarity transformation $T = U\hat{T}R$ combining (6.17), Algorithm 1 and 2. For each $i = 1, \ldots, p$, $\tilde{D}_{ii} = \hat{D}_{ii}$ in (6.20) and $||\tilde{N}_{ii}|| \leq \beta$ due to Algorithm

```
input  : $\hat{S}_{ii}$, $\beta$, $\theta$
output: $R_{ii}$
1  $N_{ii} = \hat{S}_{ii} - \mathrm{diag}(\hat{S}_{ii})$
2  if $||N_{ii}|| \leq \beta$ then
3  |    $R_{ii} = I_{q_i}$
4  else
5  |    Initialize: $r_\mathrm{u} = 1$, $r_\mathrm{l} = 0$
6  |    while $||N_{ii}|| - \beta > 0 \vee ||N_{ii}|| - \beta < -\theta$ do
7  |    |    $r = \dfrac{r_\mathrm{u} + r_\mathrm{l}}{2}$
8  |    |    $R_{ii} = \mathrm{diag}(1, r, \ldots, r^{g_i - 1})$
9  |    |    $\tilde{S}_{ii} = R_{ii}^{-1} \hat{S}_{ii} R_{ii}$
10 |    |    $N_{ii} = \tilde{S}_{ii} - \mathrm{diag}(\tilde{S}_{ii})$
11 |    |    if $||N_{ii}|| - \beta > 0$ then
12 |    |    |    $r_\mathrm{u} = r$
13 |    |    else if $||N_{ii}|| - \beta < -\theta$ then
14 |    |    |    $r_\mathrm{l} = r$
15 |    |    end
16 |    end
17 end
```

Algorithm 2: Norm bound for N_{ii}.

2. Hence, the bound in (6.11) is modified to the *improved Schur bound*

$$||e^{At}|| \leq \mathrm{isb2}_A(t) := \kappa(T) e^{\alpha(A)t} \sum_{k=0}^{q-1} \frac{\beta^k t^k}{k!}, \qquad (6.23)$$

The bound computation for $||e^{At}||$ is summarized in Algorithm 3.

```
input  : $A$, $\delta$, $\beta$, $\theta$
output: $\mathrm{isb}_A(t)$
1  Determine $S$ in (6.17)
2  Determine $\hat{S}$ according to Algorithm 1 using $\delta$
3  Adjust the norm of the strictly upper triangular part of $\hat{S}_{ii}$ using
      Algorithm 2 and $\beta$, $\theta$
4  Evaluate the bound in (6.23)
```

Algorithm 3: Overall algorithm for computing an improved Schur bound
on the matrix exponential function.

Hereby, the bound in (6.23) can be computed in a numerically stable way and

improves the bound in (6.11) from the existing literature already for small times due to the smaller polynomial degree of the block matrices and the reduced norm of the strictly upper triangular part of the block matrices.

6.3.2 Numerical Evaluation

In order to evaluate the improved bound computation, we perform numerical experiments using randomly generated matrices with different properties. In our experiments, these matrices are computed in the form

$$A = VJV^{-1} \in \mathbb{R}^{n \times n},$$

where $V \in \mathbb{R}^{n \times n}$ is an invertible matrix and $J \in \mathbb{R}^{n \times n}$ is a Jordan matrix. The real part of the eigenvalues is selected randomly (uniformly distributed) from an interval $[r_r \cdot \lambda_{\max}, \lambda_{\max}]$, whereby $\lambda_{\max} < 0$ and r_r quantifies the range of the real parts. The imaginary part of complex eigenvalues is selected randomly (uniformly distributed) from the interval $[0, r_i \cdot |\lambda_{\max}|]$. The ratio of complex eigenvalues is given as r_c (such that A has $r_c \cdot n$ complex eigenvalues) and the transformation matrix V is randomly generated with a given condition number $\kappa(V)$.

We next investigate the improvement of the bounds in (6.21) and (6.23) compared to the original Schur bound (6.11). In each experiment, we generate 100 different matrices with the respective properties and record the improvement as the logarithm of the ratio of the maxima of the different bounds over time:

$$r_1 = \log_{10}\left(\frac{\max_t \text{isb2}(t)}{\max_t \text{sb}(t)}\right), \qquad r_2 = \log_{10}\left(\frac{\max_t \text{isb2}(t)}{\max_t \text{isb1}(t)}\right) \tag{6.24}$$

That is, r_1 shows the improvement when using the bound in (6.23), whereas r_2 shows the improvement when applying the diagonal similarity transformation in Algorithm 2. Since the improvements are in the order of powers of 10, we take the logarithm of the respective ratios. We note that all our experiments are carried out using quadruple precision floating point numbers [82].

In the first experiment, we consider the dependency of r_1 and r_2 on the real part of the eigenvalues of A, which characterizes the rate of change to be ex-

pected in the dynamical system modeled by A. In this experiment, $n = 50$ and $\kappa(V) = 1000$ is chosen (the dependency on n and $\kappa(V)$ will be studied in subsequent experiments). The results are obtained for different ranges of the real part r_r, different ratios of complex eigenvalues $r_\mathrm{c} \in \{0, 0.4, 0.7, 1.0\}$ and different numbers of diagonal blocks p in (6.17). The average values of r_1 and r_2 for 100 randomly generated matrices per data point are shown for $r_\mathrm{i} = 100$ in Table 6.1 and for $r_\mathrm{i} = 10\,000$ in Table 6.2.

Table 6.1: Improvement r_1 and r_2 depending on r_r, p and r_c for $\kappa(V) = 1000$, $n = 50$ and $r_\mathrm{i} = 100$.

p	r_c	$r_\mathrm{r} = 10$		$r_\mathrm{r} = 100$		$r_\mathrm{r} = 1000$		$r_\mathrm{r} = 10000$		$r_\mathrm{r} = 100000$	
		r_1	r_2	r_1	r_2	r_1	r_2	r_1	r_2	r_1	r_2
	0.0	-126.3	-46.2	-163.1	-62.3	-182.0	-71.4	-188.4	-72.1	-190.3	-72.1
2	0.4	-158.0	-65.8	-158.4	-67.9	-170.6	-63.8	-177.8	-68.5	-183.8	-69.6
	0.7	-160.3	-69.0	-156.4	-65.4	-167.0	-64.2	-177.8	-68.5	-176.7	-68.4
	1.0	-160.5	-68.3	-158.3	-69.6	-164.7	-64.0	-175.5	-68.8	-176.8	-71.7
	0.0	-131.2	-17.9	-171.6	-26.8	-191.4	-30.6	-193.6	-30.6	-198.2	-31.9
4	0.4	-173.5	-32.1	-171.3	-33.0	-181.7	-28.8	-193.5	-31.2	-194.5	-31.7
	0.7	-176.0	-36.1	-171.7	-36.1	-181.6	-32.0	-189.7	-32.3	-191.2	-32.0
	1.0	-178.2	-38.8	-171.4	-35.0	-178.9	-30.4	-186.2	-30.7	-188.7	-31.2
	0.0	-133.9	-9.3	-174.9	-15.8	-193.7	-18.3	-201.4	-18.7	-201.9	-19.3
6	0.4	-178.3	-21.0	-175.9	-19.3	-187.6	-18.1	-198.8	-19.4	-199.2	-19.2
	0.7	-181.0	-21.7	-176.7	-22.5	-184.7	-18.4	-197.3	-20.0	-193.6	-18.9
	1.0	-183.4	-23.2	-176.9	-22.8	-180.6	-18.7	-191.9	-18.6	-192.9	-19.1
	0.0	-134.8	-5.6	-177.0	-10.9	-195.5	-12.4	-200.9	-12.4	-211.9	-13.2
8	0.4	-181.6	-14.5	-177.0	-13.7	-190.0	-13.6	-204.1	-13.4	-200.2	-13.1
	0.7	-183.1	-16.4	-180.0	-16.4	-188.0	-13.7	-195.6	-13.3	-200.0	-12.8
	1.0	-186.9	-16.6	-180.3	-16.4	-185.7	-14.6	-195.1	-13.6	-192.9	-11.7
	0.0	-135.1	-3.1	-177.5	-7.0	-199.1	-9.8	-207.4	-9.5	-208.8	-9.5
10	0.4	-183.5	-11.3	-181.6	-11.8	-193.8	-10.1	-199.7	-10.3	-201.9	-8.8
	0.7	-185.1	-12.3	-181.5	-13.7	-194.7	-11.6	-199.7	-9.8	-201.7	-9.6
	1.0	-187.4	-12.9	-182.9	-13.0	-188.3	-11.6	-195.8	-8.3	-196.1	-8.6

The observations are summarized as follows. First a considerable improvement is observed in all cases. This improvement is mostly achieved because of the block diagonalization in Algorithm 1. The contribution of Algorithm 2 is more significant if the number of blocks p is small. Conversely, the overall improvement is generally large if more blocks p are used. This observation corresponds to the fact that q in (6.23) is expected to be smaller if p is larger. The effect of the

113

Table 6.2: Improvement r_1 and r_2 depending on r_r, p and r_c for $\kappa(V) = 1000$, $n = 50$ and $r_i = 10000$.

p	r_c	$r_r = 10$		$r_r = 100$		$r_r = 1000$		$r_r = 10000$		$r_r = 100000$	
		r_1	r_2	r_1	r_2	r_1	r_2	r_1	r_2	r_1	r_2
	0.0	-126.3	-46.2	-163.1	-62.3	-182.0	-71.4	-188.4	-72.1	-190.3	-72.1
2	0.4	-201.9	-69.9	-199.0	-67.7	-185.2	-63.2	-163.7	-59.4	-166.4	-55.7
	0.7	-205.7	-70.7	-201.6	-69.3	-182.2	-64.8	-162.1	-60.2	-167.1	-57.8
	1.0	-207.3	-72.8	-201.3	-69.0	-185.5	-67.7	-159.2	-59.5	-159.9	-55.7
	0.0	-131.2	-17.9	-171.6	-26.8	-191.4	-30.6	-193.6	-30.6	-198.2	-31.9
4	0.4	-239.6	-33.7	-235.2	-34.9	-216.6	-31.4	-185.5	-30.0	-185.7	-27.5
	0.7	-243.1	-35.1	-237.2	-34.1	-215.2	-33.3	-185.1	-30.7	-183.9	-25.8
	1.0	-245.3	-37.6	-235.3	-38.1	-213.8	-36.0	-181.5	-31.5	-182.2	-27.6
	0.0	-133.9	-9.3	-174.9	-15.8	-193.7	-18.3	-201.4	-18.7	-201.9	-19.3
6	0.4	-254.7	-22.5	-247.2	-22.5	-227.0	-21.4	-196.8	-21.3	-194.7	-17.8
	0.7	-255.3	-23.5	-248.0	-24.1	-226.1	-22.7	-198.6	-20.9	-189.3	-17.4
	1.0	-256.9	-23.1	-249.9	-24.1	-228.1	-22.3	-198.6	-20.5	-187.5	-18.6
	0.0	-134.8	-5.6	-177.0	-10.9	-195.5	-12.4	-200.9	-12.4	-211.9	-13.2
8	0.4	-261.8	-16.2	-254.8	-16.0	-229.5	-15.8	-205.2	-15.5	-195.6	-13.1
	0.7	-263.4	-17.9	-255.2	-16.6	-234.7	-17.5	-201.4	-16.1	-197.1	-13.4
	1.0	-265.5	-17.6	-257.4	-17.6	-233.7	-16.9	-197.2	-17.2	-192.9	-14.6
	0.0	-135.1	-3.1	-177.5	-7.0	-199.1	-9.8	-207.4	-9.5	-208.8	-9.5
10	0.4	-266.3	-12.0	-259.8	-12.7	-234.7	-12.9	-204.2	-11.7	-202.8	-10.2
	0.7	-268.4	-13.7	-262.2	-14.1	-234.2	-13.1	-202.2	-12.1	-198.4	-10.8
	1.0	-270.5	-14.5	-263.0	-14.0	-238.0	-13.9	-200.5	-13.1	-194.4	-11.0

ratio r_c of complex eigenvalues depends on r_i and r_r. If $r_r > r_i$, less improvement is obtained when r_c increases. The reverse effect is observed if $r_i > r_r$. In addition, the improvement is smaller if r_i and r_r are in the same range. That is, the ratio of real parts and imaginary parts has an effect on the improvement.

In the second experiment, we study r_1 and r_2 when generating matrices A with different dimensions $n \in \{10, 20, 50, 100, 200\}$, different ratios $r_c \in \{0, 0.4, 0.7, 1.0\}$ of complex eigenvalues and different numbers of diagonal blocks p. The real part of the eigenvalues is generated with $r_r = 1000$ and $r_i = 100$. The average values of r_1 and r_2 for 100 randomly generated matrices per data point are shown in Table 6.3.

It can be seen from Table 6.3 that the improvement increases with an increasing dimension n, which is an expected result. In analogy to experiment 1, larger improvements are observed if more blocks p in (6.17) are used and the improve-

Table 6.3: Improvement r_1 and r_2 depending on n, p and r_c for $\kappa(V) = 1000$, $r_r = 1000$ and $r_i = 100$.

p	r_c	$n = 10$		$n = 20$		$n = 50$		$n = 100$		$n = 200$	
		r_1	r_2	r_1	r_2	r_1	r_2	r_1	r_2	r_1	r_2
2	0.0	-20.5	-7.0	-57.2	-20.0	-182.0	-71.4	-379.4	-138.7	-597.4	-287.9
	0.4	-21.7	-7.9	-50.8	-17.3	-155.7	-52.6	-365.9	-133.7	-580.3	-280.3
	0.7	-20.4	-7.4	-48.6	-15.4	-156.6	-53.0	-360.6	-132.1	-581.6	-284.6
	1.0	-20.4	-7.7	-47.5	-16.0	-156.6	-54.0	-353.5	-130.0	-578.5	-281.2
4	0.0	-26.3	-3.1	-63.9	-8.0	-191.4	-30.6	-407.9	-60.3	-627.4	-144.2
	0.4	-25.1	-3.1	-60.5	-8.7	-182.0	-25.9	-401.0	-60.8	-612.3	-146.6
	0.7	-25.2	-3.5	-58.6	-9.2	-177.3	-26.6	-391.6	-61.0	-612.4	-143.0
	1.0	-24.5	-3.3	-58.3	-9.8	-173.2	-27.0	-384.6	-62.0	-611.2	-146.6
6	0.0	-27.0	-1.6	-65.9	-5.3	-193.7	-18.3	-414.9	-37.6	-642.5	-89.7
	0.4	—	—	-64.3	-6.2	-186.6	-16.3	-405.4	-37.2	-624.5	-88.2
	0.7	—	—	-64.5	-6.5	-184.7	-18.4	-400.7	-39.2	-624.6	-90.1
	1.0	—	—	-64.2	-6.3	-180.6	-18.7	-396.1	-41.2	-624.2	-92.0
8	0.0	-28.0	-0.8	-76.8	-3.7	-195.5	-12.4	-420.8	-25.3	-650.7	-65.5
	0.4	—	—	-65.5	-5.5	-190.6	-13.2	-412.2	-28.9	-631.0	-61.6
	0.7	—	—	-64.7	-5.6	-188.0	-13.7	-405.1	-28.3	-630.5	-65.0
	1.0	—	—	-64.4	-5.7	-185.7	-14.6	-399.2	-31.9	-628.6	-66.7
10	0.0	-28.4	0	-68.8	-2.6	-199.0	-9.8	-426.5	-19.1	-653.6	-51.5
	0.4	—	—	-65.7	-5.2	-193.9	-10.5	-414.7	-22.6	-635.0	-48.5
	0.7	—	—	-65.4	-5.0	-194.7	-11.6	-409.4	-23.3	-634.8	-50.1
	1.0	—	—	-65.7	-4.4	-188.3	-11.6	-401.9	-24.6	-633.3	-52.1

ment slightly decreases for larger ratios r_c of complex eigenvalues. It is further important to note that the contribution of Algorithm 2 becomes more significant for large dimensions n.

The third experiment evaluates the dependency of r_1 and r_2 on the condition number $\kappa(V)$. The experiment is performed with $n = 50$, $r_r = 1000$ and $r_i = 100$.

Table 6.4 shows that a larger improvement is achieved if $\kappa(V)$ is large. Otherwise, the observations regarding the dependency on p and r_c are analogous to the previous experiments.

In the fourth experiment, we study the effect of the imaginary part of the eigenvalues by changing r_i. The representative case of $n = 50$, $\kappa(V) = 1000$ and $r_r = 1000$ is investigated.

It can be seen from Table 6.5 that the improvement moderately increases with

Table 6.4: Improvement r_1 and r_2 depending on $\kappa(V)$, r_c and p for $n = 50$, $r_r = 1000$ and $r_i = 100$.

p	r_c	$\kappa(V) = 10$		$\kappa(V) = 1000$		$\kappa(V) = 100000$	
		r_1	r_2	r_1	r_2	r_1	r_2
2	0.0	-94.8	-24.5	-182.0	-71.4	-246.2	-94.1
	0.4	-85.5	-19.9	-170.6	-63.8	-240.7	-95.2
	0.7	-85.4	-20.6	-167.0	-64.2	-233.4	-91.0
	1.0	-83.7	-21.6	-164.7	-64.0	-229.5	-90.8
4	0.0	-105.9	-9.0	-191.4	-30.6	-264.9	-41.9
	0.4	-98.6	-7.5	-181.7	-28.8	-261.9	-46.8
	0.7	-93.9	-7.7	-181.6	-32.0	-258.4	-45.4
	1.0	-93.6	-8.6	-178.9	-30.4	-255.0	-44.9
6	0.0	-109.8	-5.1	-193.7	-18.3	-272.2	-24.1
	0.4	-101.5	-4.7	-187.6	-18.1	-271.1	-30.8
	0.7	-99.7	-5.3	-184.7	-18.4	-267.9	-30.5
	1.0	-96.3	-5.2	-170.6	-18.7	-267.2	-33.3
8	0.0	-111.2	-2.9	-195.5	-12.4	-278.9	-17.6
	0.4	-101.6	-3.5	-190.0	-13.6	-280.9	-25.5
	0.7	-99.3	-3.6	-188.0	-13.7	-280.2	-26.0
	1.0	-97.5	-3.6	-188.3	-14.6	-271.5	-27.1
10	0.0	-111.5	-1.8	-199.1	-9.8	-284.6	-15.0
	0.4	-102.7	-2.5	-193.8	-10.1	-283.9	-21.6
	0.7	-104.7	-2.9	-194.7	-11.6	-279.4	-22.2
	1.0	-96.4	-2.8	-188.3	-11.6	-276.2	-22.6

an increasing value of r_i. Similar to the observation in Table 6.1 and 6.2, it further holds that an increase in the ratio r_c of complex eigenvalues has a negative effect on the improvement as long as $r_i < r_r = 1000$, whereas a positive effect on the improvement is confirmed for $r_i > r_r$.

The fifth experiment considers the case of matrices with multiple eigenvalues and up to 4 Jordan blocks per eigenvalue. The representative case of $n = 50$, $\kappa(V) = 1000$ and $r_r = 1000$ is investigated. In addition, δ in Proposition 7 is varied such that ordered Schur decompositions with a *large* number of blocks ($\delta = 0.1$), a *medium* number of blocks ($\delta = 10$) and a *small* number of blocks ($\delta = 20$) are computed. The results are shown in Table 6.6 together with the

Table 6.5: Improvement r_1 and r_2 depending on r_i, p and r_c for $\kappa(V) = 1000$, $n = 50$ and $r_r = 1000$.

		$r_i = 10$		$r_i = 100$		$r_i = 1000$		$r_i = 10\,000$	
p	r_c	r_1	r_2	r_1	r_2	r_1	r_2	r_1	r_2
	0.0	-182.0	-71.4	-182.0	-71.4	-182.0	-71.4	-182.0	-71.4
2	0.4	-175.8	-68.5	-170.6	-63.8	-195.7	-76.9	-192.9	-73.9
	0.7	-175.2	-68.2	-167.0	-64.2	-171.5	-73.3	-199.8	-80.5
	1.0	-171.8	-67.7	-164.7	-64.0	-171.5	-73.2	-196.0	-78.2
	0.0	-193.9	-30.2	-193.9	-30.2	-193.9	-30.2	-193.9	-30.2
4	0.4	-186.0	-30.8	-181.7	-28.8	-188.1	-35.0	-221.5	-39.0
	0.7	-187.3	-32.1	-181.6	-32.0	-189.5	-38.4	-221.2	-38.8
	1.0	-182.6	-30.5	-178.9	-30.4	-187.1	-37.7	-221.5	-40.6
	0.0	-196.7	-18.2	-196.7	-18.2	-196.7	-18.2	-196.7	-18.2
6	0.4	-192.9	-19.5	-187.6	-18.1	-196.1	-24.4	-227.9	-26.5
	0.7	-189.0	-18.5	-184.7	-18.4	-195.0	-23.8	-233.8	-26.6
	1.0	-187.3	-18.0	-180.6	-18.7	-193.7	-24.1	-232.4	-28.4
	0.0	-199.1	-12.5	-199.1	-12.5	-199.1	-12.5	-199.1	-12.5
8	0.4	-193.4	-13.0	-190.0	-13.6	-195.0	-16.1	-235.6	-18.1
	0.7	-193.5	-11.9	-188.0	-13.7	-196.9	-17.3	-237.1	-20.4
	1.0	-186.7	-11.5	-185.7	-14.6	-196.6	-19.1	-237.1	-19.7
	0.0	-201.3	-10.1	-201.3	-10.1	-201.3	-10.1	-201.3	-10.1
10	0.4	-196.1	-9.7	-193.8	-10.1	-199.3	-11.0	-238.8	-15.2
	0.7	-195.4	-10.3	-194.7	-11.6	-198.4	-12.5	-239.9	-16.2
	1.0	-191.5	-9.7	-188.3	-11.6	-197.8	-12.7	-237.8	-15.3

corresponding numbers for the case of *single* eigenvalues.

Similar to the results in Table 6.3, Table 6.6 indicates larger improvements for matrices with higher dimensions. In general, a larger number of blocks p leads to larger improvements, whereby the improvements achieved in the case of multiple eigenvalues are slightly smaller than the improvements in the case of single eigenvalues and in the case of a larger ratio of complex eigenvalues r_c. It is interesting to note that the contribution of the diagonal transformation according to Algorithm 2 is more significant for large dimensions n and for small numbers of blocks p.

The last experiment investigates the convergence of the impulse response bound.

Table 6.6: Improvement r_1 and r_2 depending on n, p and r_c for $\kappa(V) = 1000$, $r_r = 1000$ and $r_i = 100$.

c	p	$n = 10$		$n = 20$		$n = 50$		$n = 100$	
		r_1	r_2	r_1	r_2	r_1	r_2	r_1	r_2
0.0	single	-28.4	0	-68.8	-2.6	-199.0	-9.8	-426.5	-19.1
	small	-27.4	-8.0	-61.9	-21.4	-167.7	-64.4	-339.2	-133.6
	medium	-30.5	-3.9	-68.9	-9.7	-186.5	-34.0	-382.6	-68.4
	large	-31.8	-0.3	-73.1	-1.1	-197.5	-5.0	-406.4	-13.9
0.4	single	-25.1	-3.1	-65.7	-5.2	-193.9	-10.5	-414.7	-22.6
	small	-26.0	-7.9	-65.9	-20.1	-162.3	-49.2	-331.0	-109.3
	medium	-28.4	-4.8	65.9	-11.6	-178.1	-30.7	-367.0	-67.0
	large	-30.5	-2.5	-70.4	-4.8	-190.8	-12.5	-392.3	-26.5
0.7	single	-25.2	-3.5	-65.4	-5.0	-194.7	-11.6	-409.4	-23.3
	small	-25.4	-7.8	-58.6	-19.0	-156.4	-51.3	-323.1	-112.0
	medium	-27.7	-6.2	-64.1	-11.8	-172.6	-31.7	-355.1	-67.7
	large	-30.1	-3.6	-69.3	-6.7	-187.0	-17.1	-385.5	-35.4
1.0	single	-24.5	-3.3	-65.7	-4.4	-188.3	-11.6	-401.9	-24.6
	small	-23.0	-8.0	-57.4	-19.9	-157.1	-46.8	-317.2	-106.6
	medium	-26.0	-6.9	-63.0	-13.5	-173.4	-33.7	-351.6	-66.2
	large	-28.9	-5.3	-68.8	-9.4	-185.9	-20.9	-383.6	-37.6

To this end, the times when the impulse response bound is below a given threshold value γ is determined for the different bounds in (6.11), (6.21) and (6.23):

$$t_{sb} = \min_t sb(t) \leq \gamma, \quad t_{isb1} = \min_t isb1(t) \leq \gamma, \quad t_{isb2} = \min_t isb2(t) \leq \gamma,$$

In the experiment values of $\gamma \in \{10^{-5}, 10^{-10}, 10^{-15}\}$ are used.

Table 6.7 shows that the improved impulse response bound in (6.23) converges to zero significantly faster than the original bound in (6.11). In particular, the application of Algorithm 2 leads to a considerable additional improvement of the bound in (6.23) compared to the bound in (6.21).

We finally list the main observations from our experimental study.

1. The bound in (6.23) achieves a significant improvement compared to the bound in (6.11) in all cases, whereby the improvement increases with the

Table 6.7: Convergence times in seconds for different thresholds γ depending on n, $p = 10$, $\kappa(V) = 1000$, $r_\mathrm{r} = 1000$, $r_\mathrm{i} = 100$, $r_\mathrm{c} = 0.6$.

		$n = 20$	$n = 50$	$n = 100$	$n = 200$	$n = 500$
$\gamma = 10^{-5}$	$t_\mathrm{isb1}/t_\mathrm{sb}$ [%]	16.2	13.9	11.8	12.4	27.1
	$t_\mathrm{isb2}/t_\mathrm{sb}$ [%]	12.8	9.3	7.1	6.6	11.0
$\gamma = 10^{-10}$	$t_\mathrm{isb1}/t_\mathrm{sb}$ [%]	19.6	15.3	12.6	12.8	27.6
	$t_\mathrm{isb2}/t_\mathrm{sb}$ [%]	16.4	11.1	8.0	7.1	11.6
$\gamma = 10^{-15}$	$t_\mathrm{isb1}/t_\mathrm{sb}$ [%]	23.3	16.9	13.4	13.3	27.9
	$t_\mathrm{isb2}/t_\mathrm{sb}$ [%]	19.8	12.6	8.9	7.6	12.1

    matrix dimension.

2. It is beneficial to use a large number of blocks p in (6.17).

3. More improvement is seen if the real parts and imaginary parts of eigenvalues are not in the same range.

4. In the case of multiple eigenvalues, slightly smaller improvements are obtained compared to the case with single eigenvalues.

5. Significantly faster convergence of the impulse response bound in (6.23) is achieved compared to the bound in (6.11).

6.4 Application of Bounds for the Matrix Exponential Function

This section applies the proposed bound computation for the matrix exponential function to an automotive example. First, the example is described in Section 6.4.1. Then, the improved Jordan bound and Schur bound are compared for a small version of the example system in Section 6.4.2. Finally, Section 6.4.3 shows that the improved Schur bound gives suitable results for a large version of the system.

6.4.1 Vehicle String Example

We consider an automotive platooning application, where several vehicles follow each other in the form of a vehicle string. Specifically, we address the case where a new vehicle N enters in front of a string of up to k vehicles as can be seen in Fig. 6.3. The vehicle string can be modeled in the form of a stable linear system
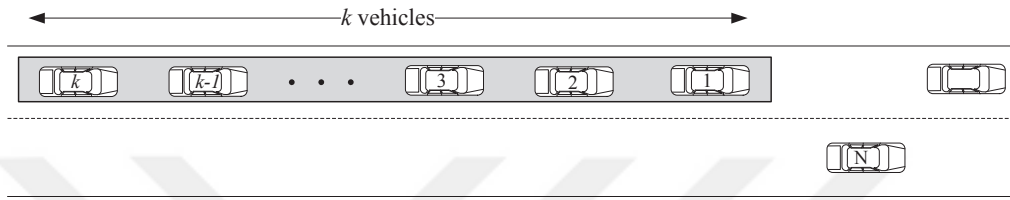

Figure 6.3: Lane change in front of a string with k vehicles.

[8, 33] with the state equations

$$
\begin{bmatrix} \dot{x}_1 \\ \dot{x}_2 \\ \vdots \\ \dot{x}_{i-1} \\ \dot{x}_k \end{bmatrix} = \underbrace{\begin{bmatrix} A_0 & 0 & \cdots & 0 & 0 \\ A_1 & A_0 & \ddots & 0 & 0 \\ \vdots & \ddots & \ddots & \ddots & \vdots \\ 0 & 0 & \ddots & A_0 & 0 \\ 0 & 0 & \cdots & A_1 & A_0 \end{bmatrix}}_{A_k} \underbrace{\begin{bmatrix} x_1 \\ x_2 \\ \vdots \\ x_{i-1} \\ x_k \end{bmatrix}}_{x} + \underbrace{\begin{bmatrix} b_1 \\ 0 \\ \vdots \\ 0 \\ 0 \end{bmatrix}}_{B_k} u. \tag{6.25}
$$

Hereby, $x_i \in \mathbb{R}^l$, $i = 1, \ldots, k$ is the state vector of vehicle i with dimension l, $u \in \mathbb{R}$ is the input signal that acts on the first vehicle and the matrices $A_0 \in \mathbb{R}^{l \times l}$ and $A_1 \in \mathbb{R}^{l \times l}$ capture the dependency of vehicle i on its own state and the state of the predecessor vehicle, respectively. Writing x for the overall state vector, an output signal can be defined as

$$
y = C_k x. \tag{6.26}
$$

Hereby, C_k can be chosen to select any relevant linear combinations of vehicle states.

Using this model, the entering maneuver can be represented by an impulse input applied to the first vehicle in the string. Then, the norm of the output response of the vehicle string is bounded by

$$||C_k e^{A_k t} B_k|| \leq ||C_k|| ||e^{A_k t}|| ||b_1||.$$

Assuming that a simulation of the linear system in (6.25) and (6.26) is available in a time interval $t \in [0, t_{\text{sim}}]$, we are particularly interested in finding a close bound for the output response that quickly converges to zero in the interval $t \in (t_{\text{sim}}, \infty)$ [64]. That is, in agreement with the discussion in Section 6.2 and 6.3, we want to find a bound for $||e^{A_k t}||$ that can be evaluated numerically and that converges to zero for sufficiently small times.

6.4.2 Jordan Bound Computation

We first consider small vehicle strings with 2 and 3 vehicles, where a Jordan canonical form of the corresponding matrix A_k in (6.25) can be obtained. Noting that different realizations of A_0, A_1 exist in the literature [13, 23, 33, 83], we choose a realization according to [33] with 8 states per vehicle and matrices

$$A_0 = \begin{bmatrix} 0 & -1 & -1 & 0 & 0 & 0 & 0 & 0 \\ 0 & 0 & 1 & 0 & 0 & 0 & 0 & 0 \\ 0 & 0 & -2.5 & 2.5 & 0 & 0 & 0 & 0 \\ 0 & 0 & 0 & -1 & 0 & 0 & 0 & 64 \\ 0.02 & 0 & 0 & 0 & 0 & 0 & 0 & -3.95 \\ 0.16 & 0 & 0 & 0 & 2 & 0 & 0 & -12.54 \\ 2.56 & 0 & 0 & 0 & 0 & 16 & 0 & -89.82 \\ 42.31 & 0 & 0 & 0 & 0 & 0 & 64 & -1\,005.73 \end{bmatrix}$$

and

$$A_1 = \begin{bmatrix} 0 & 1 & 0 & 0 & 0 & 0 & 0 & 0 \\ 0 & 0 & 0 & 0 & 0 & 0 & 0 & 0 \\ 0 & 0 & 0 & 0 & 0 & 0 & 0 & 0 \\ 0 & 0 & 0 & 0 & 0 & 0 & 0 & 0 \\ 0 & 0 & 0 & 0.06 & 0 & 0 & 0 & 0 \\ 0 & 0 & 0 & 0.20 & 0 & 0 & 0 & 0 \\ 0 & 0 & 0 & 1.40 & 0 & 0 & 0 & 0 \\ 0 & 0 & 0 & 0.16 & 0 & 0 & 0 & 0 \end{bmatrix}$$

The eigenvalues of A_k in (6.25) are the eigenvalues of A_0: $\lambda_1 = -1000$, $\lambda_{2,3} = -0.68 \pm 0.73i$, $\lambda_4 = -2.53$, $\lambda_5 = -2.24$, $\lambda_6 = -1.13$, $\lambda_7 = -0.99$ and $\lambda_8 = -1.0$.

Using the bounds in (6.14) and (6.23) with $\delta = 0.3$ and $\theta = 0.01$, we obtain the results in Fig. 6.4 and Fig. 6.5 for two and three vehicles, respectively.
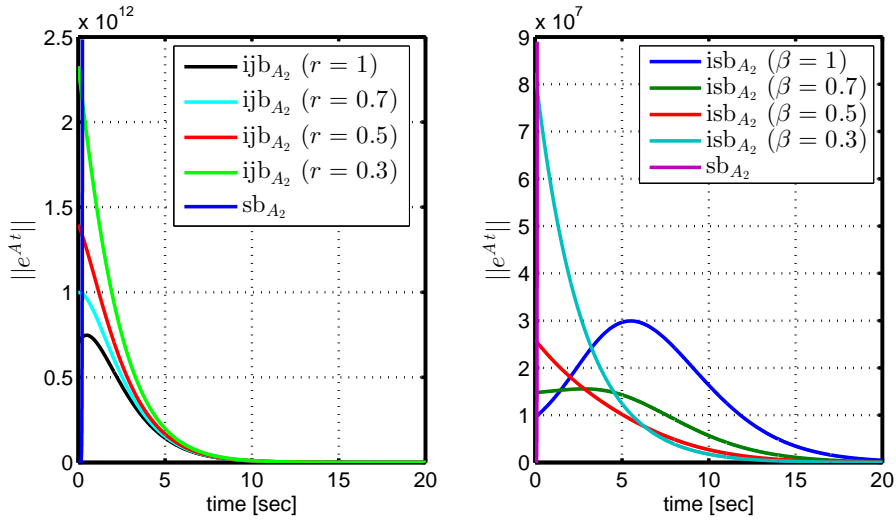
Figure 6.4: Bound comparison for a system with 2 vehicles.

It is readily observed that the bound in (6.23) using the Schur decomposition is significantly better for this example. The main reason is that the condition number of the transformation matrix for obtaining the Jordan canonical form of A is large. In both cases, the bound in (6.23) with $\beta = 0.5$ converges to zero quickly. For example it holds that $\text{isb}_{A_k}(t) \le 10^{-4}$ for $t \in (55, \infty)$ in the case of $k = 2$ vehicles
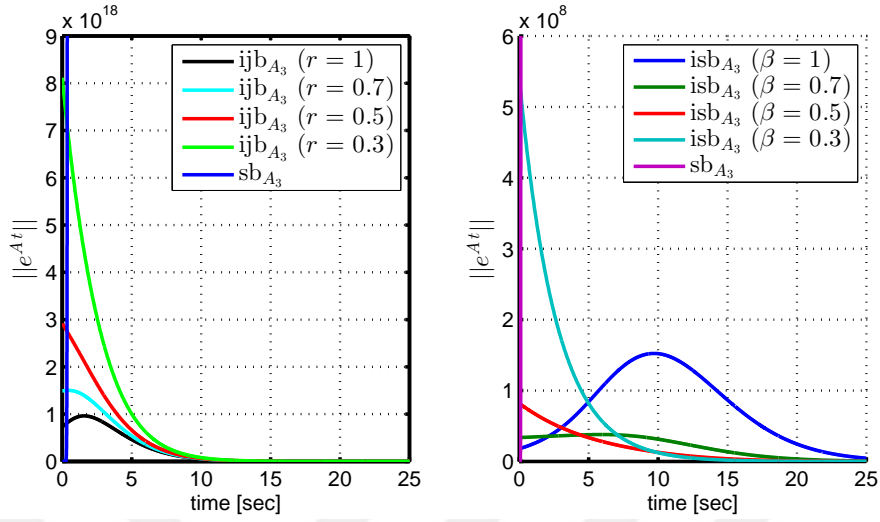
Figure 6.5: Bound comparison for a system with 3 vehicles.

and for $t \in (65, \infty)$ in the case of $k = 3$ vehicles. In comparison, the existing Schur bound in (6.11) leads to

$$\text{sb}_{A_2}(t) = e^{-0.68t} \sum_{k=0}^{15} \frac{173^k t^k}{k!} \tag{6.27}$$

for the case of two vehicles and

$$\text{sb}_{A_3}(t) = e^{-0.68t} \sum_{k=0}^{23} \frac{173^k t^k}{k!} \tag{6.28}$$

for the case of three vehicles. In both cases, this bound is much more conservative as is also indicated in Fig. 6.4 and 6.5 (note that sb_{A_2} and sb_{A_3} are only shown for very small times).

6.4.3 Schur Bound Computation

We finally consider a vehicle string with 20 vehicles. That is, the matrix A_{20} has dimension 160 and it was not possible to determine its Jordan canonical form.

Computing the Schur bound in (6.11), we obtain

$$
\text{sb}_{A_{20}}(t) = e^{-0.68t} \sum_{k=0}^{159} \frac{173^k t^k}{k!}
\tag{6.29}
$$

which cannot be evaluated numerically even for very small times due to the high polynomial order. For illustration, we compute the improved Schur bound in Section 6.3 step by step. First, we determine the ordered Schur decomposition in (6.17) with $\delta = 0.3$. As a result, we get S with 4 blocks, whereby the size of the largest block is $q = 60$. In this computation, we note that the special structure of A is helpful, since it holds that each eigenvalue of A_0 is repeated 20 times. That is, it is easy to determine similar eigenvalues for this example. Specifically, one block of size 20 contains the repeated eigenvalue λ_1, one block of size 40 contains the complex eigenvalues $\lambda_{2,3}$, one block of size 40 contains λ_4 and λ_5 and one block of size 60 contains the remaining eigenvalues. Next, we perform the transformation to the block diagonal matrix $\hat{S}$ using Algorithm 1. The resulting transformation matrix has $\kappa(\hat{T}) = 50\,140$ and the norm of the strictly upper-triangular part of $\hat{S}$ is $||\hat{S}_N|| = 12.0$. That is, without using the diagonal transformation R in Algorithm 2 (or equivalently $\beta = 12.0$), the improved Schur bound in (6.21) gives

$$
\text{isb1}_{A_{20}}(t) = 50\,140 \cdot e^{-0.68t} \sum_{k=0}^{59} \frac{12.0^k t^k}{k!}.
\tag{6.30}
$$

This bound is much smaller than the bound in (6.29) and decays below 10^{-4} for $t \in (513, \infty)$. A further improvement is achieved by limiting $||\hat{S}_N||$. Hence, we perform a transformation with R using Algorithm 2 with different values of β and a tolerance $\theta = 0.01$. The results of this computation are shown in Fig. 6.6.

Here, for example the bound for $\beta = 0.5$ is suitable. Although the condition number now increases to $\kappa(T) \approx 2.5 \cdot 10^{22}$, the overall bound

$$
||e^{A_{20}t}|| \leq 2.5 \cdot 10^{22} \cdot e^{-0.68t} \sum_{k=0}^{59} \frac{0.5^k t^k}{k!}
\tag{6.31}
$$

already decays below 10^{-4} for $t \in (233, \infty)$ and can be computed in a stable way.
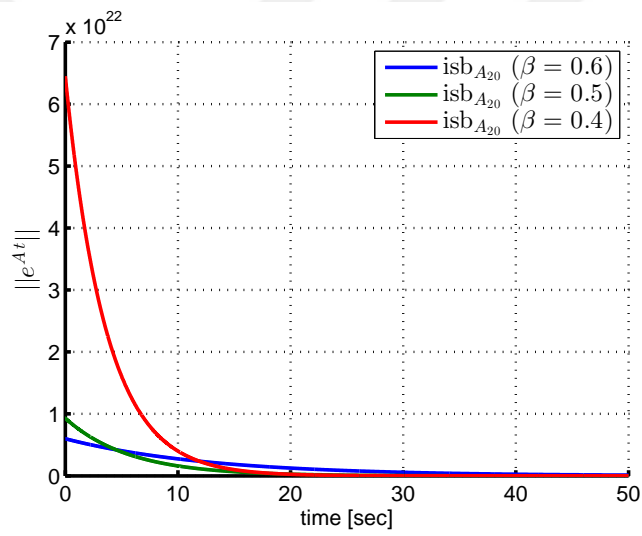
Figure 6.6: Bound comparison for a system with 20 vehicles.

CHAPTER 7

CONCLUSION

In the scope of intelligent transportation systems (ITS), cooperative adaptive cruise control (CACC) is a recent technology that enables vehicle following in the form of vehicle strings at small inter-vehicle spacings. Here, the fulfillment of string stability is essential in order to ensure driving comfort and driving safety. String stability guarantees that fluctuations and disturbances are attenuated along a vehicle string.

In the literature, string stability is commonly studied based on the fact that a disturbance is introduced by the leader vehicle and hence occurs at the beginning of the string. Such disturbance should not grow or amplify while propagating through the string. In contrast, this thesis identifies the occurrence of additional disturbances within the string when performing lane changes. When completing a lane change, impulses are encountered due to state jumps when switching predecessor vehicles. In addition, the preparation of lane changes requires opening gaps, which are achieved by applying time-limited input signals. Hence, the thesis extends the classical setting to scenarios including repeated state jumps (impulse inputs) and repeated exogenous time-limited input signals within vehicle strings.

In order to address the stated problem, the thesis first introduces the relevant background information on vehicle strings, CACC and string stability. As the first contribution, the thesis presents methods for computing norm bounds on output signals when applying repeated input impulses and time-limited input signals to stable LTI systems. In this context, it is desired that output signals such as the distance error between vehicles remain bounded in order to ensure driving safety even if maneuvers are repeatedly executed. Accordingly, the thesis first shows that

126

a bound on the output signal norm exists if the repeated input signals (impulses or time-limited signals) are separated by a non-zero dwell-time. Moreover, an original computational procedure for finding a close bound on the output signal norm is developed. Moreover, the concepts that are first developed for general LTI systems are extended to the case of distributed interconnected systems with multiple inputs and outputs.

The bound computations are formulated for general LTI systems. In accordance with the aim of studying lane changes in vehicle strings, the developed methods are applied to vehicle strings as the second main contribution of the thesis. Suitable analytical bounds for the relevant output signals such as distance error or acceleration are determined and validated by simulations. Together, it is shown that a safe and comfortable driving distance is guaranteed even if an arbitrary number of longitudinal maneuvers is performed in vehicle strings with many vehicles.

When determining the analytical output signal bounds, it is observed that the numerical computation of a certain bounding function for the norm bound of the impulse response matrix becomes infeasible for large LTI systems. To this end, the third contribution of the thesis is the development of numerical methods for bounding the matrix exponential function for the analysis and design of linear dynamical systems. Two new bounds are proposed. The first bound is based on the Jordan canonical form. Using a particular diagonal similarity transformation, it is possible to achieve fast convergence of this bound to zero. Nevertheless, the usability of this bound depends on determining the Jordan canonical form of a matrix, which is numerically difficult. Accordingly, the second method proposes a computational procedure that can be evaluated for general matrices. Using an ordered Schur decomposition, it is first possible to transform a given matrix to a block diagonal form. Then, an additional diagonal transformation is used to achieve fast convergence of the bound to zero. It is shown by examples that both bounds are suitable for systems of small size when the Jordan canonical form is available. Furthermore, the bound based on the Schur decomposition also provides satisfactory results for large systems, which is demonstrated by the practical

127

example of vehicle strings.

The current formulation is for the case of homogeneous vehicle strings with linear models, where each vehicle has the same dynamic properties. Future research will extend the obtained results to the case of heterogeneous vehicle strings. Additionally vehicle experimental tests may be done to validate our models and compare then verify our results. Another direction apart from intelligent transportation systems is that our system and control contributions might be applied to completely different areas of interconnected distributed systems such as irrigation flow systems or supply chains.

REFERENCES

[1] **M. A. Chowdhury, A. W. Sadek, (2003),** "Fundamentals of Intelligent Transportation Systems Planning", *Artech House, Inc.* pp. 35–55.

[2] **B. Ran, P. J. Jin, D. Boyce, T. Z. Qiu, Y. Cheng, (2012),** "Perspectives on future transportation research: Impact of intelligent transportation system technologies on next-generation transportation modeling,", *Journal of Intelligent Transportation Systems*, vol. 16, no. 4, pp. 226–242.

[3] **Y. Ma, M. Chowdhury, A. Sadek, M. Jeihani, (2012),** "Integrated traffic and communication performance evaluation of an intelligent vehicle infrastructure integration (vii) system for online travel-time prediction", *IEEE Transactions on Intelligent Transportation Systems*, Springer-Verlag US., vol. 13, no. 3, pp. 1369–1382.

[4] **K. C. Dey, A. Mishra, M. Chowdhury, (2015),** "Potential of intelligent transportation systems in mitigating adverse weather impacts on road mobility: A review", *IEEE Transactions on Intelligent Transportation Systems*, vol. 16, no. 3, pp. 1107–1119.

[5] **Y. Ma, M. Chowdhury, A. Sadek, M. Jeihani, (2015),** "Real-time highway traffic condition assessment framework using vehicle-infrastructure integration (vii) with artificial intelligence (ai)," *IEEE Transactions on Intelligent Transportation Systems*, vol. 10, no. 4, pp. 615–627.

[6] **L. D. Baskar, B. De Schutter, J. Hellendoorn, Z. Papp, (2011),** "Traffic control and intelligent vehicle highway; systems: A survey," *IET Intelligent Transportation Systems*, vol. 5, no. 1, pp. 38–52.

[7] **B. Kerner, (2009),** "Introduction to Modern Traffic Flow Theory and Control: The Long Road to Three-Phase Traffic Theory." Berlin and New York: Springer.

[8] **J. Ploeg, N. van de Wouw, H. Nijmeijer, (2014),** "Lp string stability of cascaded systems: Application to vehicle platooning," *Control Systems Technology, IEEE Transactions on*, vol. 22, no. 2, pp. 786–793.

[9] **M. A. Samad Kamal, J. I. Imura, T. Hayakawa, A. Ohata, K. Aihara, (2014),** "Smart driving of a vehicle using model predictive control for improving traffic flow," *IEEE Transactions on Intelligent Transportation Systems*, vol. 15, no. 2, pp. 878–888.

[10] **A. Vahidi, A. Eskandarian, (2003),** "Research advances in intelligent collision avoidance and adaptive cruise control," *IEEE Transactions on Intelligent Transportation Systems*, vol. 4, no. 3, pp. 143–153.

[11] **M. Aeberhard, S. Rauch, M. Bahram, G. Tanzmeister, J. Thomas, Y. Pilat, F. Homm, W. Huber, N. Kaempchen, (2015),** "Experience, results and lessons learned from automated driving on germanys highways," *IEEE Intelligent Transportation Systems Magazine*, vol. 7, no. 1, pp. 42–57.

[12] **J. Nilsson, J. Silvlin, M. Brannstrom, E. Coelingh, J. Fredriksson, (2016),** "If, when, and how to perform lane change maneuvers on highways," *IEEE Intelligent Transportation Systems Magazine*, vol. 8, no. 4, pp. 68–78.

[13] **G. J. L. Naus, R. P. A. Vugts, J. Ploeg, M. J. G. Van de Molengraft, M. Steinbuch, (2010),** "String-stable cacc design and experimental validation: A frequency-domain approach," *Vehicular Technology, IEEE Transactions on*, vol. 59, no. 9, pp. 4268–4279.

[14] **K. C. Dey, L. Yan, X. Wang, Y. Wang, H. Shen, M. Chowdhury, L. Yu, V. Soundararaj, (2016),** "A review of communication, driver characteristics, and controls aspects of cooperative adaptive cruise control (cacc)," *IEEE*

Transactions on Intelligent Transportation Systems, vol. 17, no. 2, pp. 491–509.

[15] **J. Lioris, R. Pedarsani, F. Yildiz Tascikaraoglu, P. Varaiya, (2017),** "Platoons of connected vehicles can double throughput in urban roads," *Transportation Research Part C*, vol. 77, pp. 292–305.

[16] **S. E. Shladover, C. Nowakowski, X.-Y. Lu, R. Ferlis, (2015),** "Cooperative adaptive cruise control: Definitions and operating concepts," *Transportation Research Record*, no. 2489, pp. 145–152.

[17] **C. Desjardins, B. Chaib-draa, (2011),** "Cooperative adaptive cruise control: A reinforcement learning approach," *IEEE Transactions on Intelligent Transportation Systems*, vol. 12, pp. 1248–1260.

[18] **R. Kianfar, B. Augusto, A. Ebadighajari, U. Hakeem, J. Nilsson, A. Raza, R. S. Tabar, N. V. Irukulapati, C. Englund, P. Falcone, S. Papanastasiou, L. Svensson, H. Wymeersch, (2012),** "Design and experimental validation of a cooperative driving system in the grand cooperative driving challenge," *IEEE Transactions on Intelligent Transportation Systems*, vol. 13, pp. 994–1007.

[19] **I. Bayezit, T. Veldhuizen, B. Fidan, J. Huissoon, H. Lupker, (2012),** "Design of string stable adaptive cruise controllers for highway and urban missions," in *Communication, Control, and Computing (Allerton), 2012 50th Annual Allerton Conference on*, pp. 106–113.

[20] **S. Oncu, J. Ploeg, N. van de Wouw, H. Nijmeijer, (2014),** "Cooperative adaptive cruise control: Network-aware analysis of string stability," *Intelligent Transportation Systems, IEEE Transactions on*, vol. 15, pp. 1527–1537.

[21] **J. Ploeg, E. Semsar-Kazerooni, G. Lijster, N. van de Wouw, H. Nijmeijer, (2015),** "Graceful degradation of cooperative adaptive cruise control," *IEEE Transactions on Intelligent Transportation Systems*, vol. 16, pp. 488–497.

[22] **J. Ploeg, D. Shukla, N. Van De Wouw, H. Nijmeijer, (2014),** "Controller synthesis for string stability of vehicle platoons," *Intelligent Transportation Systems, IEEE Transactions on*, vol. 15, pp. 854–865.

[23] **C. Wang, H. Nijmeijer, (2015),** "String stable heterogeneous vehicle platoon using cooperative adaptive cruise control," in *IEEE 18th International Conference on Intelligent Transportation Systems*, pp. 1977–1982.

[24] **D. Swaroop, J. Hedrick, (1996),** "String stability of interconnected systems," *Automatic Control, IEEE Transactions on*, vol. 41, pp. 349–357.

[25] **J. Eyre, D. Yanakiev, I. Kanellakopoulos, (1998),** "A simplified framework for string stability analysis of automated vehicles," *Vehicle System Dynamics*, vol. 30, no. 5, pp. 375–405.

[26] **P. Fernandes, U. Nunes, (2012),** "Platooning with IVC-enabled autonomous vehicles: Strategies to mitigate communication delays, improve safety and traffic flow," *Intelligent Transportation Systems, IEEE Transactions on*, vol. 13, pp. 91–106.

[27] **R. Kianfar, M. Ali, P. Falcone, J. Fredriksson, (2014),** "Combined longitudinal and lateral control design for string stable vehicle platooning within a designated lane," in *Intelligent Transportation Systems, IEEE International Conference on*, pp. 1003–1008.

[28] **M. di Bernardo, P. Falcone, A. Salvi, S. Santini, (2016),** "Design, analysis, and experimental validation of a distributed protocol for platooning in the presence of time-varying heterogeneous delays," *IEEE Transactions on Control Systems Technology*, vol. 24, pp. 413–427.

[29] **W. Dunbar, D. Caveney, (2012),** "Distributed receding horizon control of vehicle platoons: Stability and string stability," *Automatic Control, IEEE Transactions on*, vol. 57, pp. 620–633.

[30] **S. H. Hosseinnia, I. Tejado, V. Milanes, J. Villagra, B. M. Vinagre, (2014),** "Experimental application of hybrid fractional-order adaptive cruise

control at low speed," *IEEE Transactions on Intelligent Transportation Systems*, vol. 22, no. 6, pp. 2329–2336.

[31] **V. Milanes, S. E. Shladover, (2014),** "Modeling cooperative and autonomous adaptive cruise control dynamic responses using experimental data," *Transportation Research Part C*, vol. 48, pp. 285–300.

[32] **S. E. Shladover, (2009),** "Cooperative (rather than autonomous) vehicle highway automation systems," *IEEE Intelligent Transportation Systems Magazine*, vol. 1, pp. 10–19, 2009.

[33] **J. Ploeg, D. Shukla, N. Van De Wouw, H. Nijmeijer, (2014),** "Controller synthesis for string stability of vehicle platoons," *Intelligent Transportation Systems, IEEE Transactions on*, vol. 15, pp. 854–865.

[34] **S. Sheikholeslam, C. Desoer, (1993),** "Longitudinal control of a platoon of vehicles with no communication of lead vehicle information: a system level study," *Vehicular Technology, IEEE Transactions on*, vol. 42, pp. 546–554.

[35] **G. Guo, W. Yue, (2011),** "Hierarchical platoon control with heterogeneous information feedback," *Control Theory Applications, IET*, vol. 5, pp. 1766–1781.

[36] **R. Rajamani, (2012),** *Vehicle Dynamics and Control*. Springer US, Mechanical Engineering Series, 2 ed.

[37] **C.-Y. Liang, H. Peng, (1999),** "Optimal adaptive cruise control with guaranteed string stability," *Vehicle System Dynamics*, vol. 32, no. 4-5, pp. 313–330.

[38] **J. Zegers, E. Semsar-Kazerooni, J. Ploeg, N. van de Wouw, H. Nijmeijer, (2016),** "Consensus-based bi-directional cacc for vehicle platooning," in *American Control Conference (ACC)*, pp. 2578–2584.

[39] **A. Kesting, M. Treiber, M. Schnhof, H. D., (2008),** "Adaptive cruise control design for active congestion avoidance," *Transportation Research Part C*, vol. 16, pp. 668–683, 2008.

[40] **J. Eyre, D. Yanakiev, I. Kanellakopoulos, (1998),** "A simplified framework for string stability analysis of automated vehicles," *Vehicle System Dynamics*, vol. 30, pp. 375–405.

[41] **A. M. Al-Jhayyish, (2016),** "Design and evaluation of cooperative adaptive cruise control (cacc) for the improvement of highway traffic flow," Master's thesis, Cankaya University, Ankara, Turkey.

[42] **S. Oncu, N. van de Wouw, H. Nijmeijer, (2011),** "Cooperative adaptive cruise control: Tradeoffs between control and network specifications," in *IEEE, 14th International Conference on Intelligent Transportation Systems*, pp. 2051–2056.

[43] **J. Ploeg, A. F. A. Serrarens, G. J. Heijenk, (2011),** "Connect and drive: Design and evaluation of cooperative adaptive cruise control for congestion reduction," *Journal of Modern Transportation*, vol. 19, pp. 207–213.

[44] **W. Lv, W.-g. Song, Z.-m. Fang, J. Ma, (2013),** "Modelling of lane-changing behaviour integrating with merging effect before a city road bottleneck," *Physica A: Statistical Mechanics and its Applications*, vol. 392, no. 20, pp. 5143–5153.

[45] **W. Lv, W.-g. Song, L. Xiao-dong, J. Ma, (2013),** "A microscopic lane changing process model for multilane traffic," *Physica A: Statistical Mechanics and its Applications*, vol. 392, no. 5, pp. 1142–1152.

[46] **W. Lv, W.-g. Song, F. Zhi-ming, (2011),** "Three-lane changing behaviour simulation using a modified optimal velocity model," *Physica A: Statistical Mechanics and its Applications*, vol. 390, no. 12, pp. 2303–2314.

[47] **Y. Wang, E. Wenjuan, W. Tang, D. Tian, G. Lu, G. Yu, (2013),** "Automated on-ramp merging control algorithm based on internet-connected vehicles," *Intelligent Transport Systems, IET*, vol. 7, pp. 371–379.

[48] **A. Uno, T. Sakaguchi, S. Tsugawa, (1999),** "A merging control algorithm based on inter-vehicle communication," in *Intelligent Transportation Systems, 1999. Proceedings. 1999 IEEE/IEEJ/JSAI International Conference on*, pp. 783–787.

[49] **L. Xiao-Yun, H.-S. Tan, S. Shladover, J. Hedrick, (2000),** "Implementation of longitudinal control algorithm for vehicle merging," in *Proceedings of AVEC 2000. 5th International Symposium on Advanced Vehicle Control*.

[50] **B. Kim, N. Maxemchuk, (2012),** "A safe driver assisted merge protocol," in *Systems Conference (SysCon), 2012 IEEE International*, pp. 1–4.

[51] **D. Marinescu, J. Curn, M. Bouroche, V. Cahill, (2012),** "On-ramp traffic merging using cooperative intelligent vehicles: A slot-based approach," in *Intelligent Transportation Systems (ITSC), 2012 15th International IEEE Conference on*, pp. 900–906.

[52] **T. Awal, L. Kulik, K. Ramamohanrao, (2013),** "Optimal traffic merging strategy for communication- and sensor-enabled vehicles," in *Intelligent Transportation Systems - (ITSC), 2013 16th International IEEE Conference on*, pp. 1468–1474.

[53] **E. Semsar-Kazerooni, J. Ploeg, (2015),** "Interaction protocols for cooperative merging and lane reduction scenarios," in *Intelligent Transportation Systems, IEEE International Conference on*, pp. 1964–1970.

[54] **V. Milanes, S. E. Shladover, J. Spring, C. Nowakowski, H. Kawazoe, M. Nakamura, (2014),** "Cooperative adaptive cruise control in real traffic situations," *IEEE Transactions on Intelligent Transportation Systems*, vol. 15, no. 1, pp. 296 – 305.

[55] **I. Deaibil, K. Schmidt, (2015),** "Performing safe and efficient lane changes in dense vehicle traffic," in *Engineering and Technology Symposium, Ankara, Turkey*.

[56] **H. Bingol, (2017),** "String stability analysis of cooperative adaptive cruise control (cacc) with actuator saturation," Master's thesis, Cankaya University, Ankara, Turkey.

[57] **E. Cankaya, (2017),** "Trajectory generation for open/close gap maneuvers in vehicle strings," Master's thesis, Cankaya University, Ankara, Turkey.

[58] **Y. W. Wang, D. S. Bernstein, (1994),** "L_2 controller synthesis with L_∞-bounded closed-loop impulse response," *International Journal of Control*, vol. 60, no. 6, pp. 1295–1306.

[59] **N. K. Rutland, P. G. Lane, (1995),** "Computing the 1-norm of the impulse response of linear time-invariant systems," *Systems & Control Letters*, vol. 26, no. 3, pp. 211–221.

[60] **H. Tokunaga, T. Iwasaki, S. Hara, (1998),** "Analysis and synthesis of the robust impulse-to-peak performance," *Automatica*, vol. 34, no. 11, pp. 1473–1477.

[61] **J. Lygeros, F. A. Ramponi, (2015),** *Lecture Notes on Linear System Theory*. Automatic Control Laboratory, ETH Zurich.

[62] **J. Baras, R. W. Brockett, P. Fuhrmann, (1974),** "State-space models for infinite-dimensional systems," *Automatic Control, IEEE Transactions on*, vol. 19, pp. 693–700.

[63] **C. V. Loan, (1977),** "The sensitivity of the matrix exponential," *SIAM Journal on Numerical Analysis*, vol. 14, no. 6, pp. 971–981.

[64] **B. Sağlam, K. W. Schmidt, (2017),** "Outputs bounds for linear systems with repeated input signals: Existence, computation and application to vehicle platooning," *Turkish Journal of Electrical Engineering and Computer Sciences (accepted)*.

[65] **Z. Wu, Y. Liu, G. Pan, (2009),** "A smart car control model for brake comfort based on car following," *IEEE Transactions on Intelligent Transportation Systems*, vol. 10, pp. 42–46.

[66] **P. Rutquist, M. Edvall, (2010),** *Matlab Optimal Control Software*. Tomlab.

[67] **G. Dahlquist, (1959),** *Stability and Error Bounds in the Numerical Integration of Ordinary Differential Equations*. Almqvist & Wiksells Boktryckeri Ab.

[68] **E. M. E. Wermuth, (1989),** "Two remarks on matrix exponentials," *Linear Algebra and its Applications*, vol. 117, pp. 127–132.

[69] **C. F. V. Loan, (1975),** "A study of the matrix exponential," numerical analysis report no. 10, University of Manchester, Manchester, UK.

[70] **C. Moler, C. V. Loan, (2003)** "Nineteen dubious ways to compute the exponential of a matrix, twenty-five years later," *SIAM Review*, vol. 45, no. 1, pp. 3–49.

[71] **G. H. Golub, J. H. Wilkinson, (1976),** "Ill-conditioned eigensystems and the computation of the jordan canonical form," *SIAM Review*, vol. 18, no. 4, pp. 578–619.

[72] **B. Kågström, A. Ruhe, (1980),** "An algorithm for numerical computation of the jordan normal form of a complex matrix," *ACM Trans. Math. Softw.*, vol. 6, pp. 398–419.

[73] **J. G. F. Francis, (1962),** "The qr transformationpart 2," *The Computer Journal*, vol. 4, no. 4, pp. 332–345.

[74] **B. N. Parlett, "The qr algorithm, (2000),"** *Computing in Science and Eng.*, vol. 2, pp. 38–42, Jan. 2000.

[75] **H. Shapiro, (1999),** "The weyr characteristic," *The American Mathematical Monthly*, vol. 106, no. 10, pp. 919–929.

[76] **P. I. Davies, N. J. Higham, (2003),** "A schur-parlett algorithm for computing matrix functions," *SIAM Journal on Matrix Analysis and Applications*, vol. 25, no. 2, pp. 464–485.

[77] **G. W. S. Connice A. Bavely, (1979),** "An algorithm for computing reducing subspaces by block diagonalization," *SIAM Journal on Numerical Analysis*, vol. 16, no. 2, pp. 359–367.

[78] **G. H. Golub, C. F. V. Loan, (2012),** *Matrix Computations*. Johns Hopkins Studies in the Mathematical Sciences, Johns Hopkins University Press, fourth ed.

[79] **H. Shapiro, (1991),** "A survey of canonical forms and invariants for unitary similarity," *Linear Algebra and its Applications*, vol. 147, pp. 101–167.

[80] **G. Moore, (2011),** "Orthogonal polynomial expansions for the matrix exponential," *Linear Algebra and its Applications*, vol. 435, no. 3, pp. 537–559.

[81] **R. C. Ward, (1977),** "Numerical computation of the matrix exponential with accuracy estimate," *SIAM Journal on Numerical Analysis*, vol. 14, no. 4, pp. 600–610.

[82] Advanpix Software Company, (2015), "Multiprecision computing toolbox for matlab." `http://www.advanpix.com/`.

[83] **A. Ghasemi, S. Rouhi, (2015),** "A safe stable directional vehicular platoon," *Proceedings of the Institution of Mechanical Engineers, Part D: Journal of Automobile Engineering*, vol. 229, no. 8, pp. 1083–1093.

CURRICULUM VITAE

PERSONAL INFORMATION

Surname, Name: Sağlam, Harun Buğra

Nationality: Turkey

Date and Place of Birth: 03 April 1982 , Trabzon

Marital Status: Married

Phone: +90 532 327 44 78

Email: bugrasaglam@gmail.com

EDUCATION

Degree	Institution	Year
M.Sc.	Middle East Technical University, Industrial Eng. Engineering Management	2010
B.Sc.	Middle East Technical University, Electrical and Electronics Engineering.	2006
High School	Ankara Ataturk Anatolian School	2000

WORK EXPERIENCE

Year	Place	Enrollment
2007-present	Turkish Aerospace Industries, Inc.	Systems Engineer
2006-2007	Aydın Yazılım Elektronik Sanayi A.S.	Software Engineer

PUBLICATIONS

B. Sağlam, K. W. Schmidt, (2017), "Outputs bounds for linear systems with repeated input signals: Existence, computation and application to vehicle platooning," *Turkish Journal of Electrical Engineering and Computer Sciences (accepted)*.

FOREIGN LANGUAGES

English, French

HOBBIES

Art, Traveling, Sport, Reading